

INDIVIDUAL TRAPPED ATOMS FOR CAVITY QED QUANTUM  
INFORMATION APPLICATIONS

A Thesis  
Presented to  
The Academic Faculty

by

Kevin M. Fortier

In Partial Fulfillment  
of the Requirements for the Degree  
Doctor of Philosophy in the  
School of Physics

Georgia Institute of Technology  
May 2007

INDIVIDUAL TRAPPED ATOMS FOR CAVITY QED QUANTUM  
INFORMATION APPLICATIONS

Approved by:

Michael Chapman, Advisor  
School of Physics  
*Georgia Institute of Technology*

Alex Kuzmich  
School of Physics  
*Georgia Institute of Technology*

Chandra Raman  
School of Physics  
*Georgia Institute of Technology*

T. A. Brian Kennedy  
School of Physics  
*Georgia Institute of Technology*

Robert Dickson  
School of Chemistry  
*Georgia Institute of Technology*

Date Approved: 22 February 2007

*Dedicated to my wife and my parents*

## ACKNOWLEDGEMENTS

I would first like to thank my advisor, Professor Mike Chapman, who gave me an opportunity to work in his lab and provided an environment where I could succeed. His wealth of ideas guide the experiments and his patient and encouragement kept me motivated.

As a beginning graduate student I had the opportunity to learn from two talented students. Jake Sauer introduced me to experimental physics when I joined the lab as his understudy. I worked closely with Jake for two years as he shared his expertise of lasers, cavities, and optics. Ming-Shien Chang joined the the lab at the same time I did from Duke University. Ming-Shien's work ethic and dedication are amazing and an inspiration to all of us.

I am extremely fortunate to work closely with two graduate students who joined the lab after me. Soo Kim has worked with me for the last 3 years on the cavity experiment and with her dedication the experiment will continue to expand and improve. Michael Gibbons split off from the cavity experiment to work on a side project that has developed into a beautiful single atom experiment. I'm grateful for Soo's and Michael's positive attitude which has eased my frustration when the experiments weren't working. I've enjoyed the camaraderie of Layne Churchill, Adam Steele, Eva Bookjans and Chris Hamley.

Paul Griffin joined our lab as a postdoc in October 2005. Besides being a friend, he shares my birthday and taste in "good" music. Paul has taught me to appreciate his native Irish culture and generously let me sleep on his couch for the last two months. I appreciate his editing and his efforts to distract me from the writing. Peyman Amahdi joined our lab in September 2006 as postdoc and I especially want to thank him and his wife, Ghazal, for editing my thesis.

I would like to thank Professor Phil First who invited me to Georgia Tech as a REU summer researcher in 2000. I enjoyed that summer working in his lab and when it came time to decide on a graduate school this experience brought me back to Georgia Tech.

The completion of this thesis is due to the support of my family. My parents sacrificed to ensure my education was what I wanted. The continent that separates us makes seeing each other difficult, but they have always pushed me to follow my dreams. This thesis is dedicated partially to them.

Finally I would like to thank my wife, Lici. She has always supported through the good and bad times in graduate school. The completion of this thesis is largely due to her and I dedicate it to her.

# TABLE OF CONTENTS

DEDICATION		iii
ACKNOWLEDGEMENTS		iv
LIST OF TABLES		x
LIST OF FIGURES		xi
SUMMARY		xiv
<b>I</b>	<b>INTRODUCTION</b>	<b>1</b>
	1.1 Quantum Computing	2
	1.2 Quantum Computing History	3
	1.3 Quantum Computing Requirements	5
	1.4 Cavity QED at Georgia Tech	8
	1.5 Organization of This Thesis	8
<b>II</b>	<b>ATOM TRAPPING</b>	<b>9</b>
	2.1 Magneto Optical Trap	9
	2.2 Optical Molasses	9
	2.3 One-Dimensional MOT	11
	2.4 Doppler and Sub-Doppler Cooling	13
	2.5 Optical Trapping of Neutral Atoms	14
	2.6 Optical Trapping History	15
	2.7 Optical Trap Theory	16
	2.7.1 Lorentz Model of the Atomic Polarizability	16
	2.8 Gaussian Beams	19
	2.9 Single Focus Traps	20
	2.10 Optical Lattices	21
	2.10.1 Walking Wave Velocity	23
	2.11 Trap Frequencies	23
	2.12 AC Stark shift computation	24
	2.13 Magic Wavelength	27

III	CLASSICAL AND QUANTUM CAVITY THEORY . . . . .	28
	3.1 Classical Cavity Physics . . . . .	28
	3.1.1 Resonator g Parameters . . . . .	29
	3.1.2 Mirror Losses and Delta Notation . . . . .	31
	3.1.3 Cavity Transmission . . . . .	33
	3.2 Quantum Development of Cavity QED system . . . . .	35
	3.3 Strong Coupling . . . . .	37
	3.4 Master Equation and Cooling Forces . . . . .	39
	3.5 Cavity QED based Quantum Computer . . . . .	41
IV	EXPERIMENTAL SETUP . . . . .	43
	4.1 Vacuum System . . . . .	43
	4.2 MOT Coils . . . . .	43
	4.3 Rubidium Properties . . . . .	44
	4.3.1 Rubidium Source . . . . .	45
	4.4 Diode Lasers . . . . .	46
	4.4.1 MOT Laser System . . . . .	48
	4.4.2 Repump Laser System . . . . .	49
	4.4.3 Cavity Laser System . . . . .	50
	4.5 Cavities . . . . .	54
	4.5.1 Science Cavity Construction . . . . .	54
	4.5.2 Science Cavity Stabilization . . . . .	56
	4.5.3 Science Light Detection: Photon Counting . . . . .	59
	4.5.4 Transfer Cavity Construction . . . . .	60
	4.5.5 Transfer Cavity Stabilization . . . . .	61
	4.6 Optical Trap Lasers . . . . .	62
	4.7 CCD Imaging Setup . . . . .	64
	4.8 Quantitative Analysis of Images . . . . .	66
	4.8.1 Number . . . . .	66
	4.8.2 Temperature . . . . .	66
	4.9 Computer Control . . . . .	67

V	ATOM TRAPPING EXPERIMENTS . . . . .	68
5.1	Optical Trap Diagnostics . . . . .	68
5.1.1	Trap Lifetimes . . . . .	68
5.1.2	Atom Positioning Experiments . . . . .	71
5.1.3	Imaging Atoms inside the Optical Cavity . . . . .	72
5.2	Experiments with Single Atoms . . . . .	72
5.2.1	Single Atom MOT Production . . . . .	73
5.2.2	Single atom Stark Shift Probe . . . . .	74
5.2.3	Imaging Single Atoms in an Optical Trap . . . . .	77
5.2.4	Non-Destructive detection . . . . .	78
5.2.5	Preparing Chains of Atoms . . . . .	79
5.3	Summary of Atom Trapping Experiments . . . . .	81
VI	PROBING THE ATOM-CAVITY SYSTEM . . . . .	82
6.1	Characterization of Cavity Parameters . . . . .	82
6.1.1	Determination of $g_0$ . . . . .	82
6.1.2	Determination of the Cavity Linewidth . . . . .	84
6.2	Optical Trap Cavity Mode Alignment . . . . .	85
6.3	Deterministic delivery of atoms to an optical cavity . . . . .	87
6.4	General Experimental Protocol for Cavity QED experiments . . . . .	88
6.5	Cavity Absorption . . . . .	90
6.6	Observation of Cavity Emission and Cooling . . . . .	91
6.6.1	Cavity Cooling of many atoms . . . . .	94
6.6.2	Lifetime of Many Atoms cooled in the Cavity . . . . .	98
6.7	Transfer into the intra-cavity Dipole Trap . . . . .	99
6.8	Deterministic Delivery and Cooling of Single atoms . . . . .	101
6.9	Experiments with Single Atom Scatter Rate . . . . .	103
6.9.1	Scatter rate versus Atomic Position . . . . .	103
6.9.2	Scatter rate versus cavity-pump Detuning . . . . .	105
6.9.3	Scatter rate versus Rabi Frequency . . . . .	105
6.10	Current Limitations of the Cavity QED System . . . . .	105
6.10.1	Count Rate . . . . .	108

6.10.2	Drifting count rates . . . . .	109
6.11	Summary of Atom-Cavity System Results . . . . .	110
VII	CONCLUSION AND OUTLOOK . . . . .	112
7.1	Future Directions . . . . .	112
7.1.1	Qubit in a cavity . . . . .	112
7.1.2	Two Lattices in the Cavity . . . . .	114
	REFERENCES . . . . .	115

## LIST OF TABLES

2.1	Ground state transitions used for AC Stark shift calculation. . . . .	26
2.2	Excited State transitions used for AC Stark shift calculation. . . . .	26
4.1	Parameters for the two imaging lenses. . . . .	65
6.1	Resonant wavelengths of the science cavity used to measure cavity length. .	83
6.2	Cavity parameters that can be determined from the length of cavity. . . .	84
6.3	The cavity QED parameters for the current cavity. . . . .	86

## LIST OF FIGURES

2.1	Force experienced by an atom due to radiation pressure. . . . .	11
2.2	A schematic of a Magneto Optical Trap. . . . .	12
2.3	Zeeman energy shift versus magnitude of magnetic field. . . . .	15
2.4	A schematic of single focus trap. . . . .	21
2.5	A schematic of a 1-D optical lattice. . . . .	22
2.6	AC stark shift computation for the $^{87}\text{Rb}$ $5S_{1/2}$ and $5P_{3/2}$ states. . . . .	25
3.1	A basic Fabry-Perot cavity. . . . .	28
3.2	The transmission spectrum of a Fabry-Perot cavity. . . . .	33
3.3	A single atom coupled to a high finesse cavity. . . . .	35
3.4	Jaynes-Cummings ladder of energy states. . . . .	38
3.5	Geometry used for cavity-assisted cooling. . . . .	41
3.6	A cavity QED based quantum computer model. . . . .	42
4.1	AutoCAD drawing of the quartz cell . . . . .	44
4.2	Hyperfine structure of $^{87}\text{Rb}$ for the $D_2$ transition. . . . .	45
4.3	Saturated absorption spectroscopy of the $D_2$ transition in rubidium. . . . .	45
4.4	Optical setup of the MOT laser. . . . .	48
4.5	Saturated absorption spectroscopy of the MOT transition. . . . .	49
4.6	Optical setup of the repump laser. . . . .	50
4.7	Repump saturated absorption and detuning setup. . . . .	50
4.8	The optical setup of the cavity laser system. . . . .	52
4.9	Cavity probe laser saturated absorption and detuning setup. . . . .	53
4.10	A machined science cavity mirror. . . . .	55
4.11	A high finesse optical cavity suspend by springs. . . . .	56
4.12	Current mount for the high finesse optical cavity. . . . .	57
4.13	The optical setup for the science cavity. . . . .	58
4.14	Generation of error signal for science cavity. . . . .	59
4.15	Heterodyne RF setup for de-modulating the cavity transmission. . . . .	60
4.16	Optical setup of the Yb doped fiber laser. . . . .	63
4.17	Experimental setup for producing an optical trap. . . . .	63

4.18	Geometric diagram to compute the percent solid angle. . . . .	65
5.1	Lifetime of atoms in an optical trap. . . . .	70
5.2	Atomic transport efficiency in walking-wave lattice. . . . .	71
5.3	Optically transported atoms imaged inside the cavity. . . . .	72
5.4	Individual atoms detected in the high-gradient MOT. . . . .	74
5.5	Histogram of integrated fluorescence signal of the single atom MOT. . . . .	75
5.6	Histogram of Stark shifted atoms in high-gradient MOT. . . . .	76
5.7	A chain of individual atoms that are imaged non-destructively. . . . .	78
5.8	Lifetime of atoms in a continuously observed lattice. . . . .	79
5.9	Expansion of atoms in an optical lattice. . . . .	80
6.1	Cavity mode number plotted versus inverse wavelength. . . . .	84
6.2	Technique to measure linewidth . . . . .	85
6.3	Cavity linewidth measurement results . . . . .	86
6.4	Experimental setup for aligning the optical trap with the cavity mode. . . . .	87
6.5	Results of the cavity-optical trap alignment experiment. . . . .	88
6.6	Calculation of atom-cavity system when probed by intra-cavity field. . . . .	91
6.7	The interaction of atoms with the intra-cavity field. . . . .	92
6.8	Calculation of single atom emitting into the cavity mode. . . . .	93
6.9	Calculation of atomic emission rate versus atom number. . . . .	94
6.10	Atomic steps from atoms cooled in the cavity. . . . .	95
6.11	Histogram of data from Figure 6.10. . . . .	96
6.12	Long storage times of atoms in the optical cavity. . . . .	97
6.13	Lifetime of atoms cooled with the cavity. . . . .	98
6.14	Lifetime of atoms versus pump-cavity detuning. . . . .	99
6.15	Transferring atoms into the intra-cavity dipole trap. . . . .	100
6.16	Individual atoms non-destructively observed in cavity. . . . .	102
6.17	A single atom cooled in the cavity. . . . .	103
6.18	Position dependence of the single atom scattering rate. . . . .	104
6.19	Many single atom transits over the cavity mode. . . . .	106
6.20	Single atom scattering rate as a function of cavity-pump detuning. . . . .	107
6.21	The single atom scatter rate as a function of cooling beam power. . . . .	107

6.22	Drifting count rate signals. . . . .	110
7.1	Rabi flopping in an optical lattice . . . . .	113

## SUMMARY

To utilize a single atom as a quantum bit for a quantum computer requires exquisite control over the internal and external degrees of freedom. This thesis develops techniques for controlling the external degrees of freedom of individual atoms. In the first part of this thesis, individual atoms are trapped and detected non-destructively by the addition of cooling beams in an optical lattice. This non-destructive imaging technique led to atomic storage times of two minutes in an optical lattice. The second part of thesis incorporated the individual atoms into a high finesse cavity. Inside this optical cavity, atoms are cooled and non-destructively observed for up to 10 seconds.

# CHAPTER I

## INTRODUCTION

The interaction of a single dipole with a monochromatic radiation field presents an important theoretical problem in electrodynamics. It is an *unrealistic* problem in the sense that *experiments are not done with single atoms or single-mode fields* [1].

This quote is from the book, “Optical Resonance in Two-Level Atoms,” by Allen and Eberly, published in 1975. What was unrealistic to consider, namely experiments with single atoms and single photons, is now the focus of experiments are carried out regularly in a handful of laboratories around the world.

The principle technical advances that have been developed in the intervening years are the development of laser cooling and trapping of atoms and the advances in optical cavity technology. Laser cooling offers the scientist sources of cold atoms, even at the single atom level.

Since the introduction of laser cooling in 1975 [2, 3], applications and development of these techniques continues to expand. A hallmark result of laser cooling and trapping was the achievement of a Bose-Einstein condensate (BEC) of alkali atoms [4]. This new form of matter was predicted by Bose and Einstein in 1925 and took 70 years produce experimentally.

The importance of the laser cooling to physics has been recognized by the Nobel Prize committee three times in the last decade. In 1997, the Nobel prize was awarded to Chu, Cohen-Tannoudji, and Phillips, with the citation: “for development of methods to cool and trap atoms with laser light” [5, 6, 7]. In 2001, the Nobel prize was awarded to Cornell, Ketterle, and Wieman. Their citation is: “for the achievement of Bose-Einstein condensation in dilute gases of alkali atoms, and for early fundamental studies of the properties of the condensates” [8, 9]. Finally in 2005, Glauber, Hall and Hänsch shared the Nobel

Prize. Glauber's pioneering work in quantum optics was cited: "for his contribution to the quantum theory of optical coherence." Hall and Hänsch were awarded the prize "for their contributions to the development of laser-based precision spectroscopy including the optical frequency comb technique."

Using the techniques of laser cooling, it is now possible to study experimentally one of the most fundamental paradigms in quantum optics: the interaction of single atoms and single photons. Besides providing an important test bed for quantum optics, this system has important applications in quantum information processing.

### ***1.1 Quantum Computing***

A remarkably consistent advance in computing power was noticed by one of the co-founders of Intel, Gordon Moore, in 1965. Moore observed that approximately every 18 months the number of transistors placed on an integrated chip doubled. Moore's Law, as it has come to be known, has been a good prediction of the increase in computing power over the last 40 years. These advances have been due to the miniaturization of transistors, which allows increased number and density of components that can be placed on integrated circuits. If chips to continue to evolve at this rate, transistors will reach the scale of individual atoms by 2020, and their quantum nature must be addressed before this point.

Even with the power of modern classical computers, there are still problems which they solve inefficiently. Particularly, there are classes of computer problems in which no algorithm is known to solve the problem in polynomial time. For this reason these problems are known as NP (Non-Polynomial). For certain NP problems, namely factoring large numbers, a quantum computer can solve these problems faster than a classical computer. The possibility of increased performance has sparked the development of quantum information and computing over the last decade.

A successful implementation of a quantum computer will require unprecedented control over quantum systems. Construction of a quantum computer will require the ability to engineer large entangled states, manage decoherences, and exercise control over individual quanta.

## 1.2 *Quantum Computing History*

Modern quantum information and computing was greatly influenced by one of the 20th century most famous physicists, Richard Feynman. Feynman, while attempting to simulate quantum systems with his classical computer, noticed the difficulty of these problems. In 1982, Feynman suggested building a computer that worked with the principals of quantum mechanics to simulate quantum systems [10]. David Deutsch advanced quantum computing by developing the idea of a universal quantum computer that operated using quantum gates and capable of simulating quantum systems [11].

Until the development of quantum algorithms, it was unsure whether there were problems that a quantum computer could solve faster than a classical one. The most famous quantum algorithm to-date was developed by Peter Shor at Bells labs in 1994 [12]. This algorithm solved the important problem of factoring large numbers into prime factors. For a classical computer this is a difficult, or NP problem. Shor's algorithm factorizes numbers exponentially faster than any known classical algorithm and with this algorithm Shor showed that there are important problems that can be solved with a quantum computer that are impossible with a classical computer. Factoring is such a difficult problem for a classical computer that many current cryptography schemes, such as the commonly used RSA encryption, are based on the difficulty in factoring large numbers [13]. Hence, the possibility of decrypting information gave quantum computing an application that is important to commercial banking and national security.

Another important quantum algorithm was developed by Lov Grover, who addressed the problem of searching in an unordered database. Classically this search takes on the order of  $N$  operations for a database of  $N$  items. Using a quantum computer and a quantum algorithm, Grover showed that search can be performed in only  $\sqrt{N}$  operations [14].

With the development of quantum algorithms scientists began to look for physical systems to implement these algorithms. In 1995, Two atomic physics theorists, Peter Zoller and Ignacio Cirac, published a seminal paper entitled "Quantum Computation with Cold Trapped Ions," which suggested building a quantum computer using trapped ion qubits [15].

Since Cirac and Zoller's paper in 1995, many of the first steps required to build a

quantum computer have been demonstrated in ion traps. To highlight just a few of the many results of the group of Dave Wineland at NIST boulder has implemented a C-NOT gate [16] and deterministic generation of entanglement between two trapped ions [17]. Additionally, they have been able to teleport the quantum information from one trapped ion to another, implementing a quantum teleportation protocol [18]. Rainer Blatt's group at the University of Innsbruck has created a quantum byte by deterministically entangling 8 calcium ions [19], and also independently implemented quantum teleportation [20]. Chris Monroe's group at the University of Michigan has implemented Grover's search algorithm [21] and has demonstrated entanglements between trapped ions and photons [22]. Thanks to the initial success of ion trap quantum computers, large scale implementation of ion trap quantum computer is currently being developed [23], though scaling an ion trap computer from 8 to 100s of ions required to do quantum error correction still remains a challenging technical problem.

Trapped ions are just one physical implementation of a quantum computer currently being actively investigated. A review of the state of quantum information and quantum computing can be found at the Quantum Information Science and Technology Roadmap website hosted by Los Alamos labs<sup>1</sup> [24]. The breadth of this document speaks to the diverse research directions that scientists and engineers have developed in the pursuit of quantum information. Trapped neutral atoms, trapped ions, nuclear magnetic resonance (NMR), cavity quantum electro-dynamics (QED) with neutral atoms and ions, optical quantum computation, solid state (quantum dots), and superconducting systems have all been proposed as possible quantum computers. Information on these developing technologies can be found in the references in the roadmap [24]. Additionally, new journals have been created, such as the journal Quantum Information and Computation, where scientists from diverse fields interact as they strive to develop a quantum computer.

---

<sup>1</sup>[http://qist.lanl.gov/qcomp\\_map.shtml](http://qist.lanl.gov/qcomp_map.shtml)

### 1.3 Quantum Computing Requirements

In 2000, David DiVincenzo articulated a set of basic requirements that any physical realization of a quantum computer must satisfy [25]. These requirements, known as the DiVincenzo requirements, have guided scientists developing quantum computation. These five requirements are presented here as a brief an introduction to quantum information.

#### 1. A scalable physical system with well characterized qubits.

A classical bit has two states, 0 and 1. Similarly a quantum bit, or qubit, is a two state quantum system, described in general by,

$$|\psi\rangle = \alpha|0\rangle + \beta|1\rangle , \quad (1.1)$$

where  $\alpha$  and  $\beta$  are complex amplitudes that are normalized with the following condition,

$$|\alpha|^2 + |\beta|^2 = 1 . \quad (1.2)$$

Two qubits can become entangled, which means their wave function can not be factored into a product state. A general state is represented by,

$$|\psi\rangle = \alpha|00\rangle + \beta|11\rangle + \gamma|10\rangle + \delta|01\rangle . \quad (1.3)$$

In general, if there are  $n$  entangled qubits we can represent  $2^n$  values in the qubit. If we have 300 qubits, this number,  $2^{300}$ , is larger than the number of particles in the universe. Thus an enormous amount of information can be represented by a small number of qubits.

#### 2. The ability to initialize the state of the qubits.

In all computing, classical and quantum, it is necessary to prepare the register before a computation starts. This requires a method to initialize the qubit's state deterministically.

3. **Long relevant decoherence times, much longer than the gate operation time.**

Every quantum system that is in contact with the environment experiences a loss of coherence on a time scale known as the decoherence time. This arises from the undesired, irreversible coupling between the quantum system and the reservoir of modes of the environment. To observe coherent quantum dynamics, the relevant quantum operations must occur faster than the decoherences.

4. **A “universal” quantum gate.**

In classical computation, there are a number of different operations. Some examples are OR, AND, NOT, and XOR logic gates. All of these gates can be constructed from NAND gates, making this gate universal.

The operations performed by a quantum computer are also called gates. These gates are unitary operations that operate on one or two qubits. In classical computing, an example of a single bit gate is the NOT gate which follows the simple truth table,

input	output
1	0
0	1

A quantum version of this gate, the quantum NOT gate, obeys the same truth table with 1 replaced by the state  $|1\rangle$  and likewise 0 by  $|0\rangle$ . The quantum NOT gates is an example of a single qubit quantum gates and is defined by a simple  $2 \times 2$  matrix,

$$U_{\text{NOT}} = X = \begin{pmatrix} 0 & 1 \\ 1 & 0 \end{pmatrix}. \quad (1.4)$$

The second type of quantum gates required for computation are two-qubit gates. The most widely discussed universal gate in quantum computing is the controlled-note (CNOT) gate [26]. This gate has two inputs; a control qubit and a target qubit. Depending on the state of the control bit, the target qubit is flipped. The truth table for the CNOT gate is,

input	output
00⟩	00⟩
01⟩	01⟩
10⟩	11⟩
11⟩	10⟩ .

This can be represented as a 4x4 matrix,

$$U_{\text{CNOT}} = \begin{pmatrix} 1 & 0 & 0 & 0 \\ 0 & 1 & 0 & 0 \\ 0 & 0 & 0 & 1 \\ 0 & 0 & 1 & 0 \end{pmatrix} \quad (1.5)$$

**5. A qubit-specific measurement capability.** Another fundamental part of the quantum computer is the ability to read out the final state. This requires the capability to measure the state of an individual qubit without effecting other qubits.

The quantum efficiency of the measurements does not need to be unity, but in general if the efficiency is  $q$ , then the measurement must be repeated  $1/q$  times to build up enough statistics to produce a statistically valid outcome.

DiVincenzo added two more criteria that a quantum computer must possess relating to quantum communication and quantum key distribution (QKD):

1. The ability to inter-convert stationary and flying qubits.
2. The ability to faithfully transmit flying qubits between specific locations.

A flying qubit is a term for a qubit that can travel between stationary qubits and carry quantum information. Most proposals for long distance quantum communication suggest encoding the quantum information in the polarization or the spatial wave function of photon. Photons are natural choice because of fiber optic technology and the existing fiber optic communication networks.

## ***1.4 Cavity QED at Georgia Tech***

The initial cavity QED experiments at Georgia Tech were constructed by Jacob Sauer, beginning in the summer of 2002 and I joined Jacob in the fall 2002. The interaction of transported atoms with the cavity was first observed in March of 2003. This first generation experiment developed a deterministic technique to transport atoms into an optical cavity by employing an optical trap. This was the first demonstration of deterministically delivered atoms to a high finesse cavity [27]. Although these initial experiments demonstrated the ability to deterministically load atoms into the cavity, much work remained before the system could be used for quantum information. Namely, improvements in the optical trap performance and the locking of the cavity needed to be developed.

The goal of this thesis is to advance the state of the art in experimental cavity QED research. This thesis develops experimental techniques to trap single atoms in a magneto-optical trap and an optical trap. Using the optical trap, this single atom is delivered to the cavity where the atom is non-destructively detected, cooled and stored for up-to 10 seconds. This trapped atom on demand in an optical cavity is an excellent starting point for quantum information experiments and the evolution of this cavity QED system is described in the following chapters.

## ***1.5 Organization of This Thesis***

This thesis is detailed over six additional chapters. Chapter 2 focuses on the theoretical background of trapping atoms in magneto-optical and purely optical traps. Chapter 3 presents the fundamentals of cavity physics and a brief introduction to the Jaynes-Cummings Hamiltonian and cavity QED. Chapter 4 details the experimental apparatus. The next two chapters, Chapters 5 and 6, present the results of atom trapping experiments and the implementation of a cavity QED system. In these chapters, techniques are presented to trap and detect single atoms in the MOT and in an optical trap. Finally, Chapter 7 concludes with the outlook for future developments of this experiment.

## CHAPTER II

### ATOM TRAPPING

To date, three basic techniques have been developed to trap neutral atoms. They are, the Magneto-Optical Trap (MOT), the optical dipole trap and the magnetic trap. This chapter describes the theoretical background of the MOT and the optical dipole trap.

#### *2.1 Magneto Optical Trap*

The MOT is the workhorse of atomic physics and is the beginning stage of many modern atomic physics experiments. The MOT is used as a robust source of laser cooled atoms. The availability of single frequency tunable dye lasers near the sodium D<sub>2</sub> line helped sodium to become the first MOT built in 1987 [28]. Sodium was the natural choice for the first trap because of the availability of single frequency tunable dye lasers near the sodium D<sub>2</sub> line. With the development of the titanium sapphire laser and diode lasers, MOTs now span the periodic table, with MOTs being constructed from all the other alkali elements (Li, Rb, Cs and Fr), many alkali earth elements (Ca, Sr, Ra), the noble gases (He, Ar, Kr, Xe) and even some other elements (Cr, Yb, Ag, Hg, Er, Cd).

A typical MOT has anywhere between a single atom to  $10^9$  atoms of laser cooled atoms. The Doppler temperature is an equilibrium condition; for typical alkali atoms, this temperature is on the order of 100  $\mu\text{K}$ . For  $^{87}\text{Rb}$ , the Doppler temperature is 146  $\mu\text{K}$ , and with sub-Doppler cooling it is possible to get temperatures as low as 1-10  $\mu\text{K}$ .

#### *2.2 Optical Molasses*

Optical molasses is an experimental technique used to laser cool atoms. The optical molasses cools atoms by a momentum transfer from the atom to photons scattered from laser beams that are detuned from atomic resonance. The first optical molasses trapped sodium atoms and was constructed at Bell Labs in 1985 [29].

To develop the theory of the optical molasses, consider a laser of frequency  $\omega$  incident

on a two-level atom with a transition frequency,  $\omega_0$ . In the absence of frequency shifts due to the Doppler and Zeeman shifts, the spontaneous force experienced by the atom is [30],

$$F_{sp} = \hbar k \frac{s_0 \gamma / 2}{1 + s_0 + (2\delta / \gamma)^2}, \quad (2.1)$$

where  $k = 2\pi/\lambda$  is the laser's wave vector,  $s_0 = I/I_s$  is the on-resonance saturation parameter,  $\gamma$  is the linewidth of the atomic transition and  $\delta = \omega - \omega_0$  is the detuning of the laser's frequency from the atom's resonance frequency. Since the atoms are not at rest they experience a Doppler shift which add an effective detuning. If the atom is subject to two counter propagating laser beams, one in the  $+k$  direction and the other in the  $-k$  direction the total force is given by  $\vec{F} = \vec{F}_+ + \vec{F}_-$ , where

$$\vec{F}_\pm = \pm \frac{\hbar \vec{k} \gamma}{2} \frac{s_0}{1 + s_0 + (2\delta_\pm / \gamma)^2} \quad (2.2)$$

and the detuning  $\delta_\pm$  is

$$\delta_\pm = \delta \mp \vec{k} \cdot \vec{v} \quad (2.3)$$

where the velocity dependent part of the detuning,  $\omega_D = -k \cdot \vec{v}$ , is the Doppler shift.

The sum of the forces around  $v = 0$  can be approximated as a linear function with respect to velocity as shown in Figure 2.1. In this linear region the force is a viscous damping force,

$$F \approx -\alpha v. \quad (2.4)$$

The damping coefficient is given by [31]

$$\alpha = 4\hbar k^2 s_0 \frac{-2\delta / \gamma}{1 + s_0 + (2\delta / \gamma)^2}. \quad (2.5)$$

When  $\alpha$  is positive, this force opposes and damps the atomic motion. For typical experimental values for an optical molasses of  $^{87}\text{Rb}$  atoms,  $k = 8.05 \times 10^6 \text{ m}^{-1}$ ,  $\gamma = (2\pi) 6.06 \text{ MHz}$ ,  $\delta = -12.3 \text{ MHz}$  and  $s_0 = 0.9$ . This results in a damping coefficient of

$$\alpha = 5.48 \times 10^{-21} \text{ Kg/s}$$

Looking at the form of Eq. (2.4), it is clear that the optical molasses is not a trap. A trap requires a position dependent restoring force and in the next section it is shown how the addition of a magnetic field gradient which transforms the optical molasses into a trap.

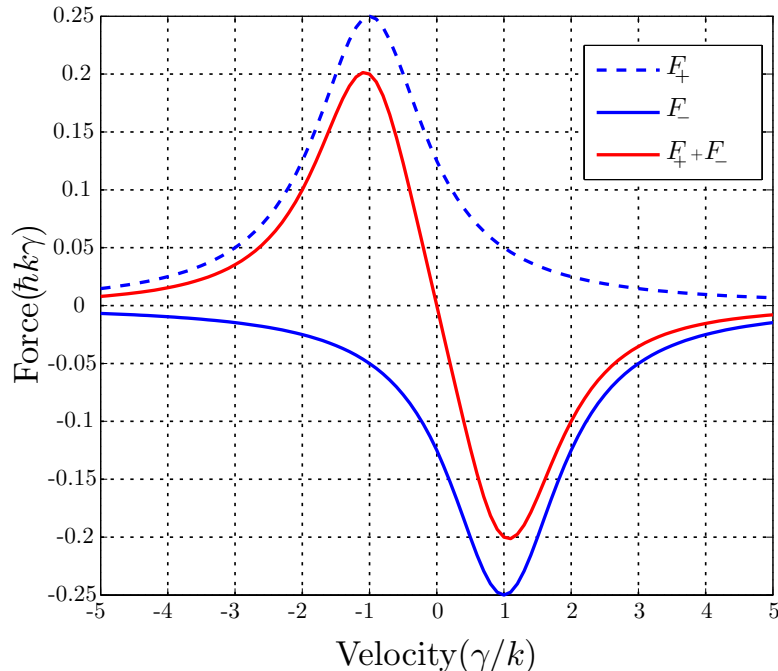


**Figure 2.1:** The force experienced on an atom in one dimension as it scatters and emits photons from two laser beams, Eq. (2.2). The saturation parameter  $s_0 = 1$  for these plots.

### 2.3 One-Dimensional MOT

The MOT can be explained by a simple one dimensional model. Imagine an atom placed in an inhomogeneous magnetic field that varies linearly with position. The field has a magnitude of,  $B(z) = Az$ , in the  $\hat{z}$  direction.

Consider an atom with an idealized electronic structure of zero spin ( $J = 0$ ) in the ground state and spin one ( $J = 1$ ) in the excited state. Due to the Zeeman effect, the degeneracy of the  $m_J$  states is lifted by the magnetic field. The Zeeman energy shift is given by

$$\Delta E = \vec{\mu} \cdot \vec{B} = \mu m_J B = \mu m_J Az, \quad (2.6)$$

where  $\mu$  is the magnetic dipole moment of the atom and  $A$  is the magnitude of the magnetic field. From Eq. (2.6), the energy shift is proportional to the  $m_J$  quantum number and the  $B$  field, therefore the state  $m_J = -1$  experiences the opposite shift of the  $m_J = 1$  state.

Two laser beams are incident on the atom with opposite wave-vectors. The laser from the left is polarized  $\sigma^+$ , which causes transitions that obey the selection rule  $\Delta m_J = 1$ .

From the right, the laser has the opposite polarization  $\sigma^-$ , with selection rule,  $\Delta m_J = -1$ . Due to the Doppler and Zeeman effects, the detuning of these lasers beams are,

$$\delta_{\pm} = \delta \mp \vec{k} \cdot \vec{v} \pm \beta z , \quad (2.7)$$

where Zeeman shift is  $\beta = \mu m_J A/\hbar$ .

In Figure 2.2, if an atom is at a position  $z = Z'$ , the detuning of the  $m_J = -1$  state is closer to the laser's frequency than that of the  $m_J = 1$  state. Therefore the atom will scatter more photons from the  $\sigma^-$  and experience a net force directed toward  $z = 0$ . Once the atom crosses the origin, the roles are reversed. The  $\sigma^+$  transition is closer to the laser's frequency, and the atom scatters more photons from the  $\sigma^+$  beam. The atom again experiences a force that directs it toward  $z = 0$ .

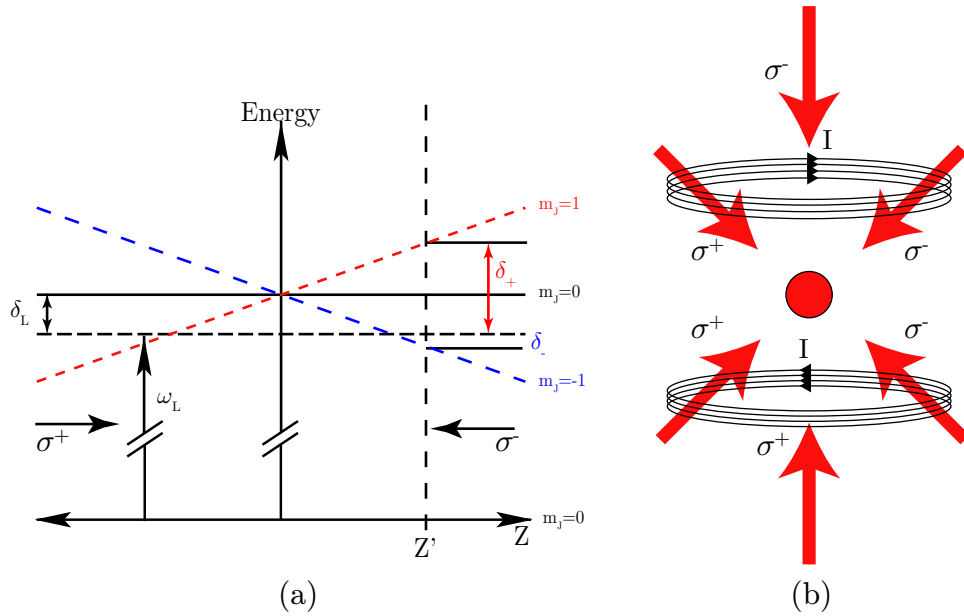


**Figure 2.2:** (a) The  $J_g = 0 \rightarrow J_e = 1$  transition of a two-level atom in an inhomogeneous magnetic field,  $B(z) = Az$ . The magnetic field breaks the excited state degeneracy and provides a spatially dependent scattering rate. (b) The experimental configuration for the MOT. Shown is the three sets of laser beams with opposite polarization, and the anti-Helmholtz coils that provide the spherical quadrupole magnetic field.

Performing an expansion of the force for small Doppler and Zeeman shift relative to the detuning,  $\delta$ , results in,

$$F = \alpha v - \beta z . \quad (2.8)$$

Where the addition of the magnetic field adds a linear restoring force required to produce a trap.

Real MOTs have a few additional complexities over the idealized one dimensional MOT described above. They must provide confinement in 3 dimensions for atoms with more complicated electronic level structure. First, we need to add two more sets of laser beams in orthogonal axis, for a total of six laser beams. Second, few alkali atoms have such a simple level structure. For example, in  $^{87}\text{Rb}$  the ground state has  $F = 1$  and  $F = 2$  hyperfine states. Laser cooling is done on the  $F = 2$  to  $F' = 3$  transition which can be made into a cycling transition. Occasionally the atom can off-resonantly be transferred into the dark  $F = 1$  state via the  $F' = 2$  state. This dark state doesn't participate in the cooling. So an additional laser, known as the repump laser, is needed to de-populate the  $F = 1$  state.

To produce the spherical quadrupole field, one uses a set of anti-Helmholtz coils, where the current flows in opposite directions in the two coils. Typical gradient strengths are approximately 10 G/cm for normal MOT operation with alkali elements.

## 2.4 Doppler and Sub-Doppler Cooling

The cooling presented in the optical molasses section is known as Doppler cooling. Atoms are subject to a velocity dependent force, Eq. (2.4), that in the absence of heating should cool the atoms to rest with a temperature,  $T = 0$  K. In addition to this cooling, the atom is heated from recoils experienced when it absorbs and scatters a photon. The steady-state between cooling and heating is known as the Doppler temperature [30, 31],

$$T_D = \frac{\hbar\gamma}{2k_B}, \quad (2.9)$$

where  $\gamma$  is the linewidth of the transition. For  $^{87}\text{Rb}$  the natural linewidth of the  $D_2$  transition is,  $\gamma = (2\pi) 6.07$  MHz which gives a Doppler temperature of  $T_D = 146 \mu\text{K}$  [30].

Early experiments with laser cooled sodium resulted in measured temperatures six times smaller than the theoretical Doppler temperature [32]. New theoretical models were developed to explain this sub-Doppler cooling mechanism [33, 34]. To fully explain this sub-Doppler cooling method one needs to take into account the multi-level structure of real atoms.

This cooling was due to the spatial variations of the light polarization of the optical molasses beams. This spatial variation of the polarization leads to a spatially dependent light shift potential for the Zeeman levels of the atoms. This cooling force was described by Dalibard and Cohen-Tannoudji, and Chu *et al.* as a Sisyphus mechanism [33, 34]. In this model, atoms in motion are more likely to make the transition to the excited state at the top of the light shift potential hill of the ground state. The atoms preferentially emit a photon that changes the ground  $m_F$  state such that the atom is now at the bottom of the potential hill, and begins to climb the potential again. It is this continual transfer between kinetic to potential energy that leads to a lower temperature. The limiting temperature is approximately  $2 E_{rec} = 2\hbar\omega_r$ , where  $E_{rec}$  is the recoil energy, and  $\omega_r$  is the recoil frequency which is defined as

$$\omega_r = \frac{\hbar k^2}{2m} . \quad (2.10)$$

For  $^{87}\text{Rb}$ , the recoil frequency is,  $\omega_r = (2\pi) 3.771$  kHz, resulting in a recoil limited temperature of  $T_r = 361.95$  nK.

## 2.5 Optical Trapping of Neutral Atoms

Optical traps have become a major research tool used by physicists in diverse fields. In atomic physics, optical traps are used to study and trap neutral atoms, produce Bose-Einstein condensates (BECs) [35], and make high precision atomic clocks [36]. Additionally, proposals exist to use optical trapped neutral atoms for quantum information. In addition to atomic physics, optical trapping is utilized in biophysics. Optical traps, or optical tweezers, are used to study and manipulate DNA that is connected to glass spheres. Optical traps are very versatile; anything that can be polarized can be trapped optically.

Optical traps are also versatile because they can trap arbitrary Zeeman states of neutral atoms. In contrast, magnetic traps trap only certain Zeeman states and then anti-trap (or repel) the others. This is because the magnetic energy is proportional to the  $m_F$  number. The Breit-Rabi formula for the Zeeman shift of the ground state of  $^{87}\text{Rb}$  is plotted in Figure 2.5, showing the weak and high field seeking states [37]. Only weak field seeking states are possible to trap magnetically. If these same atoms are loaded into an optical trap

then all of the  $m_F$  states are trapped.

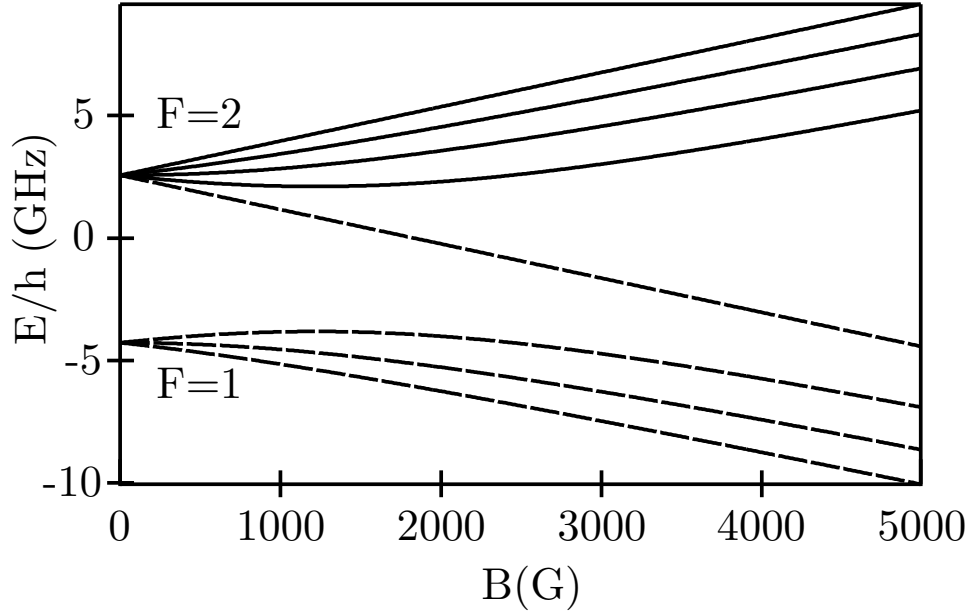


**Figure 2.3:** Energy shift vs magnitude of B field for the ground state of the  $^{87}\text{Rb}$  atom. The energies that tend toward negative energy, represented by dashed lines, are weak field seeking atoms and can be magnetically trapped, while the other states are high field seeking states and are repelled from a magnetic trap.

This section develops the theory of optical trapping. First a brief historical development of optical trapping is presented along with the Lorentz model of the atom. A review of Gaussian beams will allow the development of formulae to compute the trap frequencies and potential depths for optical traps. Additionally, a calculation of the Stark shift of the atom is presented.

## 2.6 *Optical Trapping History*

All modern optical traps can be traced back to the work of Arthur Ashkin at Bell Labs. Ashkin's first experiments in optical trapping were performed in 1970 with a focused Ar-Ion laser that trapped dielectric latex beads in a water solution [38]. In the absence of the optical trap, beads moved freely in the solution with their motion described by Brownian motion, but when the laser was unblocked, the beads were accelerated to the laser's focus and were trapped. Additionally, Ashkin proposed constructing optical trapping for neutral atoms [39].

Ashkin’s pioneering work showed the versatility of optical traps, and at Bell Laboratories the first optical trap for neutral atoms was built by Steve Chu, Ashkin and co-workers in 1986 [40]. Due to the weak trapping potential, the first neutral atom optical trap was not built until after a cold atom source, the optical molasses, was developed. The first optical trapped atoms were loaded into a tightly focused laser beam from an optical molasses. This optical trap operated at a frequency of 650 to 1300 GHz red detuned from the D<sub>2</sub> line of sodium. By turning off the optical molasses and leaving the atoms only in the optical trap resulted in a loss of half the sodium atoms in 5 ms. As we will see later in this chapter, being so close to resonance results in a large photon scattering rate, and this in turn caused a short lifetime for the optical trap.

To increase trap lifetimes many groups constructed optical traps that were far detuned from atomic resonance. The first *far-off-resonance-optical-trap* (FORT) was built by the group of Dan Heinzen in 1993 [41]. These FORTs were detuned up to 65 nm from the D<sub>1</sub> line of Rb (795 nm) which increased the trap lifetimes the 200 ms. The consequence of this far detuning is that it required a large amount of optical power to provide a deep potential.

## 2.7 Optical Trap Theory

In this section we will highlight the theoretical formalism of optical trapping relying heavily on the review article by Grimm *et al.* [42]. An optical trap works by inducing a dipole moment on the atom; this induced dipole moment can be modeled by the Lorentz model of the atom.

### 2.7.1 Lorentz Model of the Atomic Polarizability

The Lorentz model simplifies the atom-field interaction to a damped harmonic oscillator. In this model, the atom’s nucleus is connected to a smaller mass, the electron with charge  $e$  and mass  $m_e$ , via a spring. This system is driven by an electric field,  $E(t)$ , and using classical mechanics this system can be modeled as a damped driven harmonic oscillator. The equation of motion for the electron is

$$\ddot{x}(t) + \Gamma_\omega \dot{x}(t) + \omega_0^2 x(t) = -\frac{eE(t)}{m_e}, \quad (2.11)$$

where  $x(t)$  is the position of the electron,  $\omega_0$  is the resonance frequency of the atom and  $\Gamma_\omega$  is the damping coefficient of the system is

$$\Gamma_\omega = \frac{e^2 \omega^2}{6\pi \epsilon_0 m_e c^3} . \quad (2.12)$$

This differential equation can be solved by direct substitution of an oscillating solution for  $x(t)$ . It is necessary to replace the dipole moment  $p$  and the electric field with the following relations,  $p = ex$  and  $E = p/\alpha$ . Solving for  $\alpha(\omega)$  yields, where  $\alpha$  is the frequency dependent polarizability of the atom,  $\alpha(\omega)$ ,

$$\alpha(\omega) = -\frac{e^2}{m_e} \frac{1}{(\omega_0^2 - \omega^2 + i\omega\Gamma_\omega)} . \quad (2.13)$$

It is more convenient to express the atomic polarizability in terms of the on-resonance damping rate,  $\Gamma = \Gamma_{\omega_0} = (\omega_0/\omega)^2 \Gamma_\omega$ .

Armed with this expression for the polarizability, we can compute the dipole energy, the force due to an induced dipole moment, and the rate of scattered photons. The dipole potential is given by [42],

$$U_{\text{dip}} = -\frac{1}{2} \langle \vec{p} \cdot \vec{E} \rangle \quad (2.14)$$

where  $\vec{p}$  and  $\vec{E}$  are given by plane waves,

$$\vec{E}(\vec{r}, t) = \hat{e} \tilde{E}(\vec{r}) e^{-i\omega t} + c.c. \quad (2.15)$$

$$\vec{p}(\vec{r}, t) = \hat{e} \tilde{p}(\vec{r}) e^{-i\omega t} + c.c. . \quad (2.16)$$

Placing this into the dipole potential results in,

$$\vec{p} \cdot \vec{E} = \alpha \tilde{E}^2 e^{-2i\omega t} + \alpha^* |\tilde{E}|^2 + \alpha |\tilde{E}|^2 + \alpha^* (\tilde{E}^*)^2 e^{2i\omega t} . \quad (2.17)$$

Taking the time average of  $\vec{p} \cdot \vec{E}$  results in all oscillating terms averaging to zero, which leaves,

$$\langle \vec{p} \cdot \vec{E} \rangle = (\alpha + \alpha^*) |\tilde{E}|^2 . \quad (2.18)$$

This simplifies the equation for the dipole potential to,

$$U_{\text{dip}} = -\text{Re}(\alpha) |\tilde{E}|^2 . \quad (2.19)$$

One can then relate the intensity to the absolute value squared of the electric field from the relation,  $I = 2\epsilon_0 c |\tilde{E}|^2$ ,

$$U_{\text{dip}} = -\frac{1}{2\epsilon_0 c} \text{Re}(\alpha) I(\mathbf{r}) . \quad (2.20)$$

The dipole force is given by the negative gradient of the dipole potential,

$$\vec{F}_{\text{dip}} = -\nabla U_{\text{dip}} = \frac{1}{2\epsilon_0 c} \text{Re}(\alpha) \nabla I(\mathbf{r}) . \quad (2.21)$$

These two semi-classical results,  $\vec{F}_{\text{dip}}$  and  $U_{\text{dip}}$ , describe the physics that is responsible for trapping the atoms with the dipole force. Additionally, it is important to know the rate at which atoms scatter photons from the optical trap laser. This can be computed by determining the power absorbed by the oscillator, which is then later re-emitted spontaneously. The power absorbed is given by,

$$P_{\text{abs}} = \langle \dot{\vec{p}} E \rangle = \frac{\omega}{\epsilon_0 c} \text{Im}(\alpha) I(\mathbf{r}) . \quad (2.22)$$

Dividing Eq. (2.22) by the energy per photon,  $\hbar\omega$ , gives the rate that photons are scattered from the trap beams. This is given by,

$$\Gamma_{\text{sc}} = \frac{1}{\hbar\epsilon_0 c} \text{Im}(\alpha) I(\mathbf{r}) \quad (2.23)$$

Simplifying the dipole potential results in the following equation [42],

$$U_{\text{dip}}(\mathbf{r}) = -\frac{3\pi c^2}{2\omega_0^3} \left( \frac{\Gamma}{\omega_0 - \omega} + \frac{\Gamma}{\omega_0 + \omega} \right) I(\mathbf{r}) . \quad (2.24)$$

For most trapping experiments, the frequency of the trapping laser is relatively close to resonance,  $|\Delta = \omega_0 - \omega| \ll \omega_0$ . In this situation, the rotating wave approximation (RWA) can be used to develop equations for the dipole potential and the scattering rate,

$$U_{\text{dip}}(r) = \frac{3\pi c^2}{2\omega_0^3} \frac{\Gamma}{\Delta} I(\mathbf{r}) \quad (2.25)$$

$$\Gamma_{\text{sc}}(r) = \frac{3\pi c^2}{2\hbar\omega_0^3} \left( \frac{\Gamma}{\Delta} \right)^2 I(\mathbf{r}) . \quad (2.26)$$

From Eq. (2.25), the sign of the detuning determines whether the atoms are attracted or repelled from regions of maximum intensity. All of the traps that are constructed in this

thesis are red detuned traps ( $\Delta < 0$ ); for these traps the atoms are attracted to regions of high field.

From Eq. (2.25) and (2.26), scaling laws are available to give further physical insight. First, both the scattering rate and the trap depth are proportional to the intensity. Second, the trap depth is inversely proportional to the detuning and the scattering rate is inversely proportional to the detuning squared.

$$U_{\text{dip}} \sim \frac{I}{\Delta} \quad (2.27)$$

$$\Gamma_{\text{sc}} \sim \frac{I}{\Delta^2} \quad (2.28)$$

One major problem in optical traps is radiative heating due to spontaneous scattering of photons. Looking at scaling laws for the trap depth, Eq. (2.27), and the scattering rate, Eq. (2.28), a solution to this problem is evident. As one increases the detuning and the intensity of the laser field, one can preserve a deep trap while reducing the radiative heating from the scattering. This is the solution that motivates the use of FORTs as optical traps [41].

As we conclude our discussion on the theory of optical trapping, it should be noted that this theory is not limited to atoms. Optical trapping works with any material that can be polarized, and this is what makes this technique so fundamental.

## 2.8 *Gaussian Beams*

Before we go into the detail of optical trapping, we briefly need to review a few characteristics of Gaussian beams. Since a Gaussian mode is supported by an optical cavity and is generally the output mode of most lasers, the concepts developed in this section will be used throughout the thesis.

A Gaussian beam is a solution to paraxial wave equation and its properties are described in many optics textbooks [43, 44, 45]. The paraxial wave propagating in the  $z$ -direction can be written as plane wave modulated by a complex amplitude,  $A(\mathbf{r})$ . The electric field of this wave is given by,

$$U(\mathbf{r}) = A(\mathbf{r}) \exp(-ikz) . \quad (2.29)$$

The electric field,  $U(\mathbf{r})$  must satisfy the Helmholtz equation,

$$(\nabla^2 + k^2)U(\mathbf{r}) = 0 , \quad (2.30)$$

which puts a constraint on  $A(\mathbf{r})$  that it must satisfies the paraxial Helmholtz equation,

$$\left( \nabla_T^2 A - i2k \frac{\partial A}{\partial z} \right) = 0 , \quad (2.31)$$

where  $\nabla_T^2 = \partial_x^2 + \partial_y^2$ , is the transverse Laplacian operator.

The solution to this equation is given by,

$$U(\mathbf{r}) = A_0 \frac{w_0}{w(z)} \exp\left(-\frac{\rho^2}{w^2(z)}\right) \exp\left(-ikz - ik \frac{\rho^2}{2R(z)} + i\zeta(z)\right) . \quad (2.32)$$

In Eq. (2.32) there are four important factors to discuss. A Gaussian beam can be described completely by these parameters:

$$w(z) = w_0 \sqrt{\left(1 + \left(\frac{z}{z_R}\right)^2\right)} \quad (2.33)$$

$$R(z) = z \left(1 + \left(\frac{z_R}{z}\right)^2\right) \quad (2.34)$$

$$\zeta(z) = \tan^{-1} \frac{z}{z_R} \quad (2.35)$$

$$z_R = \frac{\pi w_0^2}{\lambda} . \quad (2.36)$$

Equation (2.33) describes the beam waist,  $w(z)$ , of the Gaussian beam. Twice the waist is known as the spot size, and 86% of the optical power is contained in a circle of this radius. The second important parameter is the radius of curvature of the Gaussian beam,  $R(z)$ , which is given in Eq. (2.34). The Guoy phase,  $\zeta(z)$ , is given by Eq. (2.35). The last parameter is the Rayleigh range,  $z_R$ , of the beam. This is the distance at which the beam waist expands by  $\sqrt{2}$ . More generally, twice the Rayleigh range is the depth of focus of the beam.

## 2.9 Single Focus Traps

The simplest optical trap is a focused red-detuned Gaussian laser beam. The intensity of a Gaussian beam is given by,

$$I(r, z) = \frac{2P}{\pi w^2(z)} \exp\left(-\frac{2r^2}{w^2(z)}\right) , \quad (2.37)$$

where  $P$  is the optical power and  $w$  is defined by Eq. (2.33),  $r$  and  $z$  are the standard cylindrical coordinates.

The optical dipole trap potential energy is given by,

$$U_{\text{dip}}(r, z) = U_0 \exp\left(-\frac{2r^2}{w^2(z)}\right). \quad (2.38)$$

The trap depth is defined as  $U_{\text{dip}}(r = 0, z = 0) \equiv U_0$  from Eq. (2.25). For a single focus trap in the RWA, the trap depth is given by,

$$U_0 = \frac{3c^2}{\omega_0^3} \frac{\Gamma}{\Delta} \frac{P}{\pi w_0^2}. \quad (2.39)$$

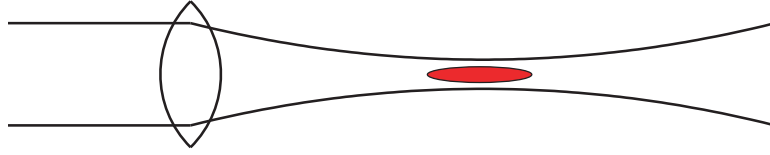


**Figure 2.4:** A focused laser beam is the simplest optical trap for atoms. For a red detuned optical trap atoms are trapped at the focus of the laser beam

## 2.10 Optical Lattices

To take a single focus trap and transform it into a 1-D optical lattice just requires an additional laser beam that is counter propagating to the first one.

Consider a standing wave made by the superposition of two counter propagating Gaussian beams: the first beam with complex amplitude,  $U_1$  coming in from the left and traveling in the  $+k$  direction and the second beam,  $U_2$  coming in from the right traveling in the  $-k$  direction. In addition, the two beams can be at different frequencies. Let the frequency of  $U_1$  be  $\omega_0$  and the frequency of  $U_2$  be  $\omega_0 + \delta$ .

If we neglect the Guoy Phase ( $\zeta(z)$ ) and the curvature of the wavefronts<sup>1</sup>, we can construct the superposition of these two waves using Eq. (2.32). The intensity is,

$$I_{\text{Tot}} = |U_1 + U_2|^2 = U_1^* U_1 + U_1^* U_2 + U_2^* U_1 + U_2^* U_2. \quad (2.40)$$

<sup>1</sup>This is valid approximation near the focus because, as  $z \rightarrow 0$ ,  $\zeta(z) \rightarrow 0$  and  $\frac{r^2}{2R(z)} \rightarrow 0$ .

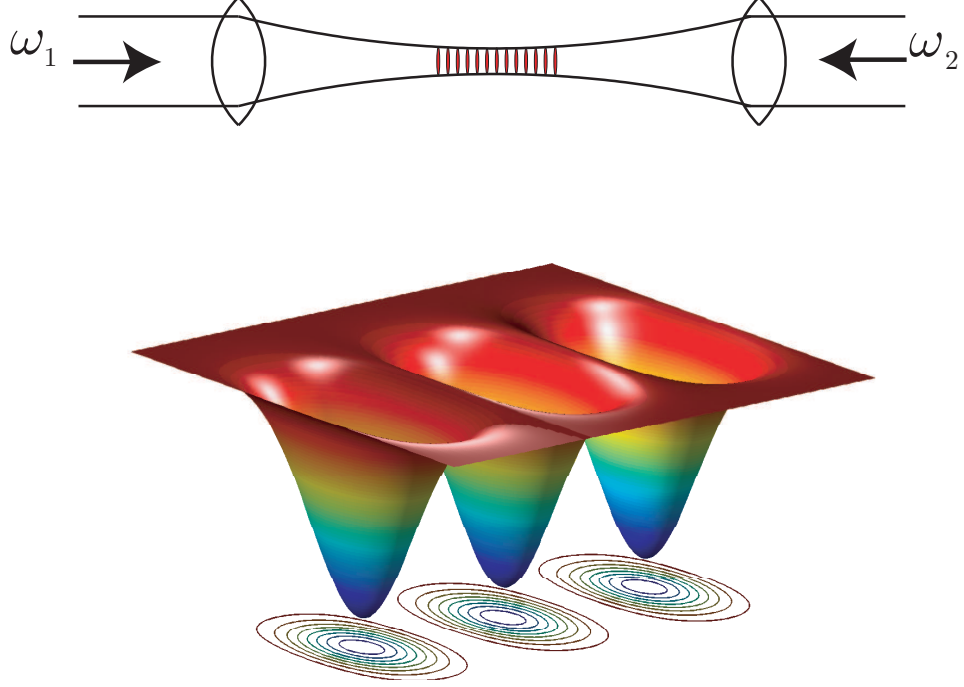


**Figure 2.5:** A standing wave is produced by two counter propagating laser beams. These laser beams form a 1-D optical lattice where the lattice sites are separated by  $\lambda/2$ . Depicted here are the lattice sites about the focus, but potential well extend throughout the overlap-region of the beams.

The two DC terms are  $|U_1|^2$  and  $|U_2|^2$ , which are

$$|U_1|^2 = |U_2|^2 = \frac{U_0}{w^2(z)} \exp\left(\frac{-2r^2}{w^2(z)}\right) = I_{\text{SF}}, \quad (2.41)$$

where  $I_{\text{SF}}$  is the single focus intensity. The cross-terms are a bit more complicated.

$$U_1^* U_2 = I_{\text{SF}} \exp\left(-2i\left(kz + \frac{\delta}{2}t\right)\right) \quad (2.42)$$

$$U_2^* U_1 = I_{\text{SF}} \exp\left(2i\left(kz - \frac{\delta}{2}t\right)\right) \quad (2.43)$$

Using the Euler formula and simple trigonometric identities, we can simplify the lattice intensity to,

$$I_{\text{Tot}} = 4I_{\text{SF}} \cos^2\left(kz - \frac{\delta}{2}t\right) \quad (2.44)$$

Since the trap depth is proportional to intensity, a 1-D optical lattice's trap depth is 4 times deeper than a single focus optical trap with identical single beam intensity. The trap depth

for a 1-D optical lattice with equal power  $P$  in each beam is given by

$$U_0 = \frac{3c^2}{\omega_0^3} \frac{\Gamma}{\Delta} \frac{4P}{\pi w_0^2}. \quad (2.45)$$

For red detuned traps, atoms are confined to the intensity maximums, the anti-nodes of the standing wave. From the equation for the lattice intensity Eq. (2.44), one can see that by modifying the frequency difference between the two traps,  $\delta$ , one can translate the lattice sites. This technique has been used to deterministically deliver atoms to a very precise location. In this work we use this walking wave optical lattice to transport atoms into an optical cavity.

### 2.10.1 Walking Wave Velocity

A standing wave must have a constant phase, therefore its time derivative must equal zero. Using this relation, one can solve for the velocity of a walking-wave lattice.

$$\frac{\partial}{\partial t} \left( kz - \frac{\delta}{2}t \right) = 0. \quad (2.46)$$

This simplifies to,

$$v = \frac{\lambda\delta}{4\pi}. \quad (2.47)$$

From the velocity, we can compute the time required to transport the atoms to the cavity. For an optical lattice with a frequency difference of 100 kHz constructed from a laser operating at  $\lambda = 1064$  nm, the velocity of the atoms is  $v = 5.32$  cm/s.

## 2.11 Trap Frequencies

For the case when atoms are well localized in the trap, one can approximate the optical trap as a harmonic oscillator potential. By performing a second order Taylor expansion for a single focus trap, the trapping potential can be approximated as,

$$U_{\text{SF}}(r, z) \simeq -U_0 \left( 1 - 2 \left( \frac{r}{\omega_0} \right)^2 - \left( \frac{z}{z_R} \right)^2 \right). \quad (2.48)$$

From this equation, we can extract the trap frequencies as,

$$\omega_r = \sqrt{\frac{4U_0}{mw_0^2}} \quad (2.49)$$

$$\omega_z = \sqrt{\frac{2U_0}{mz_R^2}}. \quad (2.50)$$

For the optical lattice, the formulae are slightly different but the technique in finding the frequencies is the same. Performing the same expansion with  $\delta = 0$ , one finds trap frequencies of,

$$\omega_r = \sqrt{\frac{4U_0}{mw_0^2}} \quad (2.51)$$

$$\omega_z = 2\pi\sqrt{\frac{2U_0}{m\lambda^2}}. \quad (2.52)$$

For an optical lattice built with a laser with wavelength,  $\lambda = 1064$  nm, focused to a waist of  $w = 34$   $\mu\text{m}$ , and power of  $P = 4$  W per beam, the trap frequencies are  $\omega_r/(2\pi) = 3.01$  kHz and  $\omega_z/(2\pi) = 428$  kHz. For this optical lattice the trap depth is  $U_{\text{dip}} = 1.08$  mK with a scattering rate of  $\Gamma_{\text{SC}} = 4.21$  photons/s. For a single focus trap with the same parameters, the frequencies are  $\omega_r/(2\pi) = 1.51$  kHz and  $\omega_z = 10.6$  Hz. The trap depth and scattering rate for this single focus trap are,  $U_{\text{dip}} = 271$   $\mu\text{K}$  and  $\Gamma_{\text{sc}} = 1.05$  photons/s.

### ***2.12 AC Stark shift computation***

So far in the calculations of trap depth we have treated the atom semi-classically with only two levels. But in reality, atoms have many energy levels, and we must take into account the fine and hyperfine structure of the atom and compute the trap depth and AC stark shift [46]. Typically, when computing the trap depth for rubidium, one only takes into account the contribution from the D<sub>2</sub> line ( $5S_{1/2} \rightarrow 5P_{3/2}$ ) and possibly the D<sub>1</sub> line ( $5S_{1/2} \rightarrow 5P_{1/2}$ ), which are typically the two strongest transitions in alkali atoms. To characterize the Stark shift of a particular state, one needs to include the energy shift from all states that the initial state can couple to. This is achieved by simply modifying Eq. (2.24) to sum over all allowed transitions, each with a resonance frequency,  $\omega_{0,k}$ , and a linewidth,  $\Gamma_k$ , to account for the other energy levels.

$$U_{\text{dip}}(\mathbf{r}) = - \sum_k \frac{3\pi c^2}{2\omega_0^3} \left( \frac{\Gamma_k}{\omega_{0,k} - \omega} + \frac{\Gamma_k}{\omega_{0,k} + \omega} \right) I(\mathbf{r}) \quad (2.53)$$

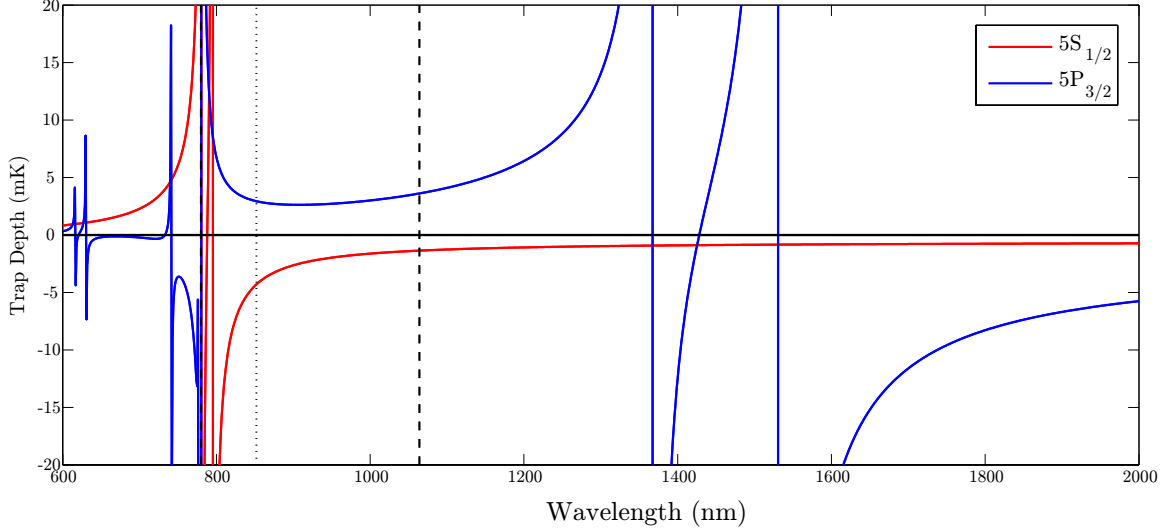


**Figure 2.6:** The dipole potential for the  $^{87}\text{Rb}$   $5S_{1/2}$  and  $5P_{3/2}$  states computed for an optical trap with  $P = 4$  W,  $w = 24$   $\mu\text{m}$ . The two dashed lines at 1064 nm and 852 nm indicate the wavelengths used for optical trapping in this thesis.

Equation (2.53) is plotted in Figure 2.6 for an optical lattice with 4 W per beam. In this figure, the dipole potential of the excited state,  $5P_{3/2}$ ,  $U_e$  is plotted in blue and the ground state dipole potential is plotted in red. The differential Stark shift experience by the atom can be related to the energy difference of the excited and ground states by,

$$\Delta_s = \frac{U_e - U_g}{\hbar} . \quad (2.54)$$

The resonant frequencies,  $\omega_{0,k}$ , and atomic linewidths,  $\Gamma_k$ , are cataloged in various databases. To compute the dipole potential, the atomic line data was used from the Kurucz and Bell atomic line database<sup>2</sup> [47]. These transitions for the ground and excited states of rubidium are reproduced in Tables 2.1 and 2.2.

For rubidium, there are 76 cataloged atomic transitions between 200 nm and 2000 nm. Looking at Eq. (2.53), the trap depth is proportional to the linewidth. The largest linewidth for rubidium is from the  $D_1$  ( $5S_{1/2} \rightarrow 5P_{1/2}$ ) and  $D_2$  ( $5S_{1/2} \rightarrow 5P_{3/2}$ ) lines, which are of the

<sup>2</sup><http://cfa-www.harvard.edu/amdata/ampdata/kurucz23/sekur.html>

order  $10^7 \text{ s}^{-1}$ . The sum is truncated to the 10 largest linewidths, where the tenth transition is 100 times weaker than the largest.

**Table 2.1:** Atomic transitions used for computing the AC Stark shift for the ground state of  $^{87}\text{Rb}$   $5\text{S}_{1/2}$  state.

Excited State Configuration	Wavelength vacuum (nm)	A coefficient (1/s)
$5\text{P}_{3/2}$	780.2405	37550000
$5\text{P}_{1/2}$	794.9783	35920000
$6\text{P}_{3/2}$	420.2972	3664000
$6\text{P}_{1/2}$	421.6706	2456000
$7\text{P}_{3/2}$	358.8070	1226000
$7\text{P}_{1/2}$	359.2593	726600
$8\text{P}_{3/2}$	334.9655	583500
$9\text{P}_{3/2}$	322.8908	329600
$8\text{P}_{1/2}$	335.1772	323300
$10\text{P}_{3/2}$	315.8441	207100

**Table 2.2:** Atomic transitions used for computing the AC Stark shift for the excited state of  $^{87}\text{Rb}$ ,  $5\text{P}_{3/2}$  state.

Excited State Configuration	Wavelength vacuum (nm)	A coefficient (1/s)
$5\text{S}_{1/2}$	-780.2405	-37550000
$6\text{S}_{1/2}$	1366.6729	13110000
$4\text{D}_{5/2}$	1529.4144	12500000
$7\text{S}_{1/2}$	741.0207	4400000
$6\text{D}_{5/2}$	630.0066	3157000
$5\text{D}_{5/2}$	775.9782	2706000
$7\text{D}_{5/2}$	572.5695	2457000
$8\text{S}_{1/2}$	616.1324	2192000
$4\text{D}_{3/2}$	1529.3116	2080000
$8\text{D}_{5/2}$	543.3035	1659000
$9\text{S}_{1/2}$	565.5309	1130000
$10\text{S}_{1/2}$	539.2057	707300
$6\text{D}_{3/2}$	630.0963	531200
$5\text{D}_{3/2}$	776.1564	478800
$11\text{S}_{1/2}$	523.5413	462600
$7\text{D}_{3/2}$	572.6190	396600
$8\text{D}_{3/2}$	543.3333	282400

### *2.13 Magic Wavelength*

A new theme in atomic physics experiments is building atomic clocks from optical transitions in optically trapped atoms [36, 48, 49]. Most of these proposals involve using earth-alkali elements which have narrow, quadrupole forbidden transitions. It is necessary in the optical traps to engineer the light shift in order to make the light shift of the excited state equal and opposite of the ground state. This ensures that when one probes the atoms in the optical trap, the frequency of the transition is equal to that of an atom in free space. The wavelength where this cancellation occurs is known as the “magic wavelength.”

As we will see in later chapters the AC stark shift experienced by the atom complicates the cavity QED picture. This complication led the Caltech group to use optical traps at the magic wavelength of cesium for their cavity QED experiments [50].

## CHAPTER III

### CLASSICAL AND QUANTUM CAVITY THEORY

This section presents the relevant theoretical background for the cavity QED elements of this research. We begin with classical cavity theory that is included for completeness and is referenced later. The chapter concludes by outlining the quantum theory of Jaynes-Cummings Hamiltonian, strong coupling in cavity QED and presenting a proposal to build a cavity QED based quantum computer. The experiments utilize two cavities, the science and the transfer cavity. The science cavity is where the atom cavity interaction is studied and the transfer cavity is used to stabilize the science cavity.

#### 3.1 Classical Cavity Physics

A Fabry-Perot optical cavity is a simple, yet subtle, optical system, consisting of two mirrors spaced by a known distance. These cavities are valuable laboratory tools used for laser diagnostics and frequency references. A schematic of a cavity can be seen in Figure 3.1.

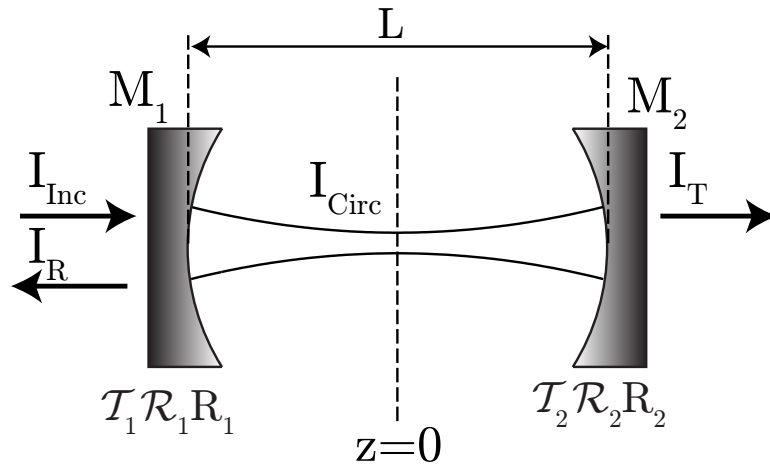


**Figure 3.1:** A basic Fabry-Perot cavity, where two curved mirrors are separated by a length  $L$ . Mirror one,  $M_1$ , at a location,  $z_1$ , has a radius of curvature of  $R_1$  a reflectivity of  $\mathcal{R}_1$ , and power transmission of  $\mathcal{T}_1$ . Mirror two,  $M_2$ , is located at  $z_2$ . The incident intensity is labeled as  $I_{\text{Inc}}$ , the reflected intensity  $I_{\text{R}}$ , the circulating intensity  $I_{\text{Circ}}$ , and the transmitted beam intensity  $I_{\text{T}}$ .

The cavity mirrors are defined by a radius of curvature,  $R_i$ , a power reflectivity,  $\mathcal{R}_i$  and power transmission  $\mathcal{T}_i$ . There are four electric fields in the cavity system, an incident, reflected, circulating and transmitted field with associated intensities of  $I_{\text{Inc}}$ ,  $I_{\text{R}}$ ,  $I_{\text{Circ}}$ , and  $I_{\text{T}}$ , respectively.

### 3.1.1 Resonator $g$ Parameters

Cavity stability and Gaussian beam parameters are often described in terms of the resonator  $g$  parameters<sup>1</sup>. The mirror's radius of curvature defines the cavity  $g$  parameter by,

$$g_i \equiv 1 - \frac{L}{R_i}, \quad (3.1)$$

where  $R_i$  is the mirror's radius of curvature and  $L$  is the length of the cavity [44, 45, 51]. To determine if a cavity is stable we need trace the beam path inside the cavity. A Fabry-Perot cavity can be represented by a periodic optical system described as:

1. propagation a distance  $L$  in free space
2. reflection from a mirror with radius  $R_2$
3. propagation of a distance  $L$  in free space
4. reflection from a mirror with radius  $R_1$

In order to have a stable cavity, the rays must remain in this periodic system, which implies that the rays fold back on themselves after one complete cycle for the lowest order mode. Using ray matrix techniques, the stability condition can be expressed in terms of the  $g$  parameters,

$$0 \leq g_1 g_2 \leq 1. \quad (3.2)$$

The eigenfunctions of the cavity are Hermite-Gaussian modes. We will focus on the TEM<sub>00</sub> mode, which is the lowest order Hermite-Gaussian mode. The TEM<sub>00</sub> mode of the cavity has the same fundamental parameters of a Gaussian beam in free space (Section 2.8);

---

<sup>1</sup>Note this is an unfortunate notation. Later when the quantum theory of cavity QED is developed  $g$  will be used for the coupling between the atom and the cavity. Context should make it clear which  $g$  is intended.

the beam waist,  $w$ , the Rayleigh range,  $z_R$ , and the radius of curvature,  $R(z)$ . It's convenient to express these quantities in terms of the cavity's  $g$  parameters.

In order to put these in terms of  $g_i$ , one needs to apply the following matching conditions,

$$R(z_1) = z_1 + \frac{z_R^2}{z_1} = -R_1 \quad (3.3)$$

$$R(z_2) = z_2 + \frac{z_R^2}{z_2} = R_2 \quad (3.4)$$

$$L = z_2 - z_1, \quad (3.5)$$

where  $L$  is the separation between the two mirrors.

The first two conditions match the radius of curvature of the Gaussian mode to the mirror's radius of curvature. Using these three conditions, with Eq. (3.1) and some algebra we arrive at equations that relate the cavity Gaussian beam parameters in terms of the  $g$  parameters,

$$w_0^2 = \frac{L\lambda}{\pi} \sqrt{\frac{g_1 g_2 (1 - g_1 g_2)}{(g_1 + g_2 - 2g_1 g_2)^2}} \quad (3.6)$$

$$z_R^2 = \frac{g_1 g_2 (1 - g_1 g_2)}{(g_1 + g_2 - 2g_1 g_2)^2} L^2. \quad (3.7)$$

Armed with the expression for the beam waist, an input laser's beam can be properly mode matched, which maximizes the overlap with the cavity mode. Also the size of the beam waist is important in computing the cavity mode volume.

The science cavity used in Chapter 6 is constructed from two mirrors with a radius of curvature  $R = 2.5$  cm separated by a length,  $L = 221.5$   $\mu\text{m}$ . At wavelength  $\lambda = 780$  nm, the  $g$ -parameters, cavity waist and  $z_R$  for this cavity are,

$$g_1 = g_2 = 0.991$$

$$g_1 g_2 = 0.982$$

$$w_0 = 20.3 \mu\text{m}$$

$$z_R = 1.66 \text{ mm}.$$

The transfer cavity is built from two mirrors with radius of curvature,  $R = 25$  cm and separated by length of  $L = 15$  cm. For this cavity the  $g$ -parameters, cavity waist and  $z_R$

are,

$$\begin{aligned}
 g_1 = g_2 &= 0.4 \\
 g_1 g_2 &= 0.16 \\
 w_0 &= 168 \mu\text{m} \\
 z_R &= 11.5 \text{ cm} .
 \end{aligned}$$

### 3.1.2 Mirror Losses and Delta Notation

In the previous section the mirror's radius of curvature was used to construct cavity  $g$  parameters. Using this notation, formulae were developed to compute the properties of the Gaussian beam. Using another property of the mirror, the reflectivity, formulae can be developed for other cavity properties, the finesse ( $\mathcal{F}$ ), the free spectral range ( $\nu_{\text{FSR}}$ ), and the linewidth ( $\kappa$ ).

To develop formulae for the finesse and linewidth we use the “delta Notation” of Siegman for the cavity losses [45]. A mirror has three loss mechanisms: transmission  $T_i$ , absorption  $A_i$  and scattering loss  $S_i$ . For mirrors to be useful for cavity QED we want the losses to be dominated by the transmission losses.

In terms of the  $\delta$ -notation, the mirror's power reflectivity is defined as,

$$\mathcal{R}_i = r_i^2 = \exp(-\delta_i) , \quad (3.8)$$

where  $r_i$  is the electric field amplitude reflection value. The  $\delta$  parameter of the mirror is given by,

$$\delta_i = \ln \left( \frac{1}{\mathcal{R}_i} \right) . \quad (3.9)$$

To account for other losses, absorptive and scatter, we introduce another delta parameter,  $\delta_0$  which is the round trip internal cavity loss. The total loss in one round trip of the cavity is given by,

$$\delta_c = \delta_0 + \delta_1 + \delta_2 , \quad (3.10)$$

where  $\delta_1$  and  $\delta_2$  are transmission losses from mirror one and two, and  $\delta_0$  is due to other losses.

The transmission through the cavity is given by the Lorentzian function [45],

$$I_T = \frac{T_{\text{Max}} I_{\text{Inc}}}{1 + (2\mathcal{F}/\pi)^2 \sin^2(\pi\nu/\nu_{\text{FSR}})} , \quad (3.11)$$

where  $\mathcal{F}$  is the finesse and  $\nu_{\text{FSR}}$  is the free spectral range. Looking at Eq. (3.11), the finesse defines the sharpness of the peaks. The larger then finesse, the narrower the transmission peak. In the limit of high quality mirrors (i.e.  $r_1, r_2 \rightarrow 1$ ), the finesse is given by,

$$\mathcal{F} = \frac{2\pi}{\delta_c} . \quad (3.12)$$

The second parameters in Eq. 3.11 is the free spectral range which is the frequency spacing between adjacent longitudinal modes. It is related to the cavity's length by,

$$\nu_{\text{FSR}} = \frac{c}{2L} . \quad (3.13)$$

Looking at Eq. (3.11), resonances occur when the frequency is equal to an integer multiple of the free spectral range,  $\nu_{\text{res}} = q \nu_{\text{FSR}}$ . In terms of length, this resonance condition is,

$$L_{\text{res}} = q \frac{\lambda}{2} . \quad (3.14)$$

The final basic cavity property is the linewidth,  $\kappa$ . This is the half-width half-max (HWHM) of the Lorentzian lineshape. The linewidth of the cavity is related to the finesse and the free spectral range by,

$$\kappa = \frac{\nu_{\text{FSR}}}{2\mathcal{F}} . \quad (3.15)$$

In Figure 3.2, the output intensity of a Fabry Perot cavity is plotted using Eq. (3.11). This figure shows the dependence of the cavity output on the finesse and the free spectral range. In Figure 3.2 (a), the cavity's transmission is repeated every free spectral range. In Figure 3.2 (b), shows the dependence of the lineshape on the finesse. As the finesse increases, the cavity's lineshape becomes narrow.

The mirrors that make the science cavity have transmission losses of  $\delta_1 = 10$  and  $\delta_2 = 100$  parts per million (ppm). Neglecting additional loss mechanisms,  $\delta_0 \approx 0$ , the science cavity has a computed finesse and linewidth of,

$$\begin{aligned} \mathcal{F} &= 57,000 \\ \kappa &= (2\pi) 5.93 \text{ MHz} . \end{aligned}$$

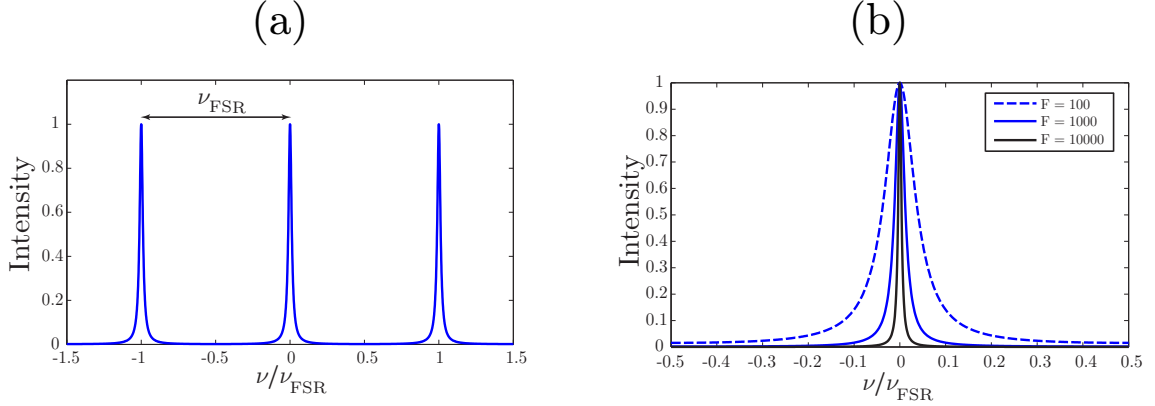


**Figure 3.2:** The transmission spectrum of a Fabry-Perot cavity. (a) The transmission of the cavity over several free spectral ranges. The Lorentzian peaks are repeated each free spectral range. (b) The Lorentzian lineshape is plotted for different finesse. As the finesse increases the lineshape gets narrower.

We will see in Chapter 6 that there are additional losses which result in a larger measured linewidth.

For the transfer cavity, the mirrors have reflectivities of 99.1% with a finesse and linewidth of,

$$\mathcal{F} = 313$$

$$\kappa = (2\pi) 1.60 \text{ MHz} .$$

### 3.1.3 Cavity Transmission

As shown in Figure 3.1, the cavity system has four electric fields and associated intensities. The fields are, an incident light beam,  $E_{\text{Inc}}$ , a circulating intra-cavity beam,  $E_{\text{Circ}}$ , a transmitted beam,  $E_{\text{T}}$ , and a beam that is reflected,  $E_{\text{R}}$ . In cavity QED experiments it is important to know properties of the intra-cavity beam. Since it is not possible to measure the intra-cavity beam directly, one has to infer its properties from the transmitted and the reflected beams.

Looking just to the right of the first mirror in Figure 3.1, the electric field amplitude,  $E_{\text{Circ}}$ , is the superposition of the incident field leaked through the first mirror, and circulating field that has completed one round trip of the cavity. This is given by,

$$E_{\text{Circ}} = it_1 E_{\text{Inc}} + g_{\text{rt}}(\omega) E_{\text{Circ}} , \quad (3.16)$$

where  $t_1$  is the electric field amplitude transmission of the first mirror.<sup>2</sup> The field circulating in the cavity experiences a complex round-trip attenuation of,

$$g_{rt}(\omega) = r_1 r_2 \exp(-i\phi) , \quad (3.17)$$

where the phase accumulated by the circulating field traveling a distance  $2L$  is  $\phi$ . This phase is given by,

$$\phi = 2kL = \frac{2L}{c} 2\pi\nu = 2\pi \frac{\nu}{\nu_{\text{FSR}}} . \quad (3.18)$$

Solving Eq. (3.16), for the circulating power results in,

$$\frac{E_{\text{Circ}}}{E_{\text{Inc}}} = \frac{it_1}{1 - r_1 r_2 \exp(-i2\pi\nu/\nu_{\text{FSR}})} . \quad (3.19)$$

Using a similar argument, formula for the transmitted field can be constructed [45],

$$E_{\text{T}} = it_2 \exp(-i4\pi\nu/\nu_{\text{FSR}}) E_{\text{Circ}} . \quad (3.20)$$

The transmitted field is given by the circulating field that transmits through the second mirror after traveling a distance  $L$ . The intensities of the fields, given by  $I = (c\epsilon_0/2)|E|^2$ , are,

$$\frac{I_{\text{T}}}{I_{\text{Inc}}} = \frac{(t_1 t_2)^2}{1 - (r_1 r_2)^2} \frac{1}{1 + \frac{4r_1 r_2}{1 - (r_1 r_2)^2} \sin^2\left(\pi \frac{\nu}{\nu_{\text{FSR}}}\right)} \quad (3.21)$$

$$\frac{I_{\text{Circ}}}{I_{\text{Inc}}} = \frac{t_1^2}{|1 - g_{rt}(\omega)|^2} . \quad (3.22)$$

From Eq. (3.21) and Eq. (3.11), we can read off the exact value of the finesse for a Fabry-Perot cavity which is given by,

$$\mathcal{F} = \pi \frac{\sqrt{r_1 r_2}}{\sqrt{1 - (r_1 r_2)^2}} . \quad (3.23)$$

Evaluating these intensity ratios on resonance results in equations that relate the transmitted field, and incident field to the circulating field in terms of the  $\delta$ -parameters are,

$$\frac{I_{\text{T}}}{I_{\text{Inc}}} = \frac{4\delta_1 \delta_2}{\delta_c^2} \quad (3.24)$$

$$\frac{I_{\text{Circ}}}{I_{\text{Inc}}} = \frac{4\delta_1}{\delta_c^2} \quad (3.25)$$

$$\frac{I_{\text{T}}}{I_{\text{Circ}}} = \delta_2 . \quad (3.26)$$

---

<sup>2</sup>Transmission through the mirror picks up a factor of  $i$ .

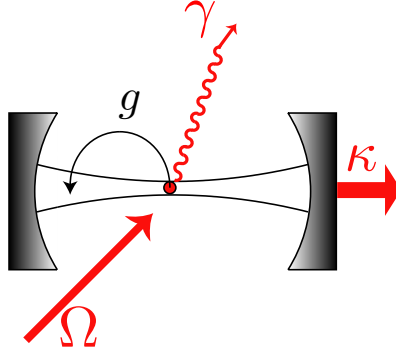


**Figure 3.3:** A single atom is coupled to a high finesse optical cavity. The atom can coherently couple to the photon at a rate of  $g_0$ , and the system can decohere via spontaneous emission ( $\gamma$ ) and by loss of the photon ( $\kappa$ ). The system can be externally pumped by a laser with Rabi rate of  $\Omega$ .

These relations provide a convenient way to measure the intra-cavity field. For the science cavity, the output mirror,  $M_2$  has a transmission of 100 ppm. Using equation Eq. (3.26), if the transmitted light is 1 pW, then the intra-cavity is 10 nW, a factor of  $10^4$  larger than the transmitted field.

### 3.2 Quantum Development of Cavity QED system

The interaction of a single atom with a single mode of the electric is field is known as the Jaynes-Cummings model [52], and represents an important paradigm in quantum optics. An atom coupled to a single mode of a cavity can be found in Figure 3.3. This system has been studied experimentally in both the microwave [53] and optical regimes [54].

The Jaynes-Cummings Hamiltonian can be broken into three parts; the atomic Hamiltonian,  $H_A$ , the Hamiltonian of the field,  $H_F$ , and the interaction of the two systems,  $H_{\text{Int}}$ . The atom is a two-level system with an excited and ground state,  $|e\rangle$  and  $|g\rangle$ , where the energy separation of these states is given by  $\Delta E = \hbar\omega_a$ . In the rotating wave approximation (RWA) the Jaynes-Cummings Hamiltonian is given by[55],

$$H_{\text{JC}} = \hbar\omega_a\hat{\sigma}_+\hat{\sigma}_- + \hbar\omega_c\hat{a}^\dagger\hat{a} + \hbar g(\hat{a}^\dagger\hat{\sigma}_- + \hat{\sigma}_+\hat{a}) = H_A + H_{\text{Field}} + H_{\text{Int}} , \quad (3.27)$$

where  $\hat{a}$  and  $\hat{a}^\dagger$  are the annihilation and creation operators for the field. The atomic raising and lowering operators are  $\hat{\sigma}_+ = |e\rangle\langle g|$  and  $\hat{\sigma}_- = |g\rangle\langle e|$ , and  $\omega_c$  is the resonant frequency

of the cavity.

The interaction term is proportional to the atom-field coupling,  $g$ , which is position dependent due to the Gaussian standing wave structure of the Fabry-Perot cavity's electric field. The cavity's TEM<sub>00</sub> electric field given by  $\psi(\vec{r})$ ,

$$\psi(\vec{r}) = \cos(kx) \exp\left(-\frac{y^2 + z^2}{w_0^2}\right), \quad (3.28)$$

where we have chosen the cavity axis to be the x direction. The volume of the electric field mode,  $V_M$ , is given by,

$$V_M = \int |\psi(\vec{r})|^2 d\vec{r} = \frac{\pi}{4} w_0^2 L. \quad (3.29)$$

The atom-field coupling is given by,  $g = g_0 \psi(\vec{r})$ , where the maximum atom-field coupling is  $g_0$  which is defined as [56],

$$g_0 = \mu \sqrt{\frac{\omega_c}{2\epsilon_0 V_M \hbar}}, \quad (3.30)$$

where  $\mu$  is the electric dipole moment. From Eq. (3.30), it is seen that the interaction coupling increases as the volume of the cavity's electric field is decreased.

The new eigenstates of the system are dressed states that are superpositions of states with the atom in the ground state,  $|g\rangle$ , and  $n$  photons in the mode, with states in which the atom is in the excited state  $|e\rangle$  and  $n - 1$  photons in the field. The eigenstates of the system are [55],

$$|-, n\rangle = \cos \theta_n |e, n - 1\rangle - \sin \theta_n |g, n\rangle \quad (3.31)$$

$$|+, n\rangle = \sin \theta_n |e, n - 1\rangle + \cos \theta_n |g, n\rangle, \quad (3.32)$$

where  $\theta_n$  is known as the mixing angle. The mixing angle is defined as,

$$\cos \theta_n = \frac{\Omega' - \delta}{\sqrt{(\Omega' - \delta)^2 + 4g^2 n}} \quad (3.33)$$

$$\sin \theta_n = \frac{2g\sqrt{n}}{\sqrt{(\Omega' - \delta)^2 + 4g^2 n}}, \quad (3.34)$$

where  $\Omega'$  is the generalized Rabi frequency, which depends on  $n$  and the detuning  $\delta = \omega_a - \omega_c$ .

The generalized Rabi frequency is given by,

$$\Omega' = \sqrt{\delta^2 + 4g^2 n}. \quad (3.35)$$

For the case when the atom and cavity share the same resonance,  $\delta = 0$ , the above equations simplify to,

$$|-, n\rangle = \frac{1}{\sqrt{2}} (|e, n-1\rangle - |g, n\rangle) \quad (3.36)$$

$$|+, n\rangle = \frac{1}{\sqrt{2}} (|e, n-1\rangle + |g, n\rangle) . \quad (3.37)$$

This gives the energy equations,

$$E_{-,n} = n\hbar\omega - \hbar g\sqrt{n} \quad (3.38)$$

$$E_{+,n} = n\hbar\omega + \hbar g\sqrt{n} \quad (3.39)$$

These dressed states lift the degeneracy of the system, and can be displayed as the well known Jaynes-Cummings ladder of states. This ladder is pictured in Figure 3.4, with energy splittings of  $\Delta_E = \hbar g\sqrt{n}$ , for the case of  $\omega_a = \omega_c = \omega_0$ .

### 3.3 Strong Coupling

In the Jaynes-Cummings Hamiltonian there are three characteristic rates,  $g$ ,  $\gamma$ , and  $\kappa$ , that describes the system's evolution. The rate  $g$  describes coherent quantum dynamics, while the other two rates,  $\gamma$  and  $\kappa$ , describe decoherences. To include decoherence in the theory presented previously, we have to use a master equation that takes into account the coupling of the quantum system to the environment. This master equation will be presented in section 3.4.

Since a quantum system can not be perfectly isolated from it's environment, it experiences decoherence. In the cavity QED system, there are two main decoherence processes. The first is decoherence associated with the atom and this loss of coherence is due to spontaneous emission. This is the emission of a photon into all other modes except the mode defined by the cavity. This process is described by the natural linewidth of the atom,  $\gamma$ . The second decoherence is due to the photon leaking out of the cavity at a rate  $2\kappa$ .

In order to have reversible quantum dynamics, the rate at which coherent interactions are performed has to be larger than the rate at which the decoherences occur. This is known as the strong coupling regime in cavity QED and is defined as,  $g_0 \gg (\kappa, \gamma)$ .

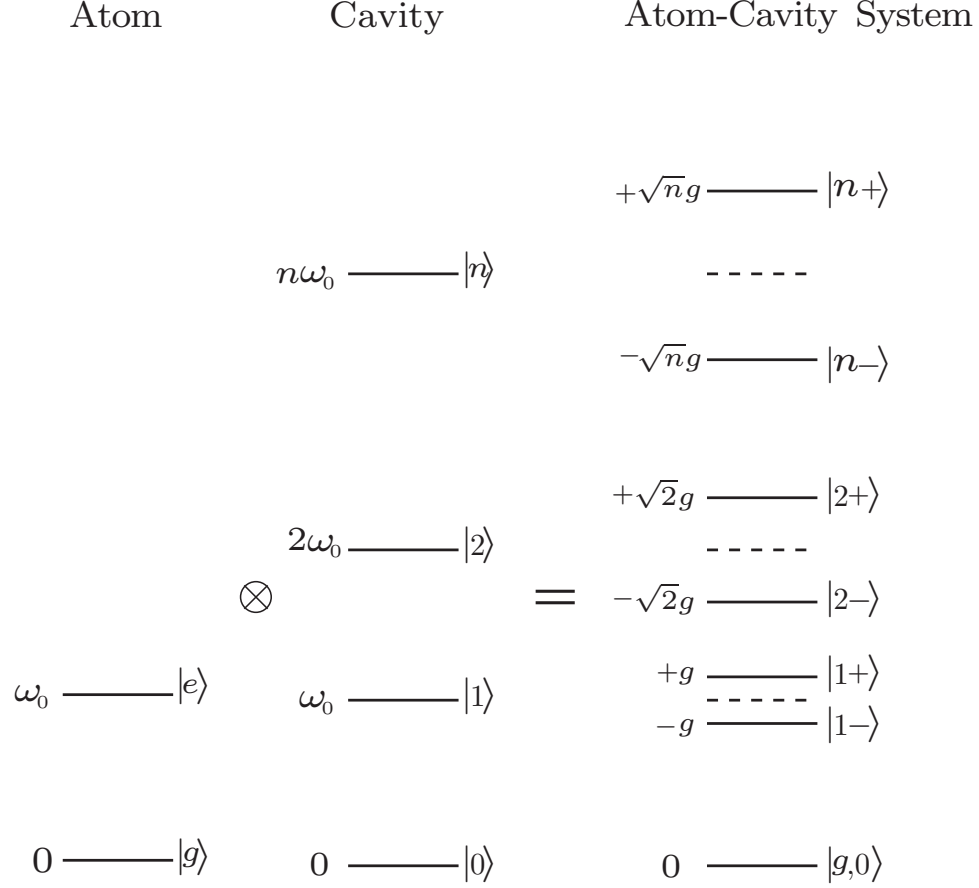


**Figure 3.4:** Energy eigenstates of the bare atom, cavity, and the coupled atom-cavity system, for the case of  $\omega_a = \omega_c = \omega_0$ . The atom-cavity system shows the Jaynes-Cummings ladder of states, where the energy levels are split by  $\Delta_E = \hbar g \sqrt{n}$ .

Three important quantities can be constructed from the three rates,  $\kappa, \gamma, g_0$  [56],

$$n_0 = \frac{4}{3} \frac{\gamma^2}{g_0^2} \quad (3.40)$$

$$N_0 = \frac{\kappa\gamma}{g_0^2} \quad (3.41)$$

$$C_1 = \frac{g_0^2}{\kappa\gamma} . \quad (3.42)$$

The first of these equation describes the saturation photon number,  $n_0$ , which is the number of photons that will saturate the atom-cavity system. The saturation photon number determines the role that a single photon plays on an atoms. The second equation describes the “critical” atom number,  $N_0$ , which describes how many atoms are required to affect the cavity field. The final equation, Eq. (3.42), is the single atom cooperativity,  $C_1$  and is

the inverse of the critical atom number. Normally in quantum optics, one operates in the regime where  $g_0 \ll (\gamma, \kappa)$  implying that  $(n_0, N_0) \gg 1$ . In this regime, it takes many photons to saturate a transition. In the strong coupling regime this is dramatically different. The saturation photon number is less than one, as is the critical atom number.

The science cavity was designed to achieve the following parameters,

$$n_0 = 0.0419$$

$$N_0 = 0.123$$

$$C = 8.14$$

Again in these calculations we assume that  $\kappa$  is only due to transmission losses. In Chapter 6, these values will be measured explicitly.

### 3.4 Master Equation and Cooling Forces

A master equation is used to describe the dynamics of the Jaynes-Cummings system which takes into account decoherences. The master equation for this system is given by [57],

$$\dot{\rho} = -\frac{i}{\hbar}[H, \rho] - \gamma(\{\hat{\sigma}_+\hat{\sigma}_-, \rho\}_+ - 2\hat{\sigma}_-\rho\hat{\sigma}_+) - \kappa(\{a^\dagger a, \rho\}_+ - 2a\rho a^\dagger), \quad (3.43)$$

where  $\rho$  is the density matrix.

To describe the cavity QED system to include external pumping and an external optical trap we need to add terms to the Jaynes-Cummings Hamiltonian. The new Hamiltonian is,

$$H = H_{\text{JC}} + H_{\text{Pump}} + H_{\text{Trap}}, \quad (3.44)$$

where  $H_{\text{Pump}}$  is given by,

$$H_{\text{Pump}} = -\hbar\Omega (\hat{\sigma}_+ e^{-i\omega_p t} + \hat{\sigma}_- e^{i\omega_p t}), \quad (3.45)$$

and  $\Omega$  is the Rabi frequency of the pump beams. This pump beam drives the cavity by exciting the atom, which then emits photons into the cavity mode. The trap Hamiltonian is a conservative potential,  $H_{\text{Trap}} = \hbar U(\mathbf{r})$ , which describes the external optical trap. In the Jaynes-Cummings Hamiltonian, we need to change the frequencies of the atomic and

field Hamiltonians to allow for detunings,

$$\omega_a \rightarrow \Delta_a = \omega_p - \omega_a - \Delta_s(\mathbf{r}) \quad (3.46)$$

$$\omega_c \rightarrow \Delta_c = \omega_p - \omega_c . \quad (3.47)$$

In these detunings,  $\omega_p$  is the frequency of the pump beams,  $\omega_a$  is the bare atomic resonance, and  $\omega_c$  is the cavity's resonance frequency. The detuning caused by the Stark shift of the optical trap is  $\Delta_s(\mathbf{r})$ , which is spatially dependent due to the structure of the trapping field. Note, the above definitions are defined as the negative of the detunings used by Murr *et al.* [58].

Cooling in optical cavities has been studied theoretically [58, 59, 60, 61, 62], and experimentally [63, 64, 65, 66] by a number of groups. This section presents the forces experienced on a atom that is located in an high finesse optical cavity. This derivation is developed by Murr *et al.* [58], and is outlined here to present the cooling forces.

The forces experienced by an atom can be found by taking the negative gradient of the Hamiltonian. The force can be split into three distinct pieces; the force on the atom due to the optical trap, the forces due to the pump beams, and the force due to the optical cavity:

$$F = -\nabla H = F_{\text{Trap}} + F_{\text{pump}} + F_{\text{cav}} . \quad (3.48)$$

We adopt the cooling method develop by the Munich group with the resulting forces for an atom moving with velocity,  $\mathbf{v}$ , have been calculated in [58],

$$F_{\text{Trap}} = 4\hbar\nabla\Delta_a(\nabla\Delta_a \cdot \mathbf{v}) \frac{\kappa\Delta_c}{(\Delta_c^2 + \kappa^2)^2} \frac{g^2 P_e}{\Delta_a^2 + \gamma^2} \quad (3.49)$$

$$F_{\text{pump}} = 4\hbar\mathbf{k}_L(\mathbf{k}_L \cdot \mathbf{v}) \frac{\kappa\Delta_c}{(\Delta_c^2 + \kappa^2)^2} g^2 P_e \quad (3.50)$$

$$F_{\text{cavity}} = 4\hbar\nabla g(\nabla g \cdot \mathbf{v}) \frac{\kappa\Delta_c}{(\Delta_c^2 + \kappa^2)^2} P_e . \quad (3.51)$$

In the above equations,  $P_e$  is the excitation probability with,

$$P_e = \langle \hat{\sigma}_+ \hat{\sigma}_- \rangle . \quad (3.52)$$

By the correct choice of axes for the trap, cavity and pump beam, cooling forces can be realized in three orthogonal directions. By the addition of a set of cooling beams at an

angle of  $45^\circ$  to the optical trap axis leads to forces in all three dimensions. The geometry of the three forces is depicted in Figure 3.5.

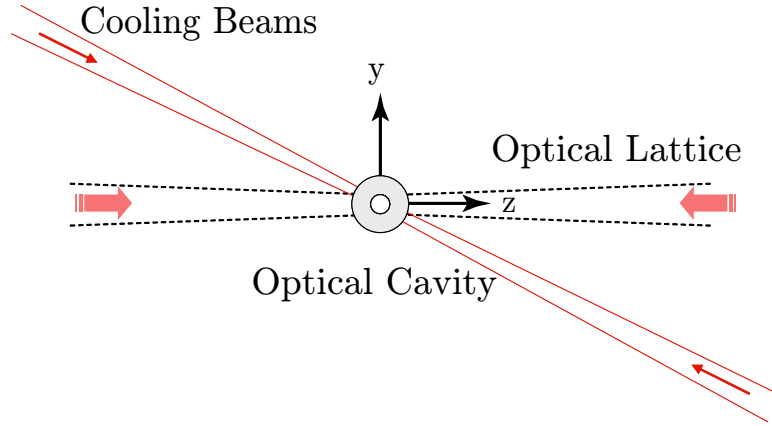


**Figure 3.5:** The geometry adopted in order to realize cooling forces in three dimensions. The cooling beams are orthogonal to the cavity axis (x-axis) and at an angle of  $45^\circ$  to the optical lattice (z-axis).

Looking at the forces, one can see that to provide a cooling the forces need to be dissipative which requires that  $\Delta_c < 0$ . Each of the forces is proportional to,  $\Delta_c(\Delta_c^2 + \kappa^2)^{-2}$ . If we take the derivative of this function with respect to  $\Delta_c$ , the maximum cooling occurs for a detuning of,

$$\Delta_c = -\frac{\kappa}{\sqrt{3}}. \quad (3.53)$$

### 3.5 Cavity QED based Quantum Computer

In 1995, Pellizzari *et al.* proposed a cavity QED based quantum computer [67]. In this proposal,  $N$  atoms are well localized and coupled to the same quantized single mode of a high  $Q$  cavity. In this model, the atoms are separated by a distance that is larger than the resonant wavelength of the cavity and with an independent addressed laser beam for each atom.

The qubit states are formed using the long-lived Zeeman ground states of the atom where each qubit can be initialized using optical pumping. Single qubit gates can be performed using microwaves between the ground state hyperfine levels or with two photon Raman processes.

In order to perform two qubit quantum gates, atoms are coupled to laser pulses and then the information is exchanged from qubit to qubit using an intra-cavity photons. After the gates have been performed, detection the quantum state are performed by measuring the output cavity photon which can be used as a flying qubit. This system satisfies all five of the DiVincenzo criteria that was presented in Section 1.3. A schematic of a proposed cavity QED implementation of a quantum computer for this thesis can be found in Figure 3.6.

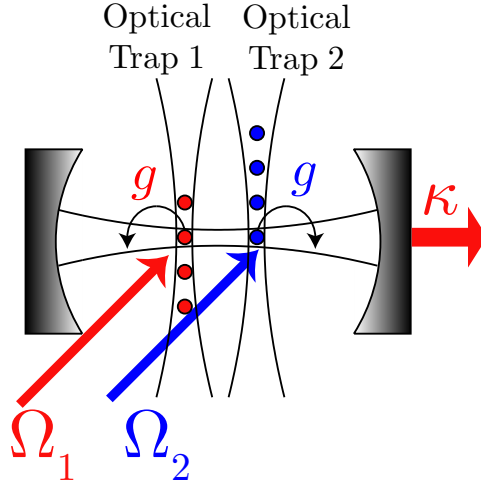


**Figure 3.6:** A scheme to implement a cavity QED based quantum computer. Two independent optical lattices shuttle atoms in and out of the optical cavity. In the cavity, independent laser beams can exciting either atom state is read out by the emitted cavity field.

This adaptation of the Pellizzari scheme implements two optical lattice traps perpendicular to the cavity mode. In each of these traps, a chain of atomic qubits form a quantum register. By constructing the optical traps in the walking wave configuration, atoms can deterministically placed in the cavity mode. When the atom is placed in the cavity mode, it can interact with it a rate of  $g$ . By placing two optical traps in the cavity it allows us to produce two qubit gates from established theoretical protocols [67, 68, 69].

## CHAPTER IV

### EXPERIMENTAL SETUP

In the preceding chapters, the theory for each of the major experimental sub-systems, MOT, optical trap and cavity were developed. This chapter focuses on the technical implementations of these systems.

#### *4.1 Vacuum System*

This experiment takes place in an ultra high vacuum environment to limit unwanted interactions between laser cooled atoms and background gases. The vacuum system is constructed from standard commercially available components and achieves a pressure of  $1 \times 10^{-11}$  Torr using an 20 l/s ion pump (Varian Valcon Plus 20 Starcell<sup>®</sup>) and a titanium sublimation pump (Varian Filament type TSP).

One custom piece of vacuum hardware is an uncoated quartz cell built by Allen Scientific Glass of Boulder, CO. The cell is a rectangular pipette with a 1" square cross section which allows the use of a high numerical aperture imaging objective. This lens has the advantage that it collects a large percentage of the light scattered by the atoms, allowing for single atom detection. A three dimensional model of the cell is depicted in Figure 4.1.

#### *4.2 MOT Coils*

The MOT requires a magnetic field gradient that is produced by anti-Helmholtz coils. Single atom trapping requires a very large field gradients,  $\sim 300$  G/cm. To produce this field, the coils are designed to be placed close together with the ability to run large electrical currents in steady state.

The coils are constructed from 1/4" outer diameter refrigerator tubing wrapped in Kapton<sup>®</sup> tape to electrically isolate the coil turns. The coils are wrapped such that there are  $4 \times 3$  (radial  $\times$  axial) turns for a total of 12 turns. The inner diameter of the MOT coils is 2.5" with an outer diameter of 4.5", and the center of the coils are separated by

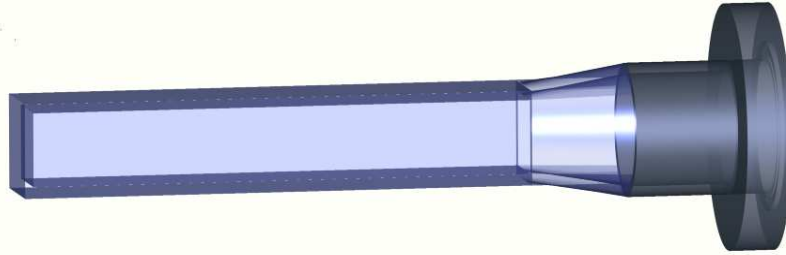


**Figure 4.1:** An AutoCAD drawing of the cell used for the experiments. The cell is made from quartz, with square cross section of 1". There is glass transition piece that takes the cell to a standard 2.75" CF vacuum connection, which connects to an ion pump.

3.5".

The current for the coils is provided by a power supply from Electronic Measurement Inc (EMI), model ESS Power supply. This power supply can provide 15kW of electrical power with a maximum of 15 V and 1000 A. The power supply becomes voltage limited at 500 A due to the circuit's resistance, giving a maximum calculated field gradient of 277 G/cm. To dissipate the heat generated in producing this magnetic field, cooling water flows through the coil tubing. At the maximum current, the coils reach a temperature of 48°C with water cooling.

### ***4.3 Rubidium Properties***

Alkali atoms are the most commonly laser cooled and trapped atoms due to their hydrogen like electronic structure and closed cycling transitions. Rubidium is a convenient atom to trap because of the commercially available of diode lasers at the  $D_2$  transition at  $\lambda = 780$  nm.

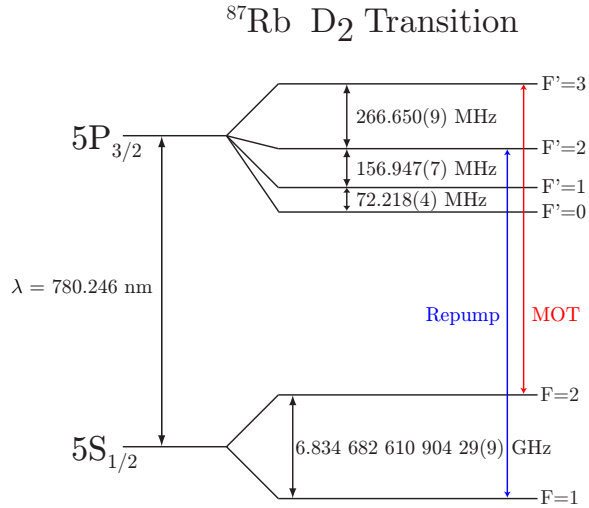


**Figure 4.2:** Hyperfine structure of the  $^{87}\text{Rb}$  atom for the D<sub>2</sub> transition at 780 nm. The red transition is known as the MOT transition and the blue transition is the repump transition.

The D<sub>2</sub> transition of  $^{87}\text{Rb}$ , with the MOT and repump transitions labeled, is shown in Figure 4.2. The MOT transition is the cycling  $F = 2 \rightarrow F' = 3$  transition and is the primary transition for cooling. An additional laser, tuned to the  $F = 1 \rightarrow F' = 2$  resonance returns atoms from the  $F = 1$  dark state to the cooling cycle. A saturated absorption signal of the D<sub>2</sub> line obtained in a vapor cell is presented in Figure 4.3.

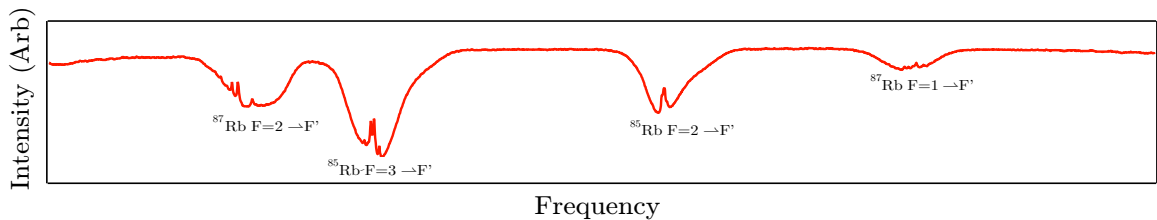


**Figure 4.3:** Saturated absorption spectroscopy of the D<sub>2</sub> transition in rubidium. The frequency increases from left to right, for frequency spacing of the  $^{87}\text{Rb}$  transitions, refer to Fig 4.2.

#### 4.3.1 Rubidium Source

The rubidium source is provided by an alkali getter source. A 4.5 mg getter releases rubidium when an electrical current resistively heats it. Typically, 3.5 W of electrical power is

used to heat the getter.

Additionally, high power light emitting diodes (LEDs) are used to enhance the vapor pressure of Rb in the chamber. These LEDs (Opto Technology, Inc.) emit blue light 440 to 460 nm that cause rubidium atoms to be de-absorbed from the quartz cell walls. This effect is called light-induced atom desorption (LIAD) and has been shown to be an effective controllable source for alkali atoms [70]. This source allows the getter to be fired sparingly, maintaining a low background vapor pressure required for long trap lifetimes. Two LEDs are mounted approximately 6" from the cell and are on during MOT loading. Then 200 ms before the MOT coils are turned off, they are switched off.

#### ***4.4 Diode Lasers***

The cavity QED experiment has four major laser systems. Two separate systems, the MOT and Repump, are diode lasers that produce the MOT. An additional group of diode lasers is used to stabilize the science cavity and to probe atoms in the cavity. This cavity laser system is built from two diode lasers and two Fabry-Perot cavities. The final laser system is a Ytterbium (Yb) doped fiber laser used to produce the optical trap.

The diode lasers are used in both a master and slave configurations. A master laser is typically an external cavity diode laser (ECDL), where a diffraction grating is used to make the external cavity for a fine frequency selection and reduced laser linewidth. These master diodes are configured in the Littrow configuration and provide a narrow linewidth laser (less than 1 MHz) with mode-hop free tuning of approximately 1 GHz. A slave diode laser is injection locked from the master laser and lacks a diffraction grating. Typically, due to poor efficiencies in double passing acousto-optic modulators (AOMs) and other optical systems, a slave diode is injection locked from a master laser to provide more optical power for the experiment. A small amount of optical power is required to injection lock a slave laser, usually less than 1 mW, while the typical slave output is approximately 100 mW.

The diode laser we use is produced by Sharp Electronics, model GH0781JA2C, and is commercially marketed for high speed CD-R burners. These lasers have a nominal center wavelength of 784 nm, but with the appropriate choice of temperature, laser current and

diffraction grating angle, the laser can be operated at 780 nm. Each of these parameters are controlled with home-built electronics.

These home-built electronics are adaptations of designs developed over the last decade. To control the temperature of the laser a temperature controller stabilizes the temperature of an aluminum block where the laser diode is mounted. This is performed with a Proportional and Integrator (PI) feedback loop that controls a current to a thermo-electric cooler (TEC) placed under the aluminum block. This PI circuit is based on a design from Hulet's group at Rice University [71] and with this feedback, it is possible to stabilize the laser's temperature to 1 mK.

The current controller is based on a design by Libbrecht and Hall [72] and produces a stable current for the diode laser by establishing a constant voltage across an extremely temperature stable resistor. In addition to the stable DC current operation, there are two inputs to add modulation to the frequency of the laser. The first modulation input has a bandwidth of approximately 1 MHz and is used to provide fast feedback to the diode current to lock laser to an atomic line or an optical cavity. The second input has a higher frequency range and is used to put RF sidebands on the laser for frequency modulated (FM) spectroscopy.

The laser frequency is stabilized by a final piece of home-built electronics, the lock box, which is also a PI circuit. Dispersive error signals are generated by using an FM spectroscopy technique which is described in Ref [73]. In the lock box circuit, the error signal is amplified and low pass filtered with a roll-off frequency of 30 kHz. The error signal is split into two branches. The first branch is integrated and then feedbacks to a piezo-electric transducer (PZT) which controls the diffraction grating angle. This integrator corrects for long term drifts of the laser frequency. The second branch is sent through a proportional circuit and servos the current of the laser diode for fast fluctuations. Using this PI circuit, the master laser remain locked for hours.

#### 4.4.1 MOT Laser System

In Figure 4.4, the optical layout of the MOT laser is shown. An ECDL laser is locked to a rubidium cell via FM spectroscopy by modulating an AOM. The output of the photodiode is mixed with the modulation frequency to generate the error signal. The error signal, saturated absorption spectrum and frequency detuning are shown in Figure 4.5.

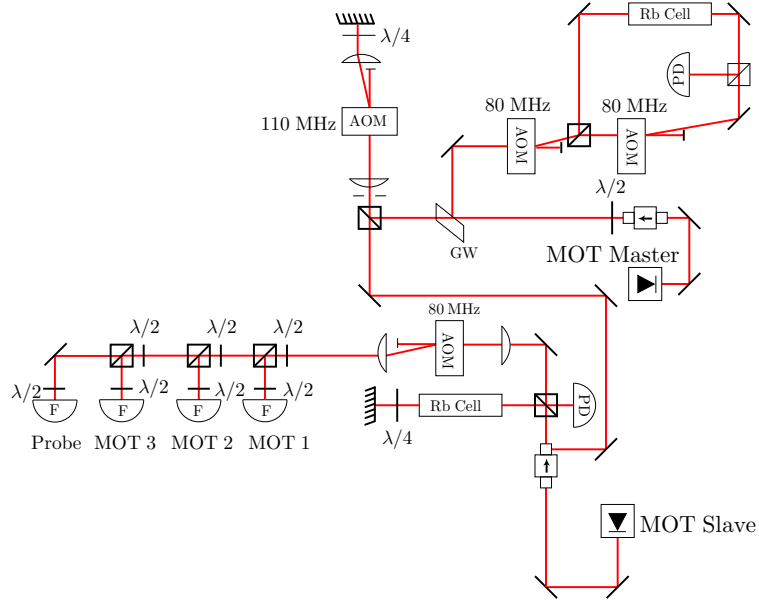


**Figure 4.4:** The optical setup for the MOT laser system where a stabilized ECDL diode laser is used to injection lock a slave laser. A double passed AOM is used to adjust the frequency of the injection locking beam that is sent to the slave diode. After the slave diode, an additional AOM is used to control the beam power. The slave laser is split into four beams and then coupled to four single mode fibers. Three of these beams are used to produce the MOT, while the fourth beam is used to generate the cavity cooling beams. A shutter is placed before each fiber coupler to switch off the beams. In the schematic the following abbreviations are used: F-polarization maintaining fiber, GW-glass wedge,  $\lambda/2$ -half wave plate,  $\lambda/4$ -quarter wave plate and PD-PDA55 photo-detector. Each of the lenses is 150 mm.

The beam from the slave laser diode passes through an optical isolator and an AOM before it is split into four fibers. The AOM, along with shutters before the fibers, controls the optical power sent to the experiment. Each of the first three fibers typically have an output of 8 mW. These fibers are used to make the MOT while the fourth fiber is used to

generate the cavity cooling beams.

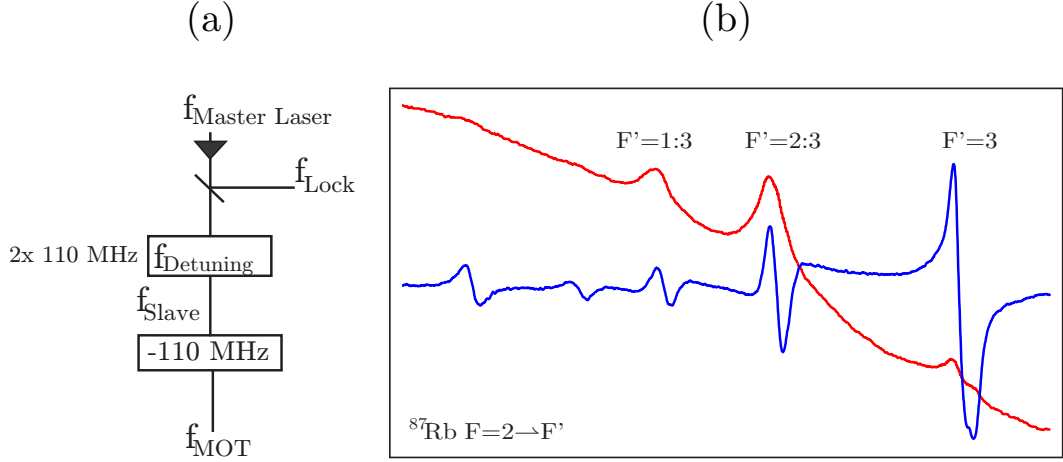


**Figure 4.5:** (a) The detuning setup for the MOT laser beams. (b) The  $F=2 \rightarrow F'$  transitions (MOT Transitions) in  $^{87}\text{Rb}$ . The 2:3 and 1:3 transitions are the crossovers peaks of the real transitions. The red curve shows the saturated absorption spectrum, and the blue curve is the FM spectroscopy signal used to stabilize the laser frequency. The frequency spacing of the transitions can be determined using Figure 4.2.

Normally, the MOT beams are red detuned from the cycling  $F = 2 \rightarrow F' = 3$  transition. The frequency detuning setup can be seen in Figure 4.5 (a). In this configuration, the MOT laser frequency can be tuned quickly by changing a double passed AOM frequency to detune the MOT beams from  $-100$  MHz to  $+10$  MHz from the cycling transition.

#### 4.4.2 Repump Laser System

The optical setup for the repump laser is presented in Figure 4.6. The repump slave is seeded by a master ECDL, which is locked 80 MHz below the  $F = 1 \rightarrow F' = 2$  transition of  $^{87}\text{Rb}$ .

The slave output is split into two beams that are fiber coupled, which provide repump light for the cavity cooling beams and for the MOT. The MOT operates with 8 mW of repump light, and an AOM before the repump fiber controls the optical power sent to the experiment. During optical trap loading, the power is reduced to  $12 \mu\text{W}$  40 ms before the MOT beams are turned off to allow the atoms to fall into the  $F = 1$  ground state. The detuning scheme of the repump laser system is displayed in Figure 4.7 (a).

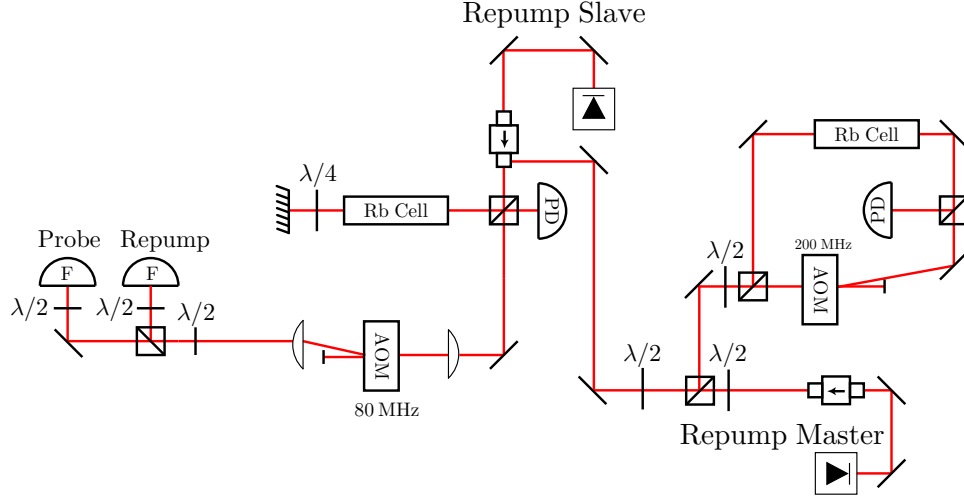


**Figure 4.6:** Optical setup for the repump laser system. An ECDL diode laser that is stabilized to a rubidium transition injection locks a slave laser. Before the slave laser is fiber coupled an 80 MHz AOM brings the laser’s frequency resonant with the  $F = 1 \rightarrow F' = 2$  transition.

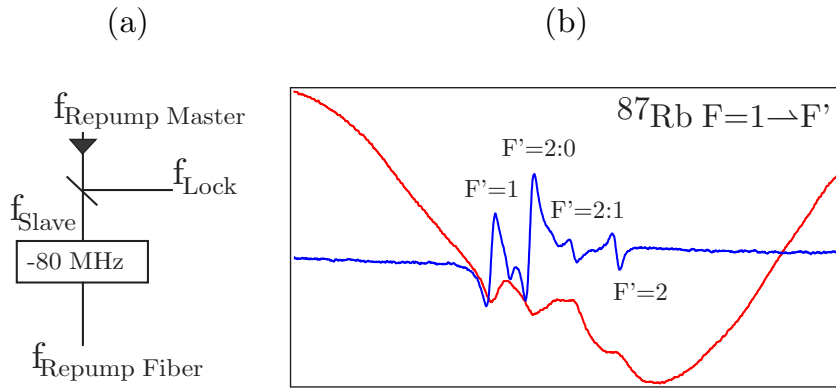


**Figure 4.7:** (a) The detuning setup for the repump laser. (b) The repump master error signal in blue and saturated absorption spectroscopy signal in red. The frequency spacing of these transitions can be determined using Figure 4.2.

#### 4.4.3 Cavity Laser System

In order to study an atom interacting with a cavity photon, we must make sure that the photon’s frequency is fixed by stabilizing the length of the cavity. Since changes in length modify the coupling between the atom and the field, it is of utmost importance to stabilize the cavity to well within its linewidth.

In our previous experiments, the science cavity light was used to stabilize the cavity [57],

a technique that has associated difficulties. This requires a more complicated locking circuit where a blanking signal is sent to the cavity's locking circuit when atoms reach the cavity. This zero volt blanking signal tells the servo system to feedback nothing and relies on the passive stability of the cavity to keep the length constant. This scheme is sufficient for short time scales, on the order of milliseconds, but it is difficult to design a system that is stable to a cavity linewidth over a timescale of seconds.

A simple calculation of the linewidth in terms of length will illustrate the performance requirements required to stabilize the cavity. The cavity has a length,  $L = q \frac{\lambda_0}{2}$ , where  $\lambda_0$  is a resonant wavelength that corresponds to the resonant frequency,  $\omega_0$ , and  $q$  is an integer mode number. The differential length per frequency is given by,

$$\frac{dL}{d\omega_0} = \frac{dL}{d\lambda_0} \frac{d\lambda_0}{d\omega_0}, \quad (4.1)$$

where,  $\frac{dL}{d\lambda_0}$  and  $\frac{d\lambda_0}{d\omega_0}$  are given by the following expressions

$$\frac{d\lambda_0}{d\omega_0} = -\frac{\lambda_0^2}{2\pi c}; \quad \frac{dL}{d\lambda_0} = \frac{L}{\lambda_0}. \quad (4.2)$$

So if the cavity changes by  $\Delta\omega_0 = \kappa$ , i.e. a linewidth, the resulting change in length is given by,

$$\Delta L = \frac{\lambda_0}{8\pi\mathcal{F}}, \quad (4.3)$$

where  $\kappa$  is replaced by  $\kappa = \frac{C}{4\mathcal{F}L}$  from Eq. (3.15).

For a finesse of  $\mathcal{F} = 10^4$  and  $\lambda_0 = 780.246$  nm, this gives,

$$\Delta L = 3.10 \times 10^{-12} \text{ m} \approx 3 \text{ pm}. \quad (4.4)$$

This is 3 *picometers*! The average atomic radius is  $\sim 1 \text{ \AA}$  ( $10^{-10}$  m), so this length stability requirement is 1/100 of the size of an atom.

With this length stability as a motivation, we developed an active locking system. The idea is to make two lasers resonant with the science cavity. One laser is resonant with the atoms, while the other laser is also resonant with the cavity but not the atoms. This second laser is used to actively stabilize the cavity length.

To accomplish this an addition laser system is needed that consists of two diode lasers: the cavity probe laser and the transfer diode laser, and two cavities: the transfer cavity and the science cavity. In Figure 4.8, the optical setup of the cavity laser system is depicted.

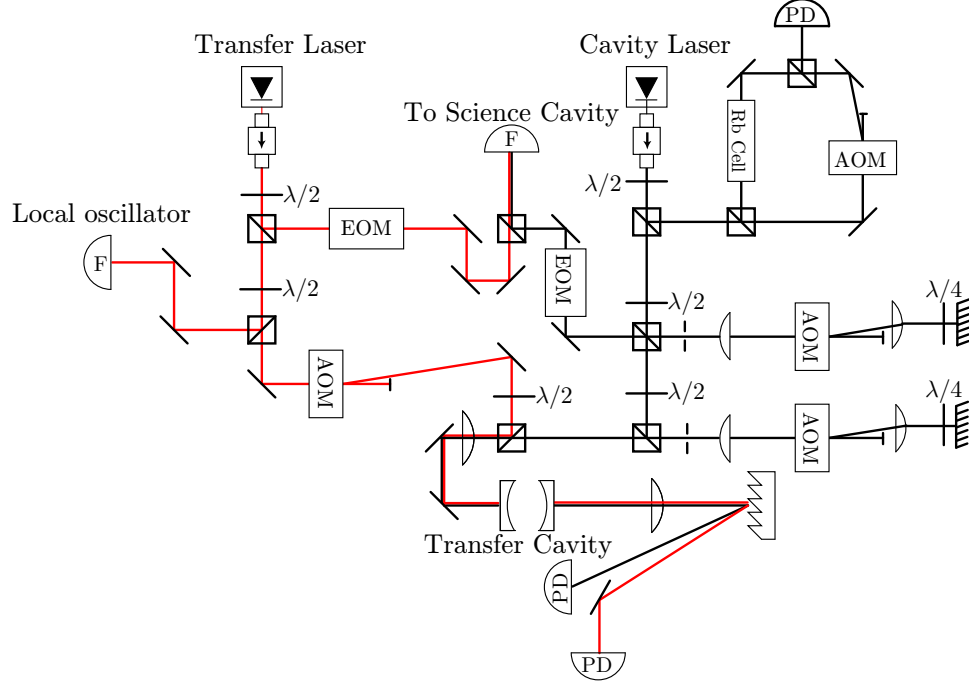


**Figure 4.8:** Optical setup of the cavity probe laser, transfer cavity, and transfer laser. The cavity probe laser is locked to rubidium and then locks the transfer cavity. Next, the transfer laser is locked to the transfer cavity; this fixes the frequency separation of the two laser beams to an integer number of the science cavity free spectral ranges.

The idea of using a transfer cavity has been introduced by many different groups [74, 75, 76]. This cavity is used to transfer the frequency stability from one laser to another laser. Explicitly in this setup, the transfer cavity transfers the frequency stability of a laser stabilized to a rubidium transition to another diode laser with wavelength,  $\lambda_{\text{Transfer}}$ . This new wavelength,  $\lambda_{\text{Transfer}}$ , can be any wavelength, with the only condition that it must produce a signal from the transfer cavity.

The cavity diode laser probes atoms in the science cavity and stabilizes the transfer cavity. This laser is a standard ECDL laser that is stabilized to the  $F = 3 \rightarrow F' = 4 : 2$  cross over of  $^{85}\text{Rb}$ . With a double-passed AOM and an electro-optic modulator (EOM), the laser frequency is brought into resonance with the  $F = 2 \rightarrow F' = 3$  transition of  $^{87}\text{Rb}$ . The

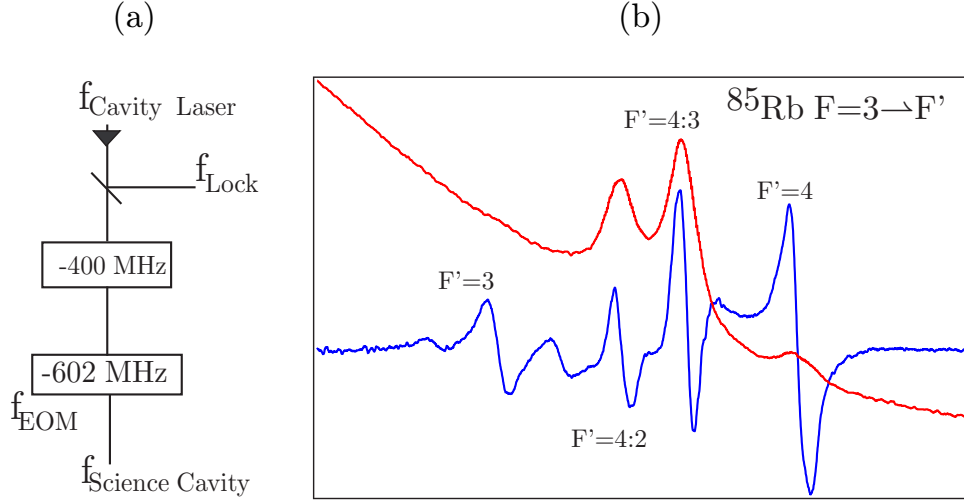


**Figure 4.9:** (a) The cavity laser’s probe detuning setup. (b) The saturated absorption spectroscopy of the  $^{85}\text{Rb}$   $F = 3 \rightarrow F'$  transition in red. The FM spectroscopy locking error signal is shown in blue.

reason to lock on rubidium-85 is to ensure that the other sidebands from the EOM are not accidentally resonant with other  $F = 2 \rightarrow F'$  transitions in  $^{87}\text{Rb}$ .

The second laser is known as the transfer diode laser, which is designed to be co-resonant with the cavity probe laser in the science cavity. This requires the transfer diode to be an integer number of free spectral ranges of the science cavity detuned from the probe laser. The laser wavelength is set to be three free spectral ranges of the science cavity detuned from the cavity probe laser, giving a wavelength of  $\lambda_{\text{Transfer}} = 784.314$  nm. At this wavelength, no rubidium atomic line exists to stabilize this laser, so it is stabilized using the transfer cavity.

The science cavity locking protocol is as follows:

### 1. Lock Cavity Probe Laser

As mentioned above, the cavity probe laser is stabilized to rubidium-85 via FM spectroscopy.

### 2. Lock Transfer Cavity

The stabilized cavity probe laser is used to lock the transfer cavity. The technical details are developed in section 4.5.4.

### 3. Lock the Transfer Laser to Transfer Cavity

The transfer laser is locked to the stabilized transfer cavity. The transfer laser and the cavity probe laser have a fixed frequency detuning that is set to be an integer number of free spectral ranges of the science cavity.

### 4. Lock the Science Cavity with Transfer Cavity

The science cavity is locked to transfer laser. This cavity length is also resonant with the  $F = 2 \rightarrow F' = 3$  transition of  $^{87}\text{Rb}$ .

Due to the cascading nature of the locking, the stability of the science cavity is only as stable as the weakest lock. Therefore, care has to be taken in each step to minimize unwanted technical noise in the servo systems. Technical noise that is introduced at any stage of the locking protocol will cascade down and eventually add noise to the science cavity lock.

## 4.5 Cavities

In this section, we will review the construction and stabilization of the Fabry-Perot cavities used in the experiments described in this thesis. The high finesse optical cavities are constructed using the same techniques presented in the thesis by Jacob Sauer [57].

### 4.5.1 Science Cavity Construction

Cavity stability begins with a good mount that is passively stable against vibrations. Three major designs for cavity mounts have been implemented, each with advantages and disadvantages.

The mirrors for the science cavity are made by Research Electro-Optic (REO). For each coating run, the reflectivity and radius of curvature for each mirror are specified and then coated by REO on a substrate with a diameter of 7 mm. In order to build short cavities, we need to have small mirror diameters. To achieve this, REO cones the mirrors down to a 3 mm diameter shank with a 1 mm diameter coned coated region. These mirrors are difficult to clean and this topic is highlighted in many student theses [57, 77, 78, 79].

Both science cavity mounts share three common features. First, they are all constructed

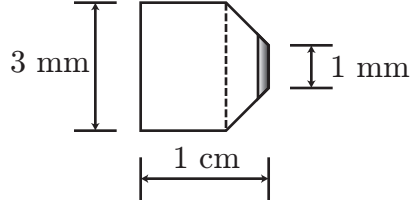


**Figure 4.10:** A coned down cavity mirror used for the science cavity. The shank of the mirror has been ground down to 3 mm and the coated portion to 1 mm. (Note: Drawing not to scale)

from a dense material to provide a large mass and a low resonance frequency of the mechanical system. For a simple harmonic oscillator, the resonance frequency is given by,

$$\omega = \sqrt{\frac{k}{m}} . \quad (4.5)$$

The larger the mass for the same spring system, the lower the resonant frequency. All the cavity mounts are constructed using oxygen free copper which is a dense UHV compatible material.

Second, there needs to be a method to change the length of the cavity. In order to scan the cavity length, the mirrors are glued to a PZT using Torr-Seal<sup>®</sup>. Using a diamond saw, sand paper, and patience, the PZT is shaped to fit the mount design. The PZT ceramic is made from Lead Zirconate Titanate (C5500) and purchased from Channel Industries. The mechanical properties of the PZT are derived from piezoelectric constants and the dimensions.

Finally, all cavity mounts need some form of vibration isolation. For this, we have used Cu-Be springs and RTV (a high temperature silicone). The following section presents the three high finesse cavity mounts that have been constructed.

**Cavity Mount 1:** The first mount used can be seen in Figure 4.11. This mount was machined from oxygen free copper and suspended by springs. As Sauer reported in his thesis, this mount had good passive stability [57].

**Cavity Mount 2:** A drawing of the current cavity design can be found in Figure 4.12. This mount has the advantage of allowing one to move the optical trap above the

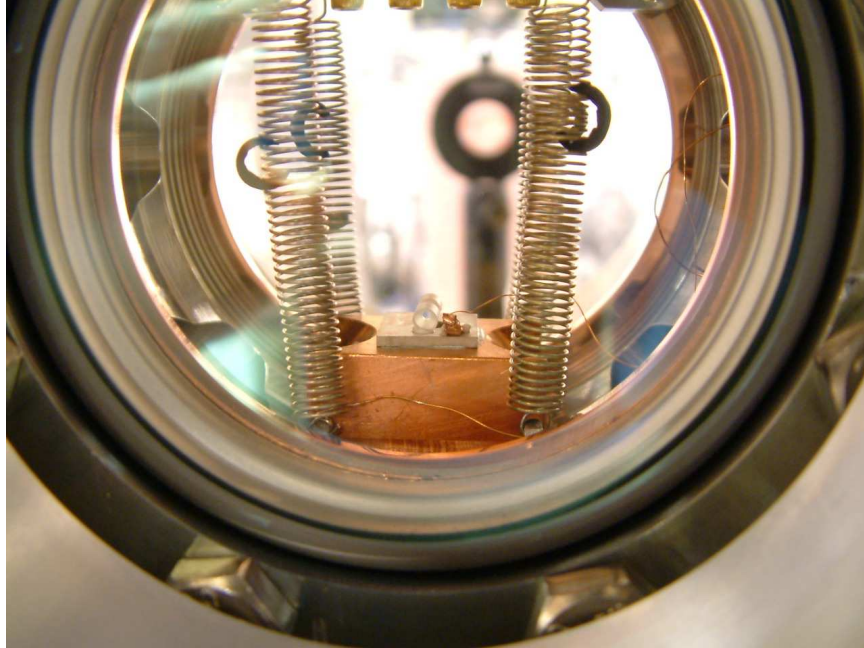


**Figure 4.11:** A high finesse optical cavity suspended from vibration isolation springs. The springs are constructed from Cu-Be springs to minimize shaking of the cavity when the MOT coils are turned on and off.

cavity and perform cavity independent measurements. The skiff is constructed from oxygen free copper and damping is provided by RTV, which is attached to the bottom of the skiff. The RTV is produced by Dow Corning (736) and is a silicone with a low Young's modulus, which provides good vibration isolation. Since RTV is typically not compatible with UHV applications, it is pre-baked to drive off any volatile elements.

#### 4.5.2 Science Cavity Stabilization

Figure 4.13 shows the optical setup for the science cavity. The transfer and cavity probe laser lights are brought to the experimental setup by a single mode fiber. The two colors of light are cross-polarized in the optical fiber and, after mode matching optics, both lights are coupled into the science cavity. After the science cavity, the light is split into two branches using polarization optics. The science light, at 780.246 nm, is sent directly into a fiber which is coupled to a photon counter for detection.

The locking light is detected via heterodyne detection, which is a technique that relies on interference to detect weak signals. In heterodyne detection, the interference between

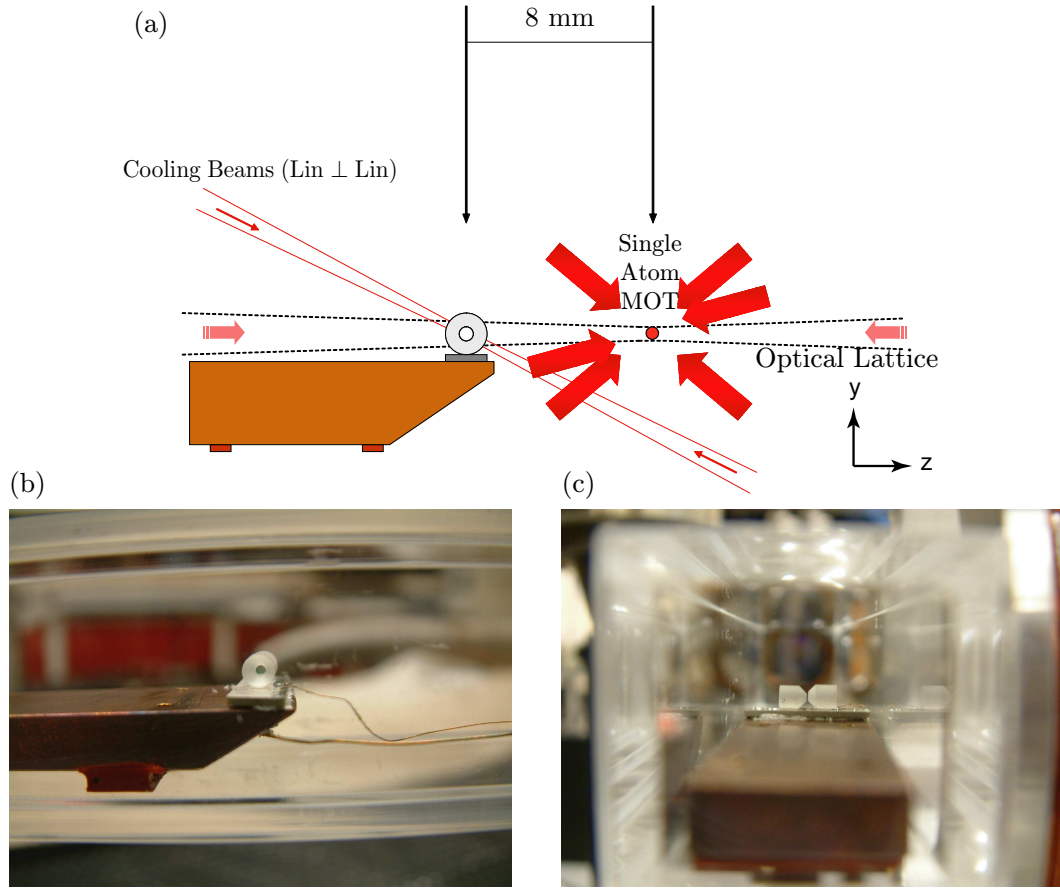


**Figure 4.12:** (a) Experimental schematic for the skiff mount. The MOT is produced 8 mm away from the cavity via a 6 beam MOT. The 1-D walking wave optical trap is used to transport the atoms 8 mm to the optical cavity. The cooling beams are at an angle of approximately 45 degrees from the optical lattice axis and intersect the cavity mode. (b) A photograph of the skiff mount. (c) A photograph looking down the optical lattice axis.

the weak signal and a reference beam is monitored, where the reference beam is used as a local oscillator. The interference is produced by mixing the two lights on a beam splitter. The signal field is detected by monitoring the interference between the two beams on a photo-detector [44].

In the heterodyne setup, seen in Figure 4.13, the signal light passes through an optical isolator to eliminate back reflections into the photon counter. After the isolator, the locking light signal is mixed with the local oscillator on a beam splitter. To achieve maximum spatial overlap, both lights are coupled into a single mode optical fiber. This fiber is then connected to a fiber coupled photo-detector (EOT-2030).

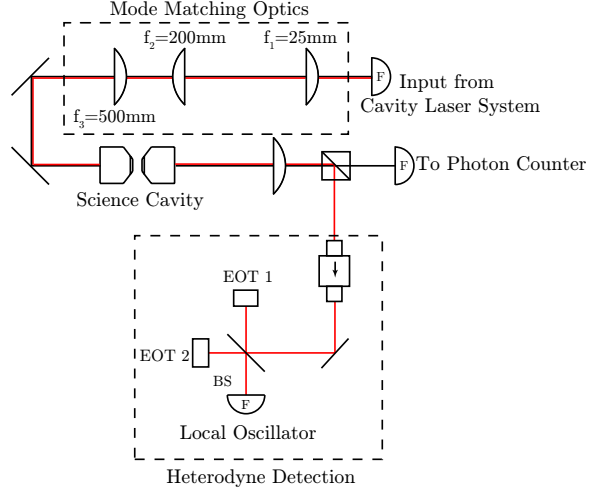


**Figure 4.13:** The science cavity optical setup. Light emitted from a fiber coupler is mode matched to the Gaussian mode of the Fabry-Perot Cavity. In the fiber, the cavity probe light is horizontally polarized while the stabilization light, the transfer laser, is vertically polarized. The transmission from the science cavity is then split into the stabilization light and the science light. The stabilization error signal is produced from the heterodyne detection, while the science light is sent to the photon counter.

The transfer diode beam passes through an EOM before it combines with the cavity probe light. This EOM serves two purposes. First, it provides a fine adjustment to ensure that the cavity probe and transfer diode are co-resonant in the science cavity. Second, it provides three different transfer diode frequencies in the science cavity.

The beams in the science cavity are the  $+\kappa$  beam, the intra-cavity dipole beam, and the  $-\kappa$  beam. The intra-cavity dipole beam is resonant with the cavity and provides an intra-cavity dipole trap. The two  $\pm\kappa$  beams provide the locking signal for the science cavity. Figure 4.14 shows the spectrum of the three beams where the locking signal is generated by subtracting the signal of the  $+\kappa$  beam heterodyne from that of the  $-\kappa$  beam signal. Performing this gives us a dispersive error signal to lock the science cavity, which is shown in Figure 4.14 (b).

To generate the error signal from the heterodyne setup, the output of the EOT-2030 photodiode is sent through a bias-T (Mini-Circuits ZFBT-4R2GW) and two 24 dB RF amplifiers (Mini-Circuits ZFL-500LN). To account for phase mismatches, one of the photocurrents from EOT 2 is sent through a digital delay line which is used to match the

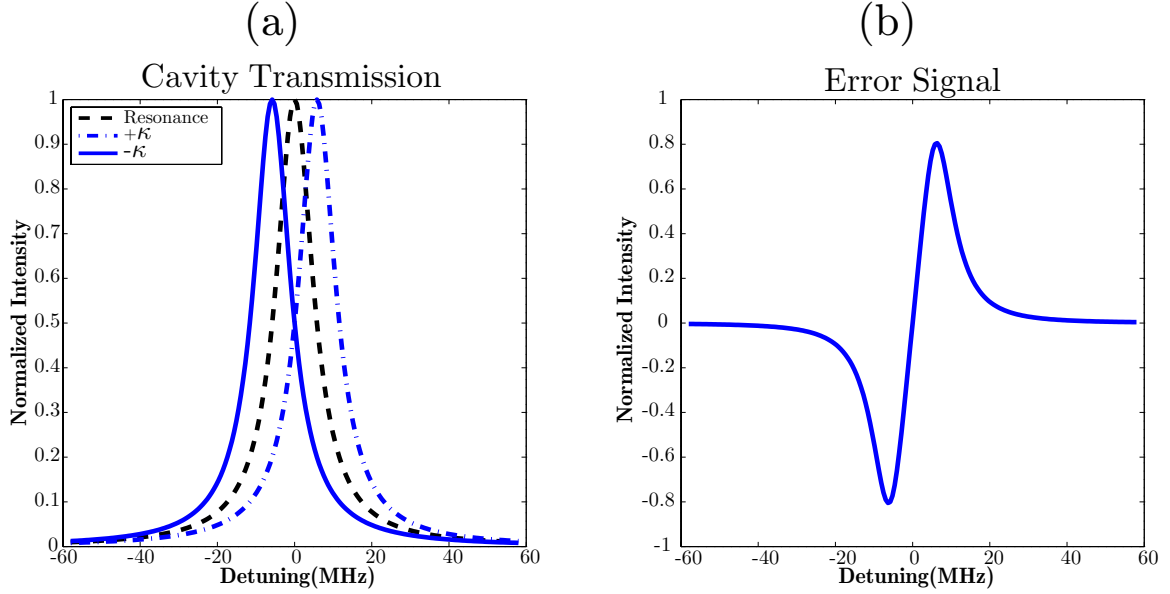


**Figure 4.14:** (a) The spectrum of the three transfer laser lights that are incident on the science cavity are shown. The two locking lights that are  $\pm\kappa$  and the intra-cavity dipole light. (b) The subtraction of the locking beams to produce the error signal. For these calculations,  $\kappa = 13.6$  MHz.

phases. The two photocurrents are combined with a RF combiner (ZFSC-2-11). The RF electrical setup can be found in Figure 4.15.

Two spectrum analyzers (HP 8590L) are set to zero span, so they act as FM receivers at the frequencies of the locking beams with a 10kHz video and resolution bandwidth. In normal operation, the center frequencies are set to  $\pm\kappa$ , but the cavity can still be locked with sidebands set to  $\pm 3\kappa$ . The video out of both spectrum analyzers is sent to an SRS preamp (SRS 560), and the two signals are low pass filtered at 3 kHz and subtracted to produce a dispersive error signal. This error signal is then sent to a PI lockbox which locks the cavity.

### 4.5.3 Science Light Detection: Photon Counting

The photon counting of the science light is performed using a single photon counting module from PerkinElmer (model SPCM-AQR-13-FC). These photon counting modules are fiber coupled, with a maximum dark counts of 200 per second. Typically photons are counted with bin times, or integration times, of  $10 \mu\text{s}$  - 20 ms. At the largest bin time (20 ms), there

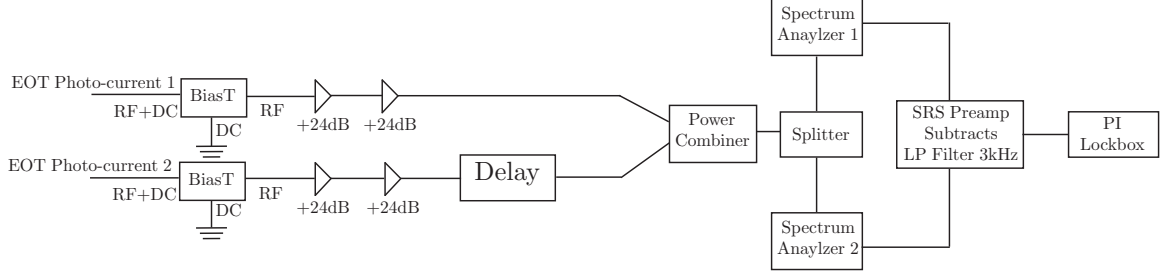


**Figure 4.15:** Heterodyne RF setup for de-modulating the cavity transmission. Light from two single mode fibers are incident on EOT detectors 1 and 2. Each signal is amplified and then recombined. Two RF spectrum analyzers in zero span mode act as FM receivers to the heterodyne signal. Before a PI lockbox, a SRS preamp subtracts the two signals and low pass filters the signal with a roll-off frequency of 3 kHz.

are 0.4 dark counts per bin time, so dark counts are not a significant noise source.

The detection efficiency is measured by comparing the light emitted from the science cavity to the percentage of light that is coupled into the photon counting fiber. This measurement is performed by inserting a flip-up mirror before the polarizing beam splitter in Figure 4.13. With the mirror flipped up, the output of the science cavity is measured with a photodiode, PDA55. With the mirror flipped down, the light is fiber coupled and measured using a fiber coupled PDA55. The typical fiber coupling efficiency is 45%. The photon counters have a quantum efficiency of 0.5 counts/photons which results in a detection efficiency of  $\eta = 0.225$  counts/photon.

To separate the science light (780 nm) from the locking light (784 nm), polarization sensitive optics are used. These polarization optics are only 95% efficient in attenuating the undesired polarization, so laser line filters are used to prevent the locking light from getting into the photon counter. The laser line filters are purchased from Semrock (Max-Line Laser-Line Filter LL01-780-12.5), and have a high throughput (95%) with a narrow bandwidth (1 nm). To attenuate the 784 nm light, two filters are placed back-to-back, resulting in an attenuation of 6 orders of magnitude (OD 6).

#### 4.5.4 Transfer Cavity Construction

The transfer cavity is constructed from mirrors coated by VLOC, with a radius of curvature of 25 cm and transmission losses of 1% (i.e. R=99%) at 780 nm. The cavity was designed

to have a free spectral range of 1 GHz. The properties of the transfer cavity are,

$$\begin{aligned}
 L &= 15 \text{ cm} \\
 \nu_{\text{FSR}} &= 1.0 \text{ GHz} \\
 \mathcal{F} &= 300 \\
 \kappa &= 1.8 \text{ MHz} .
 \end{aligned}$$

The cavity is constructed using a Thorlabs aluminum lens tube and is scanned using a cylindrical PZT. Due to its construction from aluminum, the transfer cavity is sensitive to temperature drifts. The linear thermal expansion is given by [80],

$$\frac{\Delta L}{L} = \alpha \Delta T , \tag{4.6}$$

where  $\alpha$  is the coefficient of thermal expansion. For aluminum,  $\alpha_{\text{Al}} = 23 \times 10^{-6} / ^\circ\text{C}$ .

The locking circuit can output a voltage range of 30 V, which corresponds to a total length change of the PZT of,  $\Delta L = 5.6 \text{ nm}$ . In terms of temperature, the locking circuit can stabilize against a change of temperature of only 1.67 mK. Because of this small temperature range, the transfer cavity is passively temperature stabilized by isolating it from the lab environment. The cavity is wrapped in thermal insulation, and then placed in a sealed plastic PVC tube to isolate the cavity. This passive isolation allows the cavity to remain locked for approximately 30 minutes before the integrator range needs to be reset.

Constructing a transfer cavity from a material with smaller coefficient of thermal expansion would increase the locking range. Super-Invar<sup>TM</sup> has a very low coefficient of thermal expansion,  $\alpha_{\text{SuperInvar}} = 0.66 \times 10^{-6} / ^\circ\text{C}$ . Since the coefficient of thermal expansion of Super-Invar<sup>TM</sup> is approximately 40 times smaller than that of the aluminum, this allows the integrator to compensate for a temperature drift of approximately 58.7 mK. Such a transfer cavity has been constructed and tested, but has yet incorporated in the experiment.

#### 4.5.5 Transfer Cavity Stabilization

The transfer cavity is locked by the cavity probe laser. The transfer laser and the cavity laser are combined on a beam splitter and then are coupled into a single mode fiber. At the

transfer cavity, a mode matching lens is placed to match the cavity's waist. The two colors of light are separated in transmission by a diffraction grating (Edmund optics 1800 lines/mm), and the beams are allowed to propagate  $\sim 0.5$  m before the beams are able to be picked off into two separate Thorlabs PDA55 detectors.

Each of the lasers are separately modulated via AOMs to perform FM spectroscopy. The transfer cavity length is stabilized by locking the length to the cavity probe laser using the Pound-Drever-Hall (PDH) technique [81, 82] and PI servo circuit.

#### ***4.6 Optical Trap Lasers***

In the history of the cavity QED experiment at Georgia Tech, a number of laser systems have been used for optical trapping. Jacob Sauer's thesis describes optical trapping with a titanium sapphire laser and optical traps constructed from 850 nm diode-seeded tapered amplifier systems [57]. The work performed in this thesis builds on the knowledge gained by Sauer but leaves the details of the previous traps to his thesis. This section focuses on the experimental setup for a new optical trap built with a Ytterbium (Yb) doped fiber laser.

The fiber laser was purchased from IPG photonics, model number YAR-20-LP-SF. The laser's specifications are as follows: 20 Watts of output power with single frequency output and linearly polarized. The laser operates at the Nd:YAG wavelength of  $\lambda = 1064$  nm. To control the optical power in real time, AOMs from IntraAction Corp (AOM-40) are used with RF attenuators from Mini-Circuits (ZX73-2500).

The RF frequency for the AOMs is provided by phase locked HP oscillators (HP 8647A and HP E4430B). A very stable GPS satellite based 10 MHz reference (EndRun Technologies Præcise Gfr) provides the frequency reference to phase lock these two oscillators. A frequency difference between the two AOMs is used to translate the atoms in the lattice. Typical atom transport is done with difference frequencies of 50 kHz to 70 kHz. The optical setup can be seen in Figure 4.16.

The output from the fiber laser passes through two optical isolators to protect the laser before its split into two trapping beams, Trap 1 and Trap 2. In order to send probe ( $F = 2 \rightarrow F' = 3$ ) and repump ( $F = 1 \rightarrow F' = 2$ ) light on the optical trap axis, dichroic

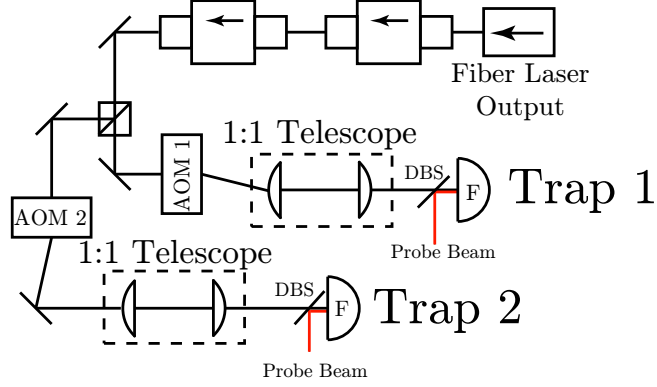


**Figure 4.16:** Optical setup for Yb doped fiber laser optical trapping system. The output of the fiber laser is sent through two isolators to protect the laser from the back reflections. Then the beam is split into two trap beams and sent through two phase locked AOMs. The light is then fiber coupled after a Dichroic Beam Splitter (DBS), where probe light is coupled into the fiber.

beam splitters (DBS) are used to combine these beams with the fiber laser. The combined beams (fiber laser, probe and repump) are coupled into large mode diameter polarization maintaining fibers from Nufern (FUD-3460 PM085-LNA) using 1:1 telescopes to maximize the collimation for greater coupling efficiency.

After the optical fiber, the beam is sent through a system of three lenses: the beam is expanded and then focused down to a waist of  $w_0 = 26.9 \mu\text{m}$  by the final 350 mm lens. All lenses in this optical setup are achromatic lenses to reduce aberrations. Figure 4.17 shows the optical setup for the cavity QED experiment. In this schematic, the path of the optical trap optics is shown as it passes through the UHV vacuum chamber. Also this schematic shows the MOT beams, the science cavity mount and the CCD detection.

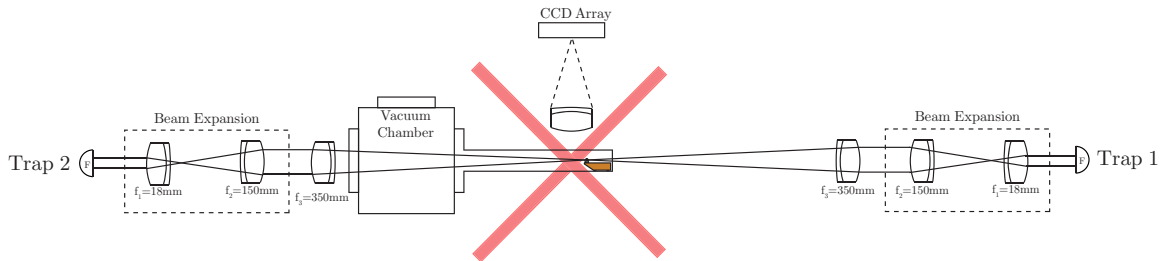


**Figure 4.17:** Optical setup for producing the optical trap. The two lattice beams each come from independent fibers and are focused down to a waist,  $w_0 = 26.9 \mu\text{m}$ . Also shown is the cavity, the MOT beams, imaging objective and CCD.

## 4.7 CCD Imaging Setup

In order to image single atoms, one needs to collect a large percentage of the solid angle with the imaging lens. The numerical aperture of the lens sets the resolution limit of the imaging system by defining a minimum spot size and depth of focus. Imaging objectives are specified by either the numerical aperture or the related parameter, f-number ( $f/\#$ ). The f-number and numerical aperture are related by [44],

$$f/\# = \frac{1}{2NA} = \frac{f}{D}, \quad (4.7)$$

where  $NA$  is the numerical aperture,  $f$  is the focal length and  $D$  is the clear diameter of the lens.

The minimum focus spot size is given by [44],

$$w_{\min} = \frac{2}{\pi} \lambda f/\#. \quad (4.8)$$

The depth of focus of the imaging system is twice the Rayleigh range,

$$2z_R = \frac{8}{\pi} \lambda (f/\#)^2. \quad (4.9)$$

The imaging technique used in this thesis is fluorescence imaging, where photons scattered from the atoms are collected with a lens. Atoms spontaneously emit photons in a randomly in all directions. To determine the calibration of the imaging system, i.e ratio of collected photons to number of atoms, the collection efficiency must be computed. This geometrical calculation can be computed with the aide of Figure 4.18.

The percent solid angle,  $\Omega$ , is given by,

$$\% \Omega = \frac{\pi \left(\frac{D}{2}\right)^2}{4\pi f^2} = \frac{NA^2}{4} \quad (4.10)$$

From Eq. (4.10), one can see that the larger the numerical aperture, the larger the percentage of solid angle that is collected by the imaging system, which in turns means more photons are collected from the atoms.

For this thesis, two basic lenses have been used for imaging; a high aperture laser objective (HALO) from Linos Optics (Part #03 8903) and a microscope objective from

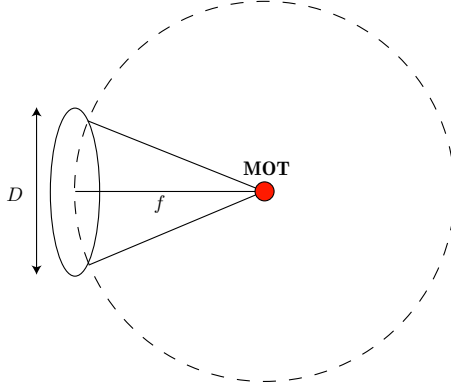


**Figure 4.18:** Geometric diagram to compute the percent solid angle.

**Table 4.1:** Parameters for the two imaging lenses.

objective	HALO	Mitutoyo Objective 5x
working distance	16.55 mm	37.5 mm
focal length ( $f$ )	30 mm	40 mm
N.A.	0.38	0.14
$w_{min}$	0.654 $\mu\text{m}$	1.77 $\mu\text{m}$
Depth of focus ( $z_R$ )	1.720 $\mu\text{m}$	12.67 $\mu\text{m}$
% SA	0.0361	0.0049

Mitutoyo Corp. (M Plan Apo NIR 5x). The specifications of these lenses is presented in Table 4.1.

As one can see from Table 4.1, the working distance of the HALO lens is much smaller than that of the Mitutoyo objective. To focus on the MOT properly the HALO lens is only a few millimeters from the quartz cell. This limits the steepness of the angle of the MOT beams and in turn, sets the distance between the MOT and the cavity. Here we have elected to lose some collection efficiency to have a lens with a larger working distance.

The light coming from the MOT is collimated by the objective lens. It is then focused down onto a Andor Ixon CCD camera with a 75 mm achromatic lens. The imaging system also has a laser line filter from Semrock to cut out background and optical trapping light. The Andor CCD has 16  $\mu\text{m}$  square pixels, which combined with magnification of imaging system, 1.88 $\times$ , yields an effective pixel size of 8.53  $\mu\text{m}$ .

## 4.8 Quantitative Analysis of Images

### 4.8.1 Number

The number of spontaneously emitted photons is [30],

$$\gamma_{sp} = \frac{s_0\gamma/2}{1 + s_0 + (2\delta/\gamma)^2} , \quad (4.11)$$

where  $\delta$  is the detuning from resonance,  $\gamma$  is the natural linewidth of that atom and  $s_0$  is the on-resonance saturation parameter. The on-resonance saturation parameter,  $s_0$ , is the ratio of the intensity of the applied laser beam to the saturation intensity. This can be related to the Rabi frequency,  $\Omega$  by

$$s_0 = \frac{2|\Omega|^2}{\gamma^2} = \frac{I}{I_s} \quad (4.12)$$

Finally, the saturation intensity is constructed from physical constants and atomic parameters. The saturation intensity is defined by,

$$I_s \equiv \frac{\pi\hbar c}{3\lambda^3\tau} , \quad (4.13)$$

where  $\tau$  is the lifetime of the transition. For  $^{87}\text{Rb}$ , the saturation parameter is approximately  $1.60 \text{ mW/cm}^2$ .

The number of photons collected on the camera is,

$$\# \text{ photons} = \eta \gamma_{sp} N_{\text{atoms}} t_{\text{exp}} , \quad (4.14)$$

where  $t_{\text{exp}}$  is the exposure time and  $\eta$  is the detection efficiency. Therefore, by measuring the number of photons collected, the percent solid angle, and by computing the scattering rate, one can determine the number of atoms in an image.

### 4.8.2 Temperature

Thermal atoms released from a trap (optical or magnetic) expand and fall due to gravity. Using this Time-of-flight (TOF) imaging it is possible to extract the atom number and temperature of the atoms. The width of the Gaussian distribution of atoms is given by,

$$\sigma^2 = \sigma_0^2 + \frac{k_B T}{m} t^2 , \quad (4.15)$$

where  $\sigma_0$  is the width of the atomic cloud at  $t = 0$ ,  $k_B$  is Boltzmann's constant,  $T$  is the temperature of the gas,  $t$  is the expansion time, and  $m$  is the mass of the atom.

For thermal atoms, the expansion is isotropic, so one can collapse the 2-D image into 1-D and perform a Gaussian fit. From this fit, the temperature, the number of atoms and the initial size of the cloud can be extracted.

#### ***4.9 Computer Control***

The computer interface of the experiment involves three computers. The first computer controls the experiment via LabView using two 8-channel analog output cards (NI-6713 and NI-6733). A second computer is devoted to the Andor CCD camera and collects the data from the CCD camera. A third computer is used for collecting analog input (AI) from the photon counter. A counter on the AI card, NI-AT-MIO-16, records the signal from the photons counters with 100  $\mu s$  time bins. The data can then be post processed to integrate over larger times.

## CHAPTER V

### ATOM TRAPPING EXPERIMENTS

This chapter presents results from experiments in atom trapping. The chapter begins with results from optical trap lifetime and transport measurements. Then the ability to trap and detect individual atoms in a MOT is demonstrated. Finally, these single atoms are transferred and detected in an optical lattice. This non-destructive measurement in the optical trap leads to extremely long trap lifetimes.

#### *5.1 Optical Trap Diagnostics*

The first experiments that deterministically loaded atoms into a high finesse cavity were limited by the quality of the optical lattice. As noted by Jacob Sauer in his thesis, the traps had short lifetimes and atoms were lost as they were transported to the cavity [57]. Sauer developed a diode seeded tapered amplifier system that provided satisfactory lifetime and transport. This improved lifetime was due to the sub MHz linewidth of the diode system, and a smaller measured intensity noise compared to previous trapping lasers. This section presents results with two trapping systems, the tapered amplifiers and a Yb doped fiber laser that was implemented in August of 2005. To characterize the optical trap system, we are most concerned with the trap lifetime and the transport efficiency.

##### **5.1.1 Trap Lifetimes**

The number of atoms in a trap can be described as  $N = N_0 \exp(-t/\tau)$ , where  $N_0$  is the initial number of atoms and  $\tau$  is the lifetime of the trap. To measure the lifetime, the number of atoms is measured versus hold time and then fit to an exponential, from which the trap lifetime can be extracted. It should be noted that there can be different lifetimes for different loss processes.

There are many different heating mechanism that have been presented in the literature of optical traps. Heating can occur from off-resonance atomic absorption and emission of

trap photons [42], and from intensity and pointing instabilities of the trap laser [83]. It should be noted that these studies have primarily focused on single focus optical traps, not optical lattices. In addition to these problems, optical lattices are also sensitive to frequency noise of the trap laser. The limiting loss mechanism for all traps is background gas collisions.

To measure the lifetime, atoms are loaded into the optical trap and the number of atoms is recorded for different hold times. While a MOT of approximately  $10^6$  atoms is loading an optical trap is turned on. During loading, the MOT and the optical lattice are spatially overlapped. To prevent energetic, hyperfine state changing collisions [84], atoms are de-pumped into the  $F = 1$  state by turning off the repump light 40 ms before the MOT beams are extinguished.

Fluorescence imaging is used to measure the number of atoms where the trapped atoms are probed by the MOT beams, or by a probe beam along the optical trap axis. The scattered photons are collected by the imaging objective and recorded on a CCD camera. In Figure 5.1, the atom number is plotted versus hold time for the 852 nm tapered amplifier and the Yb doped fiber laser optical traps.

For the tapered amplifier system, the optical trap was constructed from two independent beams where each beam was constructed from an individual tapered amplifier chip. To ensure phase stability, both tapered amplifiers were seeded by the same master oscillator with wavelength 852 nm. These tapered amplifiers were fiber coupled with 120 mW per trap beam. The trapping parameters for this trap are,

$$\begin{aligned}
 U_{\text{MOT}} &= 26 \mu\text{K} \\
 U_{\text{cavity}} &= 206 \mu\text{K} \\
 \Gamma_{\text{sc}} &= 4 \text{ photons/s} \\
 w_{\text{cavity}} &= 24 \mu\text{m} ,
 \end{aligned}$$

where  $\Gamma_{\text{sc}}$  is the scattering rate at the deepest part of the potential (i.e. at the cavity).  $U_{\text{MOT}}$  and  $U_{\text{cavity}}$ , refer to the trap depth at the MOT and the cavity, respectively and the beam waist at the cavity is  $w_{\text{cavity}}$ . In Figure 5.1, the green dataset correspond to the

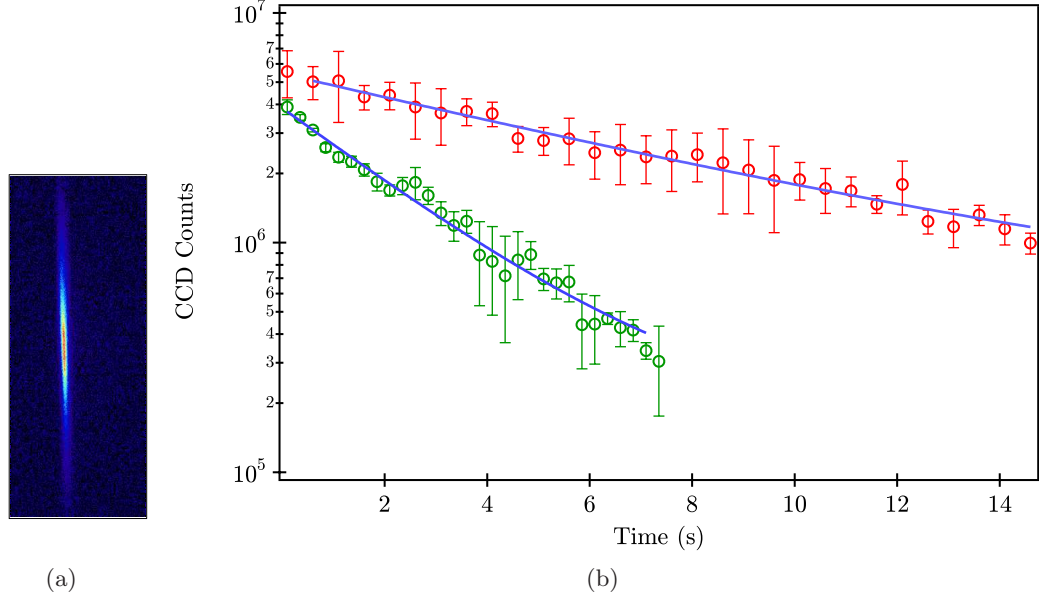


**Figure 5.1:** (a) A fluorescence image of atoms trapped in an optical lattice. (b) Lifetime measurements for atoms stored in a optical lattice constructed from 852 nm tapered amplifiers and a Yb doped fiber laser. The green dataset is for the 852 nm tapered amplifiers, with a corresponding lifetime of  $\tau = 2.58$  s. In the red dataset is the result for the Yb doped fiber laser lattice with a lifetime of  $\tau = 7.78$  s.

852 nm trap with a measured trap lifetime is,  $\tau = 2.58$  s.

The red data set in Figure 5.1 corresponds to a lifetime measurement made with the Yb doped fiber laser trap. This trap was built from two independent laser beams, with 700 mW per beam, resulting in trap parameters of,

$$\begin{aligned}
 U_{\text{MOT}} &= 16 \mu\text{K} \\
 U_{\text{cavity}} &= 381 \mu\text{K} \\
 \Gamma_{\text{sc}} &= 1.5 \text{ photons/s} \\
 w_{\text{cavity}} &= 24 \mu\text{m} .
 \end{aligned}$$

The measured lifetime of the trap was  $\tau = 7.78$  s.

The trap lifetime of the fiber laser is larger than the 852 nm tapered amplifier by approximately a factor of three. Both of these lifetimes are sufficient for the cavity QED experiment where atoms are transported to the cavity in 200 ms. The shorter lifetime of the tapered amplifier is still ten times longer than the transport time.

### 5.1.2 Atom Positioning Experiments

The walking-wave lattice is constructed from two independent laser beams where the frequency of these beam are controlled by phase locked AOMs. One of the AOMs has a tunable frequency, which can be tuned over  $\Delta\nu = \pm 1$  MHz. By introducing a frequency difference between the two beams, the nodes and the anti-nodes of the lattice translate. Since the atoms are trapped at the anti-nodes of the optical lattice, they are optically transported, with a velocity given by Eq. (2.47).

To measure the transport efficiency, atoms are transported a distance of  $z$  away from the MOT location, followed by a distance of  $-z$  to return the atoms to where they started. The number of atoms that survive the transport are compared to the number of atoms in the trap without transport. To cancel out any lifetime effects, both measurements are performed at the same time with respect to the MOT turn off. The loading of the optical trap is performed in the same manner as the lifetime measurement. Figure 5.2, plots the percentage of atoms that remain after transport at  $v \approx 5$  cm/s.

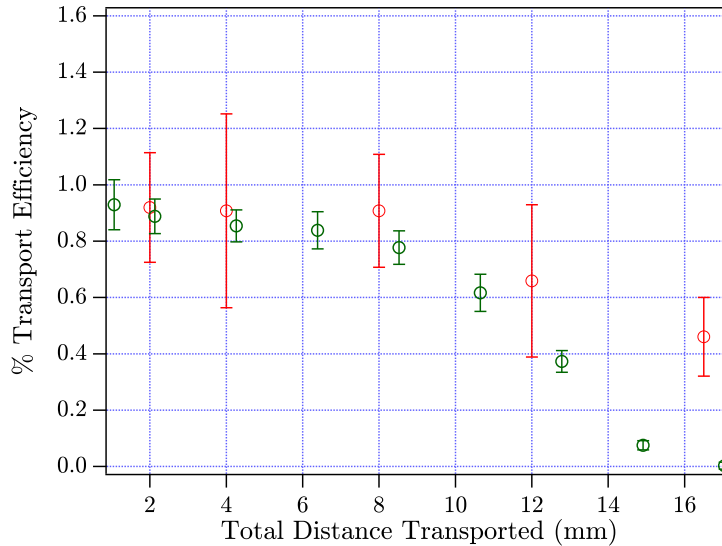


**Figure 5.2:** Atomic transport efficiency in the walking-wave lattice. The green data set shows the transport efficiency for the 852 nm diode laser trap. The red data set shows the results for the Yb doped fiber laser trap.

For the 852 nm lattice the MOT was located 5.6 mm away from the optical cavity, so a distance of 11.2 mm corresponds to travel to and from the cavity. This transport

had an efficiency of approximately 60%. For the fiber laser experiment, the MOT was located farther away from the cavity which is required to limit scatter of the MOT beams off the cavity. For the fiber laser trap the MOT was typically located 8 mm away from the cavity. So a transport of 16 mm corresponds to atom traveling to and from the cavity. The transport efficiency to and from the cavity for the fiber laser is 46%.

### 5.1.3 Imaging Atoms inside the Optical Cavity

With the current cavity mount design it is possible to image inside the cavity. By probing down the optical trap axis it possible to image atoms as they enter the cavity. Figure 5.3 shows approximately 1000 atoms as they enter the cavity after being transported 8 mm.

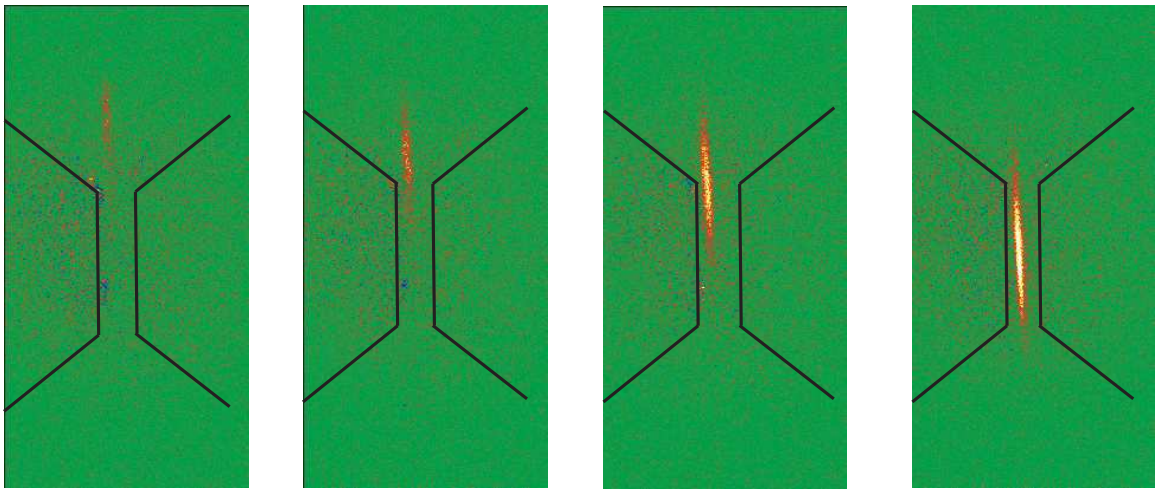


**Figure 5.3:** Atoms that have been transported 8 mm are imaged inside the cavity. The field of view is 3.2 mm in the vertical direction and 1.6 mm in the horizontal. The atoms appear weaker on the edge of the cavity because they are on the edge of the imaging field of view. Lines have been added to emphasize the location of the cavity mirrors.

## 5.2 Experiments with Single Atoms

The previous experiments started with a MOT formed with  $10^5 - 10^6$  atoms, where 10% of the atoms are loaded into an optical trap. By loading fewer atoms into the MOT and decreasing the transfer efficiency into the optical trap, single atoms can be loaded into the cavity. This top down approach starts with many atoms and then manipulates efficiencies to reach the single atom level.

In contrast, a bottom up approach has been developed which produces a single atom inside the optical cavity, by beginning with just a single atom in the MOT. This single atom is transported to, and detected by, the optical cavity. To pursue this new idea it became necessary to develop techniques to trap, detect and transport individual atoms.

### 5.2.1 Single Atom MOT Production

To construct the single atom MOT requires a large magnetic field gradient, on the order of 250 G/cm, which severely reduces the capture rate of the MOT [85], thereby limiting the average number of atoms loaded into the MOT. Constructing this large field gradient requires running 400 A through the MOT coils, which requires water cooling to prevent over heating the coils.

A second technical hurdle is the ability to detect single atoms. In order to detect individual atoms, a large percentage of the light scattered by the atoms needs to be collected. To accomplish this, a high numerical aperture microscope objective is used to collect the scattered light. These experiments take place in uncoated quartz glass cells where light scattered off the cell can mask the single atom signal. To minimize this scatter, the MOT beams are apertured down to an approximate 1-2 mm spot size.

The other main difference between a high gradient MOT and a low gradient MOT is the integration time for detection. In fluorescence imaging, rubidium atoms that are probed near saturation and near resonance scatter approximately  $10^7$  photons/s. For a low gradient MOT with  $10^5$ - $10^6$ , atoms can be probed for a short time, 1 ms, and still collect enough photons to achieve a high signal to noise ratio. In contrast, in a single atom MOT, the signal is integrated for 500 ms to collect enough photons to image a single atom. Figure 5.4 shows the fluorescence signal from individual atoms in the MOT.

The fluorescence signal is integrated over a region of  $4 \times 4$  pixels, which corresponds to a region of interest that is approximately  $25 \times 25 \mu\text{m}$ , and integrated for 500 ms. In the integrated signal, Figure 5.4 (a), one can clearly see atomic steps, indicating the individual atoms. The atom number in the MOT can increase due to collecting additional atoms from the background vapor and atoms are lost due to background gas collisions, or losses

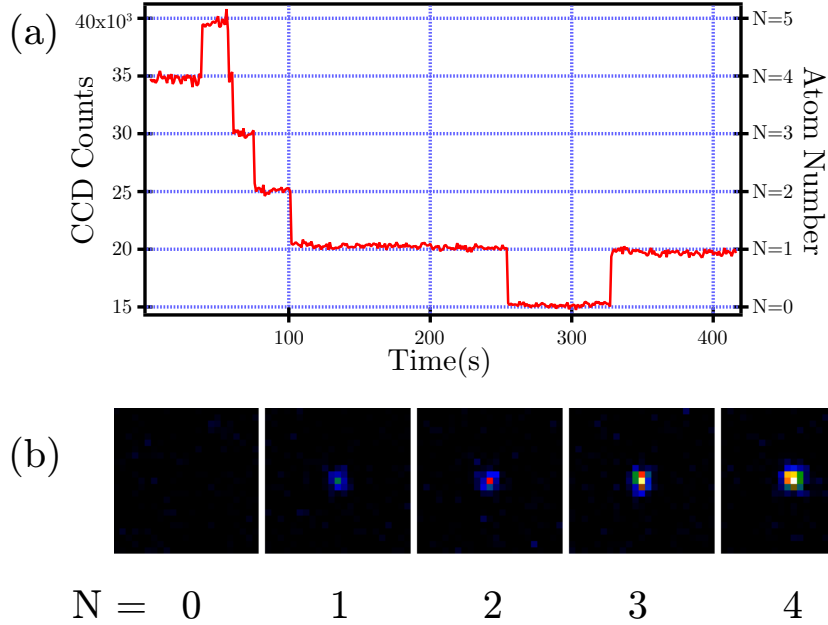


**Figure 5.4:** (a) The integrated fluorescence single from the single atom MOT. Atoms are exposed for 500 ms, and the image is integrated over a  $4 \times 4$  pixel region that contains the MOT. Atomic steps are present showing the ability to detect single atoms. (b) Fluorescence images showing: 0, 1, 2, 3, and 4 atoms.

due to collisions with other MOT atoms.

By constructing a histogram of the results from Figure 5.4, one can determine the count rate per atom per exposure time which is plotted in Figure 5.5. The resulting histogram is then fit to a sum of Gaussian functions to determine the count rate.

In Figure 5.5 the histogram is constructed from the data shown in Figure 5.4 (a). The center of each Gaussian gives the count rate for 0, 1, 2, 3, 4, and 5 atoms. The count rate per atom per integration time is given by the separation of the peaks. This histogram is constructed using bins with a width of 100 counts resulting in a count rate per atom of  $R_{\text{atom}} = 4900$  counts per 500 ms.

### 5.2.2 Single atom Stark Shift Probe

The single atom MOT signal can be used as a probe of the Stark shift experienced by the atom due to the optical trap laser. The atom will experience a spatially dependent Stark shift and by monitoring the scattering rate of an atom with and without the trapping laser,

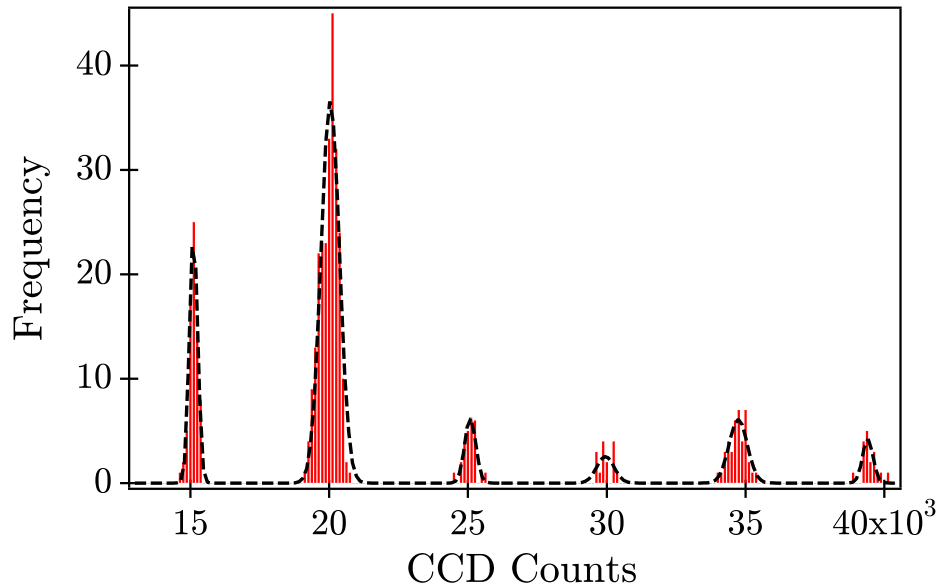


**Figure 5.5:** Histogram of the integrated fluorescence signal of the single atom MOT from Figure 5.4 (a). The histogram is fit to a sum of six Gaussian functions which is shown as a black dashed line. The peaks show  $N = 0, 1, 2, 3, 4,$  and  $5$  atoms.

a time averaged Stark shift can be computed.

An atom will scatter photons from the MOT beams at a rate given by,

$$\Gamma = \frac{\gamma}{2} \frac{s_0}{1 + s_0 + (2\delta/\gamma)^2}, \quad (5.1)$$

where  $s_0$  is the on-resonance scattering rate,  $\gamma$  is the natural linewidth of the atom, and  $\delta$  is the detuning of the MOT beams. The ratio of the scattering rate of the Stark shifted atom to the bare atom is,

$$\frac{\Gamma_{\text{bare}}}{\Gamma_{\text{Stark}}} = \frac{1 + s_0 + (2\delta_{\text{Stark}}/\gamma)^2}{1 + s_0 + (2\delta_{\text{bare}}/\gamma)^2}. \quad (5.2)$$

Using the CCD camera to measure the different count rates of a single atom, where the intensity and the detuning from bare atomic resonance remains constant, the time-average Stark shift can be computed.

In Figure 5.6, the results of the Stark shift experiment are shown. Atoms in the MOT are imaged with 500 ms exposure with a CCD camera, and the count rate per atom is determined, as in Figure 5.5. Then the optical trap laser is turned on and the new Stark

count rate is recorded. The MOT laser beams are fixed at a constant detuning of -10.6 MHz from the atomic resonance, and the power per beam is held constant. The optical trap is constructed from the fiber laser with 1 W of optical power, focused to  $w = 17 \mu\text{m}$ , and a trap depth of 1 mK.

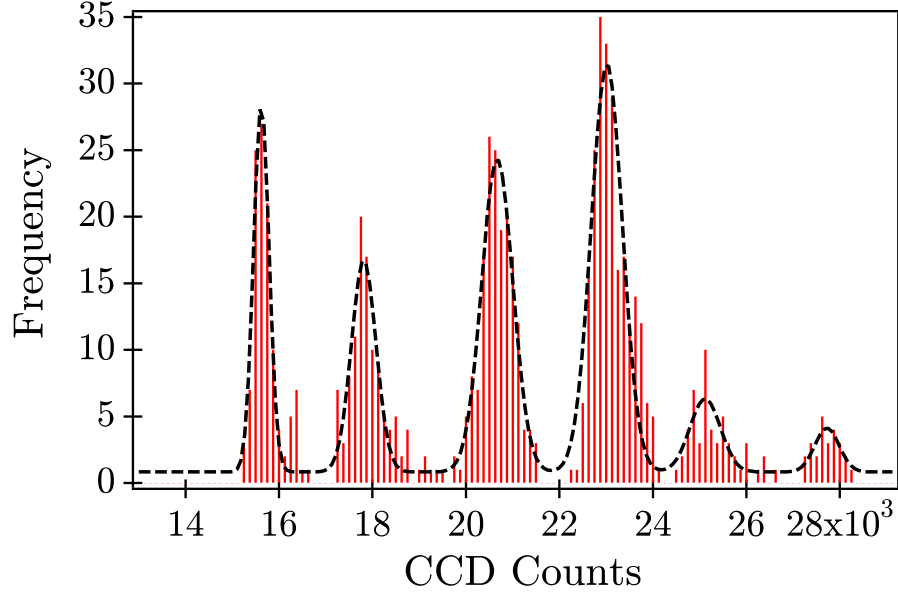


**Figure 5.6:** A histogram of the single atom fluorescence signal from Stark shifted atoms in the MOT. The histogram is fit to a sum of 6 Gaussian curves (shown as a black dashed line) to find the single atom count rate for the Stark shifted atom.

The histogram is constructed with bins of width 100 counts which is again fit to a sum of Gaussian functions, where the Stark shifted single atom count rate is 2420 counts per 500 ms.

From the fits of the two histograms (Figures 5.5 and 5.6), one can compare the count rates for Stark shifted and unshifted atoms. These rates are given by,

$$R_{\text{bare}} = 9800 \text{ cts/s}$$

$$R_{\text{Stark}} = 4840 \text{ cts/s} .$$

Using Eq. (5.2), one can compute the detuning due to the Stark shift. The detuning is computed,

$$\delta_{\text{Stark}} = 30.33 \text{ MHz} \tag{5.3}$$

This results in a trap depth of approximately,  $U_{\text{dipole}} \approx 400 \mu\text{K}$ , where the trap depth is,

$$U_{\text{dipole}} = \hbar\delta_{\text{Stark}} . \quad (5.4)$$

In addition to determining the trap depth, this measurement can be used as an alignment tool between the MOT and the optical trap. The key alignment in the cavity QED experiment is the intersection between the optical trap and the cavity mode as described in Section 6.2. Once this alignment is made, the MOT must be moved to the optical trap. To maximize this alignment and ensure good transfer to the optical trap, the Stark shift experienced by the MOT atoms is maximized.

### 5.2.3 Imaging Single Atoms in an Optical Trap

With successfully trapped and detected individual atoms in the MOT, the next experiment focused on loading individual atoms into an optical trap. Additional techniques had to be developed to detect these atoms in the optical trap, which was challenging, due to the large Stark shift of the trap.

To image individual atoms in optical traps requires much of the same experimental tools as imaging them in MOT. Again the scatter must be minimized to increase the signal to noise ratio. As before, the atom has to be exposed to near-resonant light for a long time period, in order to collect enough photons to detect the atom and discriminate it above the background.

This long integration time is strikingly different than the above fluorescence imaging of atoms in an optical trap. In the many atom experiments, atoms are exposed for a short time, less than 1 ms, with a near resonant laser probe. This is a destructive measurement where the atoms are heated out of the trap due to the absorption and emission of photons. Since there are many thousand atoms emitting photons, a large signal can be collected in this short integration time.

To image individual atoms in the optical trap required the development of a technique that could image atoms non-destructively. This was first demonstrated with Cs by the Bonn group [86, 87] and we adopt their technique here.

### 5.2.4 Non-Destructive detection

In Figure 5.7, one can see a chain of atoms that are imaged in the optical lattice, using a six beam optical molasses. The optical trap is constructed from a 1 W laser beam that is

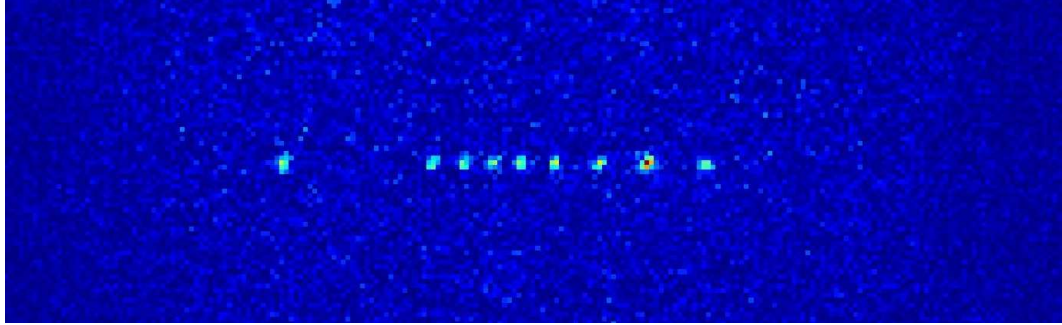


**Figure 5.7:** A chain of individual atoms that are imaged using non-destructively. There are eight individual atoms and one location where there are two atoms.

retro-reflected onto itself with a focus of  $w_0 = 17 \mu\text{m}$ . The trap depth is,  $U_{\text{dip}} \approx 1.1 \text{ mK}$ . This trap induces a Stark shift on the atom that is computed to be  $+ 82.7 \text{ MHz}$  which blue-shifts the resonance with respect to the bare atom.

Imaging the atoms in the optical trap employs a 6 beam optical molasses. Each beam of the optical molasses has 3 mW of optical power and detuned from the bare atomic resonance by  $\delta = -13.1 \text{ MHz} \approx 2.2\gamma$ . The beams of the optical molasses are thus detuned by  $\delta = 15.7\gamma$  from the light shifted atomic transition. This results in a per beam saturation parameter of,  $s = 3 \times 10^{-5}$  per beam. The atoms are imaged in the optical molasses with an exposure time of  $t_{\text{exp}} = 700 \text{ ms}$ .

In addition to the ability to detect individual atoms in the optical trap, the continuous observation increases the lifetime of the atoms in the lattice. In this chamber the lifetime of the optical trap without cooling is limited to  $\tau_{\text{no-cooling}} = 20 \text{ s}$ . With cooling, the lifetime grows by nearly an order of magnitude! The result of the lifetime measurement can be seen in Figure 5.8. The lifetime of the atoms in the continuous observation lattice is  $\tau = 125 \text{ s}$ .

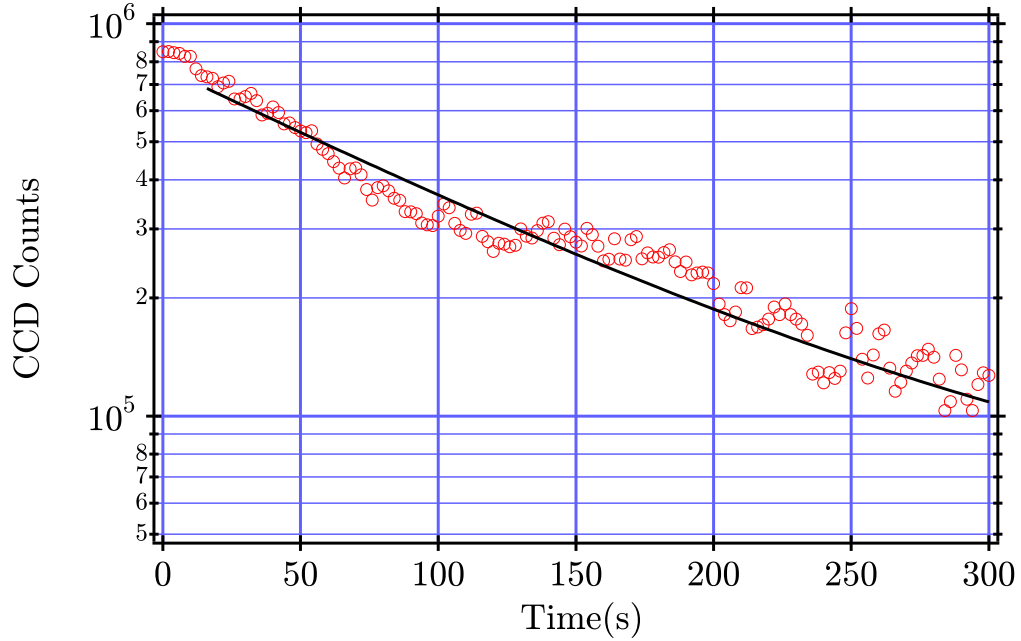


**Figure 5.8:** Lifetime measurement of atoms in the continuously observed lattice. The trap depth is  $U = 1$  mK, and each of the six beams has a  $s = 0.00003$ . The lifetime of the atoms in the trap with cooling light is  $\tau = 125$  s.

### 5.2.5 Preparing Chains of Atoms

The ability to image individual atoms in an optical trap does not require a single atom MOT. Atoms can be loaded from a normal MOT and then cooled and observed continuously. The scheme for the cavity QED based quantum computer requires a chain of atoms that can be moved in and out of the optical cavity mode. By manipulating the optical trap laser beams one can produce a chain of atoms.

In this experiment, the optical lattice was formed by two independent laser beams. Atoms are initially loaded into the trap from the MOT. The atoms are continuously observed in the optical lattice, and are localized to the region where the MOT was located. To spread the atoms into a linear chain, one laser beam is turned off for 3 ms, and the atoms are allowed to expand in a single focus trap. After the expansion time, the second laser beam is turned back on and the atomic motion is frozen. The atoms are then spread along the lattice trap. In Figure 5.9, the results of the expansion are presented.

Initially approximately 50 atoms are loaded into the optical trap. These atoms are

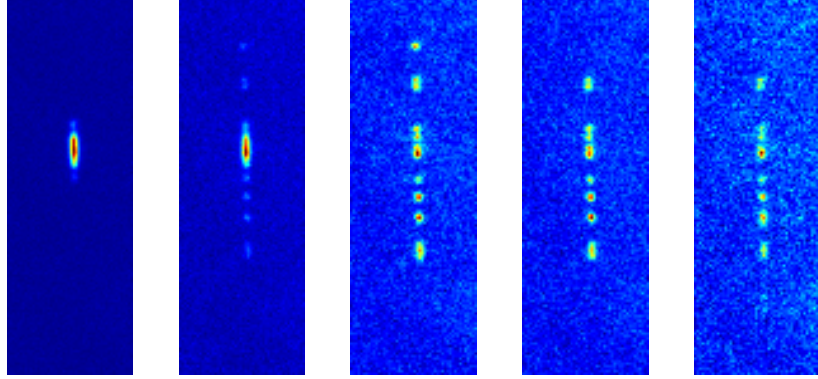


**Figure 5.9:** Expansion of atoms in an optical lattice. One lattice beam is turned off and the atoms expand for 3 ms in a single focus trap. The atoms expand and form a chain of atoms that could be used for a quantum register.

spread over a distance of approximately  $40 \mu\text{m}$ . After the expansion, individual atoms are spread over the optical lattice. By using this technique we can prepare the system envisioned in Figure 3.6, where a chain of atoms are ready to interact with an optical cavity.

A detailed study of the cooling versus detuning and other trap parameters is being investigated currently and a complete description of continuous observation will be presented in the Ph.D. thesis of Michael Gibbons. Currently the longest lifetime observed in this system is 300 seconds, or 5 minutes. For quantum information, the interactions usually occur at rates on the order of MHz. Comparing the time scale of the atom's lifetime to clock rate, the atoms are essentially stored forever.

### 5.3 Summary of Atom Trapping Experiments

In this section, experiments have been presented that show the ability to trap and manipulate atoms with an optical lattice. We have shown that we can store atoms for long lifetimes with optical traps. We have also shown the ability to transport atoms over macroscopic distances.

Additionally, tools have been developed to trap and image individual atoms. First individual atoms are trapped in a Magneto-Optical trap and detected via the CCD camera. Then single atoms are imaged in an optical trap using a balanced six beam optical molasses. This continuous observation leads to increased trap lifetimes which are greater than two minutes. The following table highlights the increase of trap lifetime in the cavity QED experiment over the last five years.

Optical Trap Source	Trap Lifetime	Years Used
Ar <sup>+</sup> pumped Ti:S	200 ms	2002-2003
Tapered Amplifier diode pumped 852 nm	2-4 s	2003-2005
Yb doped Fiber Laser	8-20 s	2005-
Continuous Observation	>120 s	2006-

## CHAPTER VI

### PROBING THE ATOM-CAVITY SYSTEM

This chapter presents the results from experiments with the atom-cavity system. First, the rate of coherent coupling and decoherence of the cavity field are measured to determine important cavity QED parameters. After the cavity QED system is characterized, we present deterministic delivery of atoms into the cavity mode. The atoms are observed in the cavity by absorption of the intra-cavity photon, and later by cooling and non-destructive emission into the cavity mode. Finally, experiments with single atoms emitting into the cavity are presented.

The experiments described in this chapter are performed with the second high finesse cavity where the distance between the MOT and the cavity is 8 mm. The walking-wave optical lattice is constructed using Yb doped fiber laser, with 4 W of optical power per beam. Unless otherwise noted, the trapping parameters are  $U_{\text{MOT}} \sim 100 \mu\text{K}$  and  $U_{\text{cavity}} \sim 1 \text{ mK}$ .

#### *6.1 Characterization of Cavity Parameters*

In order to characterize the cavity QED system, three rates need to be measured; the coherent coupling rate  $g_0$ , the cavity's linewidth  $\kappa$ , and the natural linewidth of the atom,  $\gamma$ . For  $^{87}\text{Rb}$  the linewidth of the  $\text{D}_2$  transition is,  $\gamma = (2\pi) 6.065 \text{ MHz}$  [88].

##### **6.1.1 Determination of $g_0$**

The first parameter of the cavity QED system to measure is the rate at which information can coherently be transferred from the single atom to the single photon. The coherent coupling rate,  $g_0$ , is defined as [56],

$$g_0 = \sqrt{\frac{3c\lambda^2\gamma}{2\pi^2w_0^2L}} \quad (6.1)$$

where,  $\lambda$  is the wavelength of the atomic transition,  $\gamma$  is the linewidth of the atomic transition,  $w_0$  is the cavity mode waist and  $L$  is the length of the cavity. To determine  $g_0$ , the

**Table 6.1:** Resonant wavelengths of the science cavity measured with the HP Optical Spectrum Analyzer 86142A.

Mode number	wavelength (nm)
q+3	776.113
q+2	777.357
q+1	778.874
q	780.224
q-1	781.583
q-2	782.936
q-3	784.314

cavity’s waist and length needs to be measured because the other parameters are determined from atomic properties.

To measure the length of the cavity, one can directly measure the free spectral range using two lasers. One laser with a fixed frequency, stabilized to a rubidium transition, serves as a frequency reference. The second laser is tunable with the ability to scan over many nanometers. The cavity’s length is kept constant by monitoring the fixed laser’s transmission, while the second laser’s wavelength is changed until both lasers are co-resonant with the cavity. The wavelength of the tunable laser is recorded when both lasers are resonant with the cavity. The wavelength is measured to high accuracy using an optical spectrum analyzer or a wavemeter. In Table 6.1 the co-resonant wavelengths are recorded.

The length of the cavity is related to the mode number by,

$$L = q\frac{\lambda}{2} \rightarrow \frac{1}{\lambda} = \frac{1}{2L}q. \quad (6.2)$$

By plotting the inverse wavelength versus the mode number, the slope is related to the length of the cavity. Once the length of the cavity is known to a high precision the cavity’s waist can be computed from Eq. (3.6). Armed with these values,  $g_0$  can be computed using Eq. (6.1).

It should be noted that Hood *et al.* [89], make corrections for the frequency dependence of the mirror coatings. Since this measurement is performed over a small range of wavelengths ( $\sim 10$  nm), it is assumed that mirror coatings are constant.

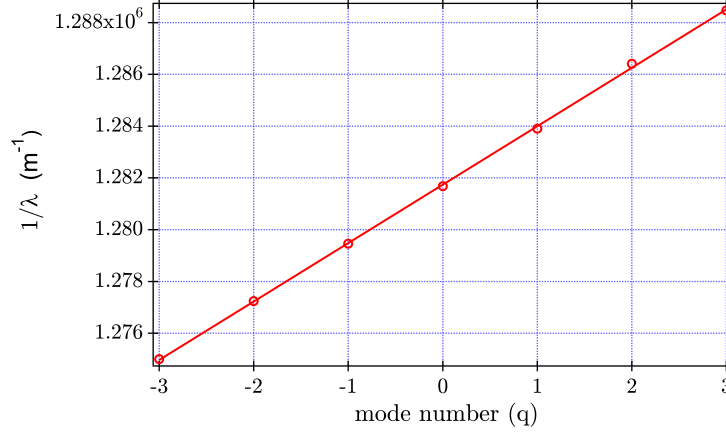


**Figure 6.1:** Plot of inverse wavelength vs. mode number. The slope of this line gives the length of the cavity. The length of the cavity is,  $L = 221.51 \pm 1.65 \mu\text{m}$ .

Table 6.2 summarizes the cavity QED parameters that can be computed with the knowledge of the length of the cavity mode.

**Table 6.2:** Cavity parameters that are computed once the length of the science cavity is determined.

Cavity QED Parameters		
$L$	221.51	$\mu\text{m}$
$\nu_{\text{FSR}}$	677.161	GHz
$w_0$	20.307	$\mu\text{m}$
$V_m$	$7.17 \times 10^{-14}$	$\text{m}^3$
$g_0$	$(2\pi) 17.11$	MHz

### 6.1.2 Determination of the Cavity Linewidth

The linewidth of the cavity,  $\kappa$ , is measured using the transfer diode laser. Figure 6.2 depicts the technique used to measure the cavity linewidth. The EOM which produces the transfer laser light for the science cavity is driven with three RF signals. Two frequencies from the EOM stabilize the cavity and are depicted as blue dashed. The frequency of these beams are,

$$\omega_{\pm} = \omega_0 \pm 2\kappa$$

where  $\omega_0$  is the resonance frequency of the cavity. A third laser with an adjustable frequency  $\omega'$ , maps out the cavity transmission spectrum by recording the transmitted power versus

frequency.

All three beams are detected via heterodyne detection where three separate spectrum analyzers are set to each of the RF frequencies. The transmitted power of the adjustable laser is fit to a Lorentzian function from which the linewidth can be determined.

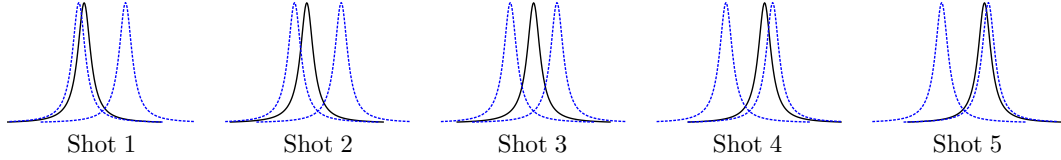


**Figure 6.2:** Experimental setup to measure the linewidth of a cavity using the transfer cavity light. The blue dashed lines are the frequencies that are centered at  $\pm 2\kappa$  that provide the cavity stabilization while, the black solid line can be tuned across cavity resonance. Once the cavity is locked we monitor the transmission versus detuning of the black frequency laser.

The results of cavity linewidth measurement is shown in Figure 6.3, with a measured linewidth of,  $\kappa = (2\pi) 13.69 \pm 1.43$  MHz. This cavity is constructed from two mirrors with transmission losses of 100 ppm and 10 ppm. For these mirror losses, the computed linewidth of  $\kappa_{\text{Theory}} = (2\pi) 5.8$  MHz is substantially smaller than the measured value. This measured linewidth implies a finesse,  $\mathcal{F} = 24,740$ , which corresponds to a total loss of  $\delta_c = 254$  ppm, This linewidth is approximately a factor of 2.5 larger than the design parameter, and possibly due to impurities on the mirror's coated surfaces.

With measurements of  $\kappa$  and  $g_0$ , all necessary cavity QED parameters can be computed, which includes saturation atom number,  $N_0$  and the saturation photon number,  $n_0$ . The formulae for these parameters are given in Eqs. (3.41) and (3.40). In Table 6.3, all the cavity QED parameters of the current cavity are presented.

## 6.2 Optical Trap Cavity Mode Alignment

To successfully position atoms in the cavity field mode, careful alignment is required to overlap the optical trap axis with the cavity mode axis. The Gaussian beams that define these two axes have small waists. The optical trap has a waist of,  $w_{\text{Trap}} = 26.9 \mu\text{m}$ , and the cavity mode has a waist of,  $w_{\text{Cavity}} = 20.3 \mu\text{m}$ . Once the focus of the optical trap is located at the cavity the only parameter to vary is the height of the optical trap. To achieve good

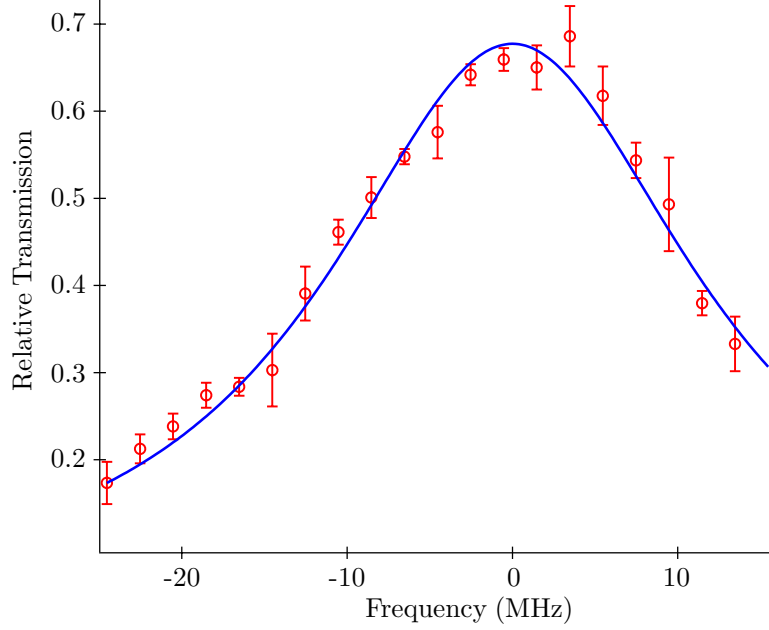


**Figure 6.3:** Cavity linewidth measurement using the 784 nm transfer laser. The measured linewidth is  $\kappa = (2\pi)13.69 \pm 1.43$  MHz. Each point is the average of 10 measurements, with the error bars showing one standard deviation.

**Table 6.3:** The cavity QED parameters for current cavity.

Cavity QED Parameters		
$L$	221.513	$\mu\text{m}$
$\nu_{FSR}$	677.161	GHz
$g_0$	$(2\pi)17.11$	MHz
$\mathcal{F}$	24,742	
$\kappa$	$(2\pi)13.69$	MHz
$\delta_c$	254	ppm
$N_0$	0.287	
$n_0$	0.0419	
$C_1$	3.48	

alignment between the cavity beam and the optical trap in the vertical height, the atoms are rolled down a single-focus optical trap into the cavity mode as depicted in Figure 6.4

Atoms start at the top of a potential hill created by the single focus optical trap. When the MOT beams and magnetic field are turned off, atoms roll down to the focus where the potential is the deepest. The height, or y position, of the optical trap beam is adjusted until atoms are detected in the cavity mode.

In Figure 6.5, the results of this experiment are presented. As atoms roll down the

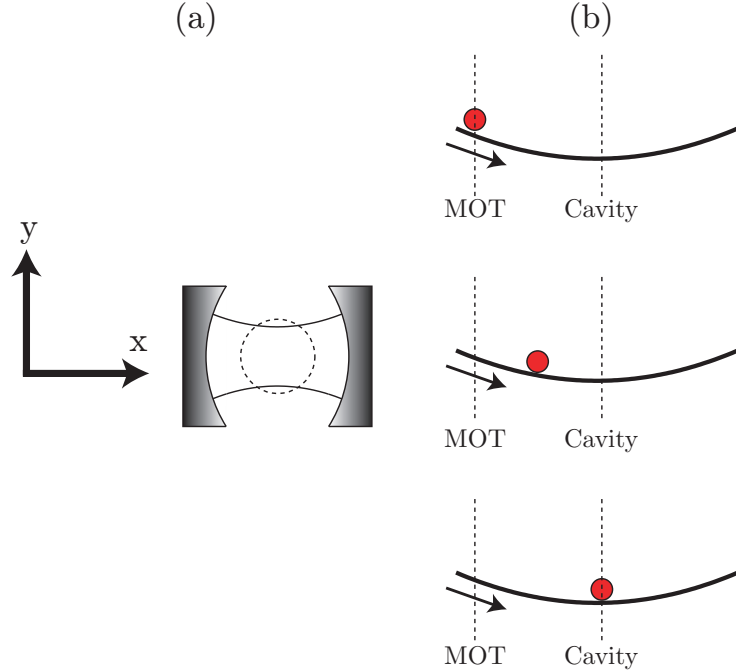


**Figure 6.4:** (a) Schematic of the optical trap beam and the cavity mode. The dashed line is the optical trap that is propagating into the page. (Note: Gaussian beams are to scale, cavity mirrors are not) (b) Experimental technique for aligning the optical trap with cavity mode. Atoms roll down the hill to the focus of the trap and are detected by the cavity if the optical trap beam intersects the cavity mode.

potential hill and miss the cavity mode, there is no effect on the cavity transmission as in Figure 6.5 (a). Once the trap beam is aligned with the cavity mode, the atoms change the cavity's transmission as in Figure 6.5 (b).

### 6.3 *Deterministic delivery of atoms to an optical cavity*

The deterministic loading of atoms into an optical cavity is a unique feature of this cavity QED system. Experiments currently performed by the Caltech group use randomly loaded atoms into a cavity. In their experiments, a cesium MOT is formed approximately 5 mm above an optical cavity. When the MOT is turned off, atoms undergo ballistic expansion and fall due to gravity. During this expansion there is a small probability that an atom will pass through the cavity mode and become trapped by an intra-cavity FORT [50].

The group led by Gerhard Rempe at the Max Planck Institut für Quantenoptik, has developed a quasi-deterministic technique to load atoms in the cavity. In these experiments,

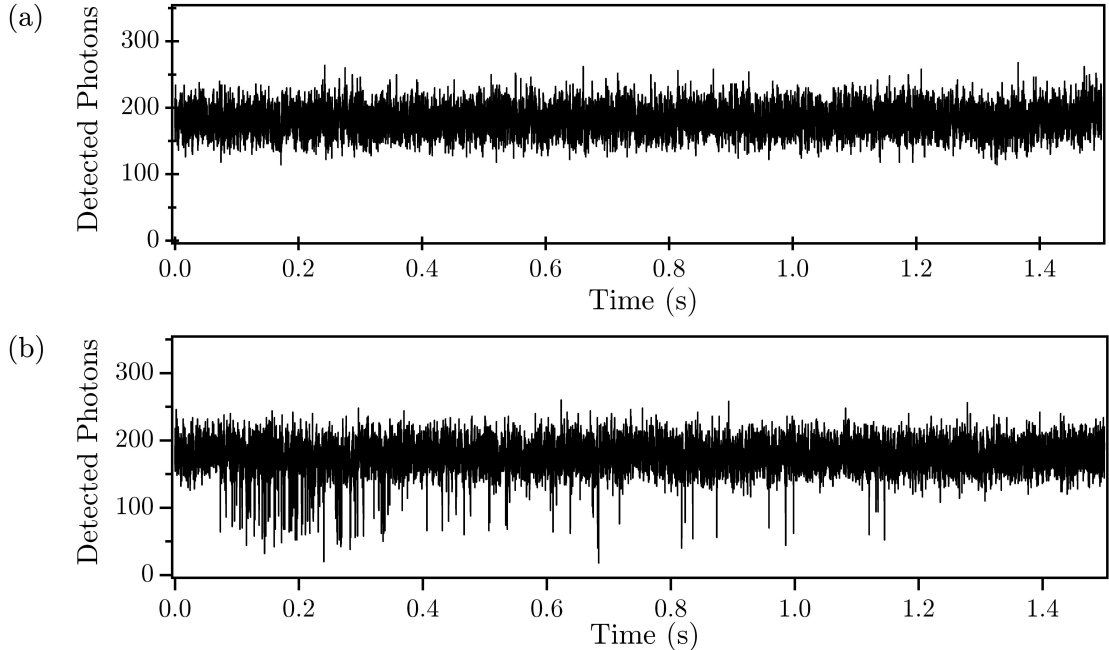


**Figure 6.5:** (a) The cavity’s transmission when the cavity and the trap are not aligned. The atoms miss the cavity mode leaving transmission unchanged. (b) The FORT and cavity mode are aligned and atoms are visibly interacting with the intra-cavity photon and changing the transmission. The photons are counted with  $100 \mu\text{s}$  time bins.

rubidium atoms are collected in a MOT 1.5 cm from an optical cavity. These atoms are then loaded into a single focus optical trap, with its focus at the optical cavity. When the MOT is released, the atoms roll down the potential hill into the optical cavity. As the atoms reach the cavity an optical lattice is turned on, stopping the motion of the atoms. For fine adjustments of atomic position, a glass wedge in the beam path can be adjusted to add a phase change to the optical lattice. This translates the nodes of the standing wave allowing for them to position the atoms into the cavity mode [66, 90].

This thesis presented a totally deterministic cavity loading technique. A one dimensional walking-wave optical lattice connects the MOT and the cavity mode, which allows for atoms to be transported to the cavity from the MOT and back again, on demand.

#### **6.4 General Experimental Protocol for Cavity QED experiments**

All the experiments performed in following sections share a common protocol. Atoms are initially collected in a MOT that is located 8 mm from the optical cavity. By controlling

the magnetic field gradient, the MOT can be loaded with as few as one atom or up to  $10^6$  atoms.

The optical trap is formed by the Yb doped fiber laser, which is focused at the cavity. The optical trap has a potential depth of approximately 1 mK at the cavity, and 100  $\mu$ K at the MOT. This optical lattice is constructed from two independent laser beams, each controlled by phase-locked AOMs. Using a frequency difference between the two trap beams, atoms can be deterministically transported and positioned in the cavity. In the optical lattice, atoms are transported at a velocity,  $v = 3.72$  cm/s and reach the cavity in 240 ms.

Once atoms are positioned in the cavity, they can be probed using two distinct techniques. The first technique is intra-cavity photon absorption, where atoms are detected by sending a probe along the cavity axis. The presence of the atoms is observed by the change in the cavity's transmission spectrum. This measurement is destructive as it results in the loss of the atoms. Alternatively, the atoms can be detected by observing their emission into the cavity mode. To perform this measurement atoms are illuminated with beams that are perpendicular to the cavity axis. The atoms scatter photons from the probe beams and emit into the cavity mode. With the correct choice of parameters, this process will cool the atom and allows for long storage times with this non-destructive probing.

For the experimental geometry, the reader should refer to Figure 4.12 in the experimental setup chapter. From this figure, the cavity axis is the x-axis, and the optical trap is along the z-axis. For the emission process, the cooling beams are perpendicular to the cavity mode, and at an angle of approximately  $45^\circ$  to optical trap axis. The cooling beams drive the  $F = 2 \rightarrow F' = 3$  transition, additionally there is  $F = 1 \rightarrow F' = 2$ , repump light on the cooling beam axis.

The photons leaked out of the cavity are detected using photon counters. The detection efficiency of the photon counting system is  $\eta = 0.225$  counts/photon. This efficiency accounts for losses as the photon is transmitted through the glass cell, fiber coupling efficiency into the photon counter and the quantum efficiency of the photon counters ( $\eta_{PC} = 0.5$  counts/photons). The cavity emits photons at a rate of  $2\kappa$  and this can be used to determine the intra-cavity photon number. The intra-cavity photon number,  $\tilde{n}$ , can be

computed by [91],

$$\tilde{n} = \frac{\text{CtRate}}{\eta} \frac{1}{\tau_p} = \frac{\text{CtRate}}{\eta} \frac{1}{2\kappa}, \quad (6.3)$$

where  $\tau_p$  is the photon lifetime.

### 6.5 Cavity Absorption

The first way to probe the atom-cavity system is to observe the atoms absorbing the intra-cavity photon. The atom-cavity system can be simulated by numerically solving the master equation, Eq. (3.43) [92]. The results are shown in Figure 6.6. In Figure 6.6 (b-d), the Stark shift is included in the simulation, while in Figure 6.6 (a), the Stark shift is set to zero.

Without a Stark shift, as in Figure 6.6 (a), the spectrum displays the characteristic vacuum Rabi splitting [93]. When the detuning between the cavity and the atom is zero, the transmission will drop from high transmission to nearly zero transmission. The introduction of the atom fundamentally changes the spectrum of the system changing the resonance frequency to  $\omega_0 \pm g_0$ .

For deep traps, the shape of the resonance changes. For a 1 mK deep optical potential, the Stark shift is approximately 75 MHz. As one can see from Figure 6.6 (d), the characteristic transmission dip at zero detuning is not present. To probe the system using the cavity field for deep traps, one has to shift the cavity to be resonant with the Stark shifted atom. The calculation in Figure 6.6 (a) describes the experiment that is presented in Figure 6.7.

In Figure 6.7 we show atoms interacting with the cavity mode. A large MOT of approximately  $10^5$  atoms is formed and then transferred into the optical trap with 10% efficiency. Using the walking-wave optical lattice, atoms are transported 8 mm into the cavity. Once in the cavity, the atoms are probed by the intra-cavity field, which has an intra-cavity photon number of  $\tilde{n} = 0.038$ . The frequency of the cavity, and the probe beam are both on bare atomic resonance ( $\omega_c = \omega_p = \omega_0$ ). As the atoms enter the field, the transmission spectrum changes, and the characteristic drop in transmission is visible.

While many important results have been studied using cavity absorption, currently this signal is used as a diagnostic. Detecting the presence of atoms in the cavity confirms that

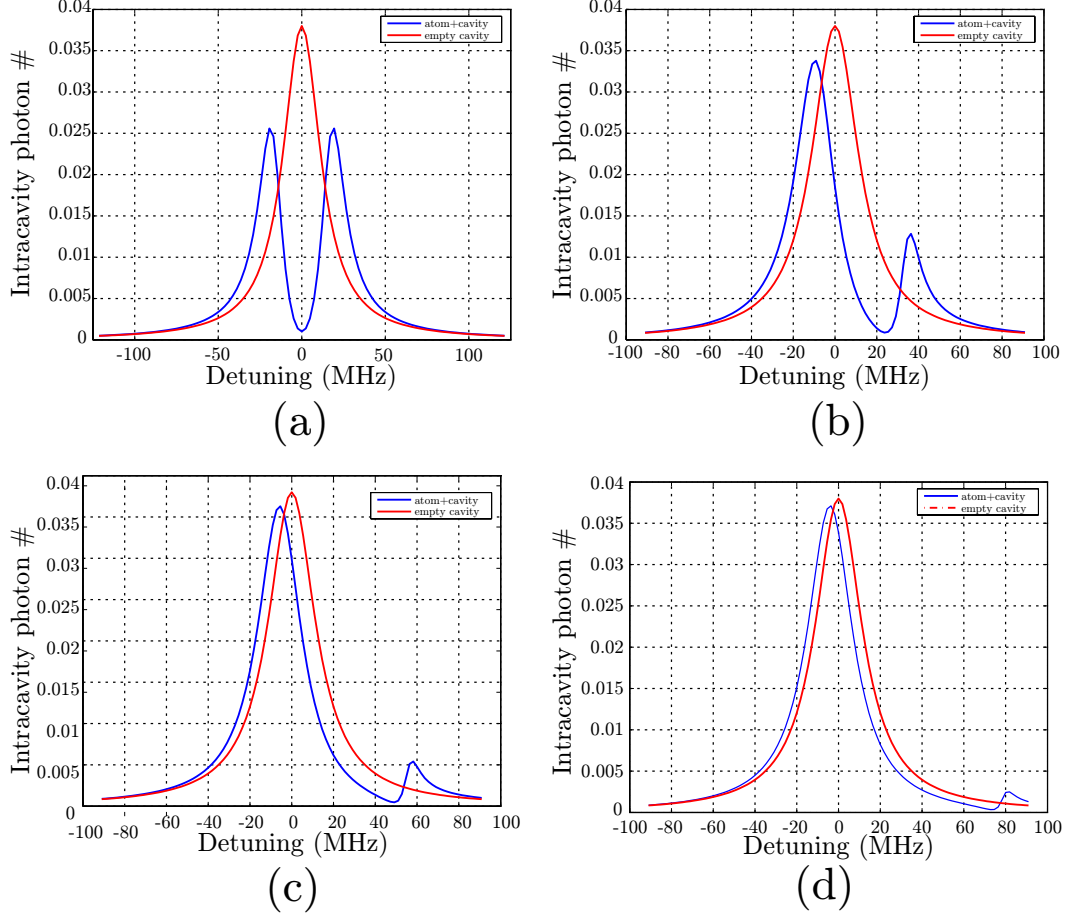


**Figure 6.6:** Calculation of atom-cavity system. The red curve represents a normal cavity spectrum with a Lorentzian lineshape. (a) When an atom enters the cavity, the lineshape splits into two peaks separated by  $2g_0$ . This simulates the experiment performed in Figure 6.7 with cavity parameters,  $(g_0, \kappa, \gamma) = (17.11, 16.68, 6.06)$  MHz and the atoms is maximally coupled ( $g = g_0$ ). (b-d) Calculations including Stark shifts of  $\Delta_S = 25, 50, 75$  MHz.

we can transport atoms to the cavity, the cavity is locked correctly and detection is working. This signal is a necessary starting point in order to cool and observe the atoms emission into the cavity mode.

### 6.6 Observation of Cavity Emission and Cooling

For all schemes of cavity QED based quantum information, it is assumed that one can store the atom inside the cavity. Minimally, it is required to store atoms longer than the time required to perform coherent quantum dynamics. Additionally, it is assumed that atom can

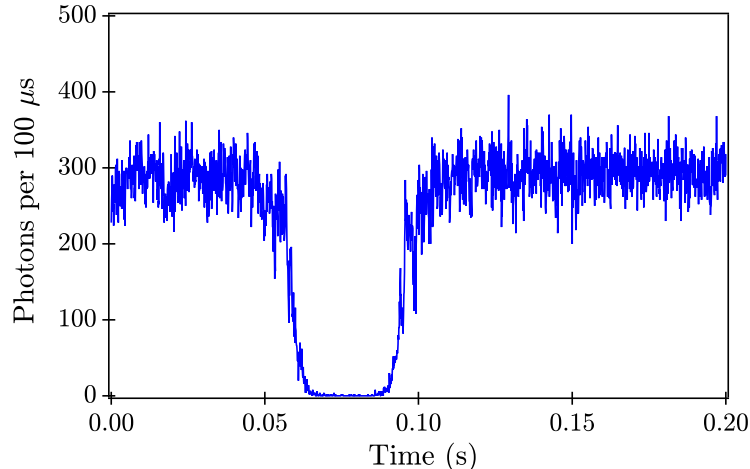


**Figure 6.7:** Cavity transmission showing the interaction of atoms with the cavity field for intra-cavity photon number,  $\tilde{n} = 0.038$ .

be well localized, so that the position dependent coupling,  $g$ , is constant. Initial experiments with single atoms in an optical cavity by Kimble *et al.* had interaction times with a single atom less than  $100 \mu\text{s}$  [94]. This was due to the fact that the atoms were falling through the cavity mode and not trapped in the mode. For the last decade, experiments have made progress in storing single atoms inside high finesse cavities in the strong coupling regime [95, 96]. With the addition of optical traps and cavity cooling, atoms can now be cooled and observed for seconds [66].

In general, to cool an atom requires dissipative forces in three orthogonal directions. In free space this is achieved by an optical molasses, and was implemented in the experiments in Section 5.2.4, to continuously cool and observe atoms in optical traps. Due to the cavity's geometry, there are only two axes in which cooling beams can be placed, but the atom will lack cooling in the third dimension.

Using the cavity mode, the atoms can be cooled along the cavity axis. Atoms that emit photons in the direction of their motion, are Doppler shifted to a higher frequency than the pump laser. If the cavity is detuned such that these emissions are favored, then the atom will continue to lose momentum as it emits into the cavity mode. This emission leads to a cooling along the cavity axis and the emission of photons which are detected provides a non-destructive technique to observe the atoms.

This system can be modeled again by numerically solving the master equation. The results for the emission of photons into the cavity mode can be found in Figure 6.8 for different Stark shifts.

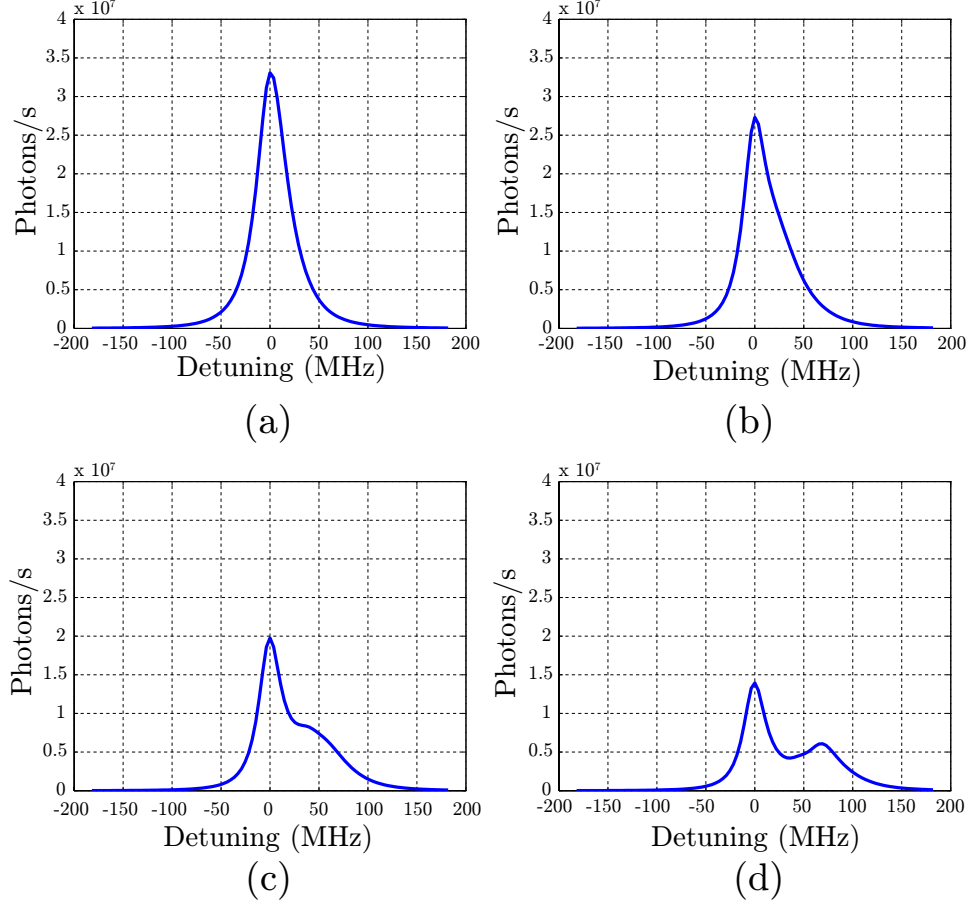


**Figure 6.8:** Calculation of the count rate of a single atom driving the cavity by emission of a photon into the cavity mode. The rate of photons emitted is plotted versus detuning, where the detuning is the pump-cavity detuning,  $\Delta_c = \omega_p - \omega_c$ . For this calculation,  $(g_0, \kappa, \gamma, \Omega) = (2\pi) (17.11, 16.86, 6.06, 35)$  MHz,  $\omega_c = \omega_0 - 12$  MHz where  $\omega_0$  is the bare atom resonance frequency and the atom is maximally coupled,  $g = g_0$ . (b-d) Calculations including a Stark shifts of  $\Delta_S = 25, 50, 75$  MHz.

Additionally the system can be modeled to include more than one atom emitting into the cavity mode. To model  $N$  atoms emitting into the cavity, one needs to change the coupling to [56],

$$g_{\text{eff}} = g\sqrt{N} , \quad (6.4)$$

where  $g$  is the single atom coupling rate. The emission rate versus atom number is plotted

in Figure 6.9, for two common experimental detunings.

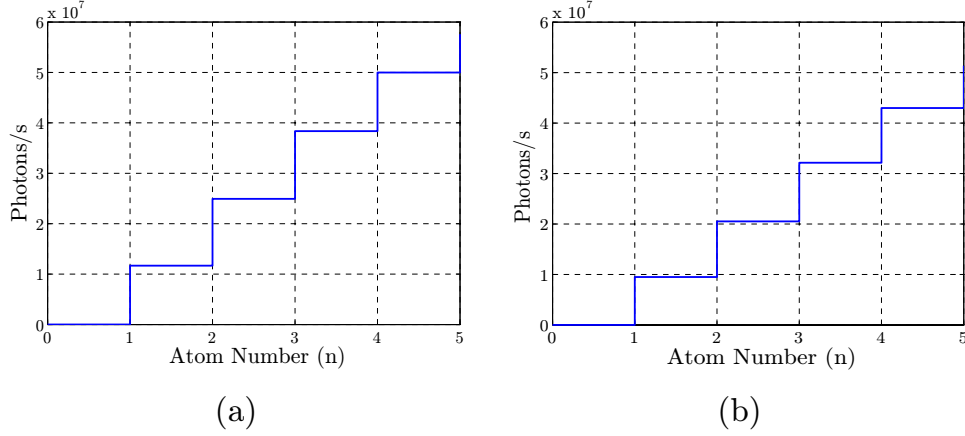


**Figure 6.9:** Calculation of the count rate as the number atoms emitting into the cavity mode changes. (a) For this calculation,  $\Delta_s = 75$  MHz,  $\omega_c = \omega_0$ , and  $\omega_p = \omega_0 - 8.9$  MHz. (b) For this calculation,  $\Delta_s = 75$  MHz,  $\omega_c = \omega_0 - 21.5$  MHz, and  $\omega_p = \omega_0 - 9$  MHz. For both calculations  $(g_0, \kappa, \gamma, \Omega) = (2\pi) (17.11, 16.86, 6.06, 35)$  MHz. For these detunings  $\omega_0$  is the bare atom resonance frequency.

### 6.6.1 Cavity Cooling of many atoms

The first experiment in cooling atoms with the cavity follows the same experiment protocol as Section 6.5. A large MOT of approximately  $10^5$  atoms is formed and then transferred into the optical trap with 10% efficiency. Using the walking-wave optical lattice, atoms are transported 8 mm into the cavity.

The optical trap is focused at the cavity, with a maximum trap depth of 1 mK and a computed Start shift of  $\Delta_S = 75$  MHz. The optically transported atoms are cooled using beams that are perpendicular to the cavity axis and oriented at  $45^\circ$  to the optical trap axis. These beams drive the  $F = 2 \rightarrow F' = 3$  transition and are in the Lin  $\perp$  Lin configuration, to avoid intensity modulation of the pump beams. Each beam has a Rabi frequency of  $\Omega = 32$  MHz, detuned 8.9 MHz below the bare atomic resonance. Co-propagating with the pump beams is repump light ( $F = 1 \rightarrow F' = 2$ ). The cavity is locked to the bare atomic resonance, i.e.  $\omega_c = \omega_0$ , and atoms scatter photons from the pump beams into the cavity mode. The results of the cooling atoms with the cavity can be seen in Figure 6.10.

The atoms are observed non-destructively by the emission of photons and survive for

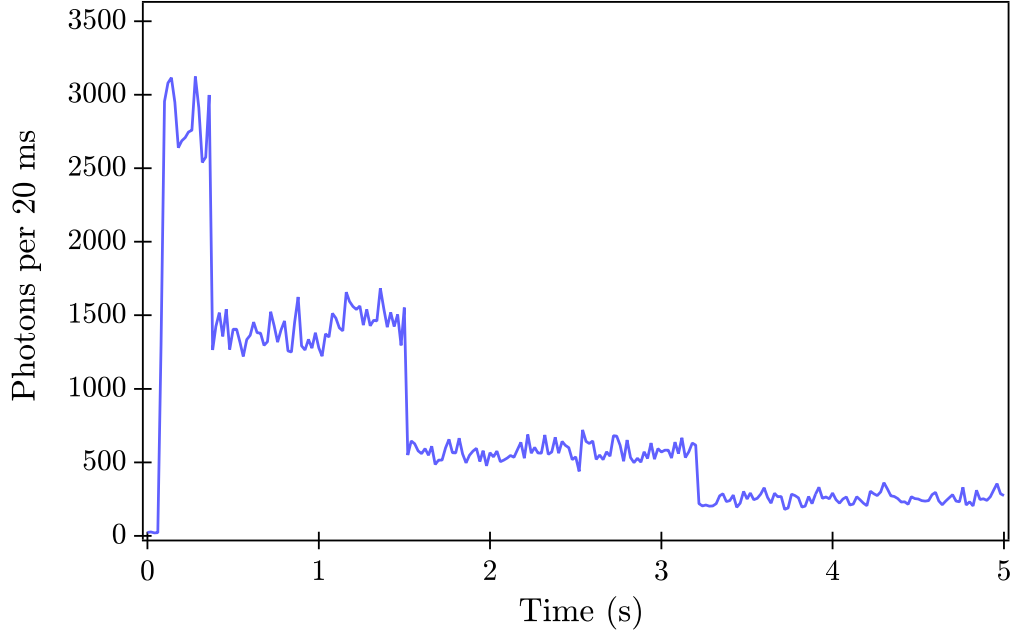


**Figure 6.10:** Atomic steps from atoms that are continuously cooled and observed in the cavity. In this data set initially six atoms are loaded in the cavity, three atoms are lost and the counts to three atom count rate. Finally, only one atom remains before it is lost at 3.2 s. Each atom is approximately 300 photons/20 ms. With a noise floor of 240 photons/20 ms. The cavity-probe detuning is  $\Delta_c = -8.9$  MHz.

many seconds in the cavity mode. In Figure 6.10, initially six atoms are loaded into the cavity mode. Three atoms are lost and the signal reduces to the three atoms emission rate. Finally, two more atoms are lost, leaving only a single atom in the cavity. This single atom is stored in the cavity approximately 1.5 seconds.

The emission signal can be built into a histogram, to determine the count rate per atom. This is done in Figure 6.11. The resulting histogram is fit to a sum of Gaussian functions.

The Gaussian fit of the histogram gives count rates for 0, and 1 atom of,

$$R_{0 \text{ atoms}} = 238.0 \text{ photons/20 ms}$$

$$R_{1 \text{ atom}} = 543.6 \text{ photons/20 ms} .$$

Where the count rate for a single atom is,  $R_{1 \text{ atom}} - R_{0 \text{ atoms}} = 305.6$  photons/20 ms. Theoretically, the rate that atoms will scatter photons into the cavity is [66],

$$R_{\text{scat}} = 2\kappa \frac{g^2}{\Delta_c^2 + \kappa^2} \frac{\Omega^2}{\Delta_a^2 + \gamma^2} , \quad (6.5)$$

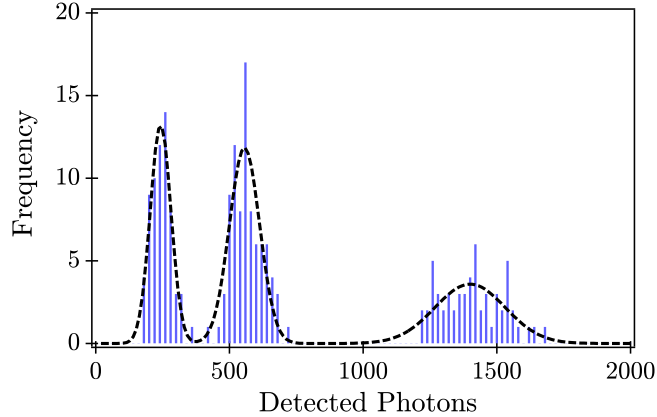


**Figure 6.11:** Histogram of data presented in Figure 6.10, showing  $N=0,1,3$  atoms in the cavity mode.

where  $\Omega$  is the Rabi frequency of the cooling beams and the detunings are defined with an overall negative sign than of Ref [58],

$$\Delta_a = \omega_p - \omega_0 - \Delta_S(r) \quad (6.6)$$

$$\Delta_c = \omega_p - \omega_c, \quad (6.7)$$

where  $\omega_0$  is the bare atomic resonance,  $\omega_p$  is the frequency of the cooling lasers,  $\omega_c$  is the cavity frequency and the spatial dependent Stark shift detuning is  $\Delta_S(r)$ .

For these detunings the theoretical predicted value of photons per ms, taking into account the detection efficiency, is  $R_{\text{scat}} = 12349$  photons/atom/ms. The detected single atom level, 16 photons/atom/ms, is a factor of 820 smaller. In section 6.10.1, we discuss possible reasons why this count rate is smaller than the anticipated value.

For some of the many atom results, we observed very long storage times in the cavity. In Figure 6.12, long storage traces are displayed for one, two and three atoms.

The single atom and the three atoms signals, Figure 6.12 (a) and Figure 6.12 (d-e), exhibit storage times of ten seconds in the cavity. In the two atoms signals, Figure 6.12 (b-c), storage times of greater than 5 seconds are observed. Individual atoms that are probed with the cavity field typically survive 1 ms before they are heated out of the cavity. Using this non-destructive technique we can observe, and store atoms for 10,000 times longer.

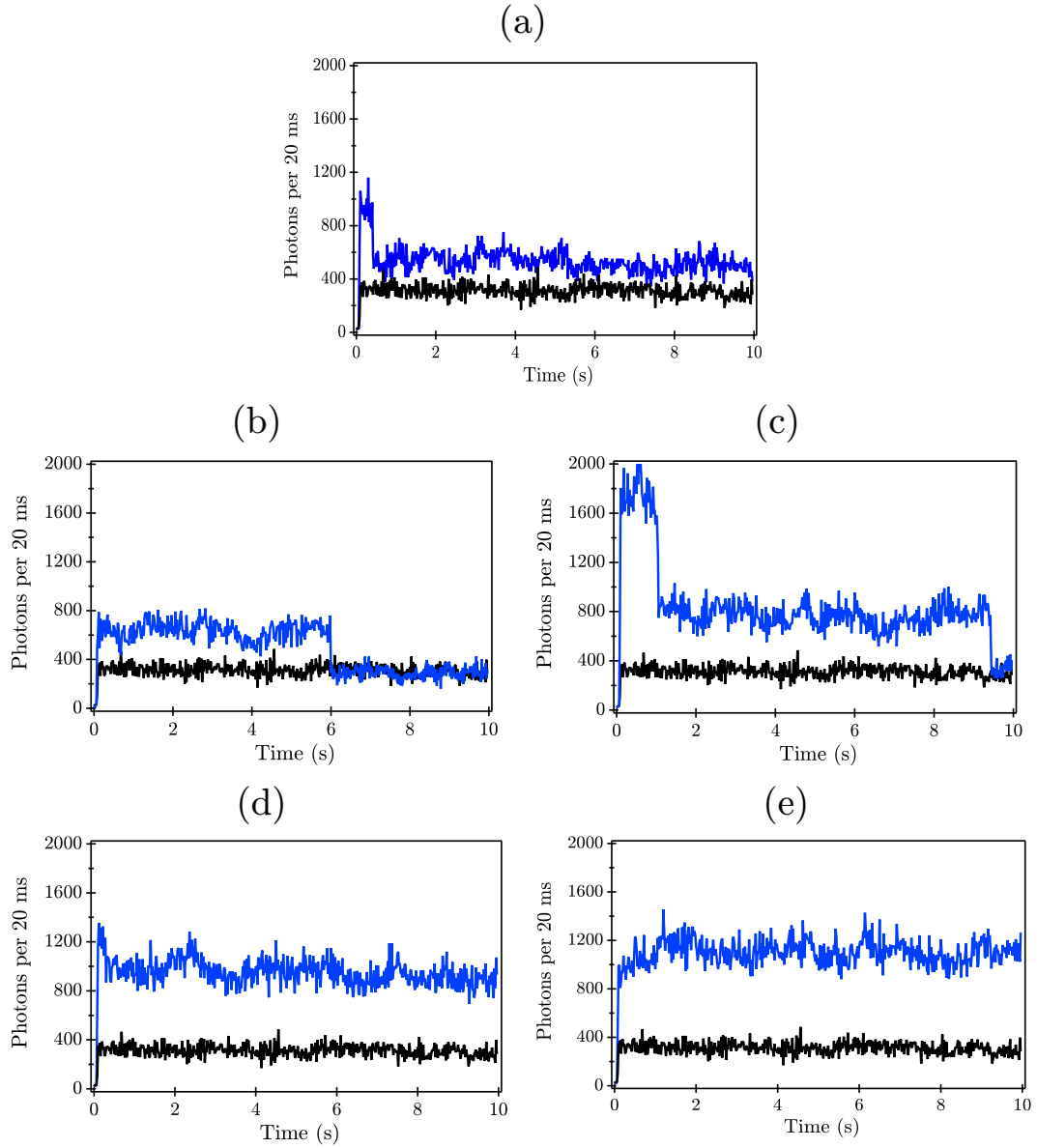


**Figure 6.12:** Graphs that show atoms cooled and non-destructively observed for long time periods. (a) A single atom stored for approximately 10 seconds in the optical cavity. (b-c) Storage of two atoms for 6 seconds and approximately 9 seconds. (d-e) Traces with three atoms stored in the cavity for 10 seconds. For each graph the black curve is the background noise level, and the data sets are taken with  $\omega_c = \omega_0$  and  $\Delta_c = -8.9$  MHz.

### 6.6.2 Lifetime of Many Atoms cooled in the Cavity

The lifetime of atoms cooled in the cavity is studied as the pump-cavity detuning,  $\Delta_c$  is varied. To perform this experiment, approximately 40 atoms are loaded in a MOT and then are transported to the cavity where they are cooled and observed. The experiment is repeated 50 times for each detuning value and the data is averaged and fit to an exponential to measure the lifetime. Figure 6.13, shows a typical data set, where the detuning  $\Delta_C = -8.9$  MHz.

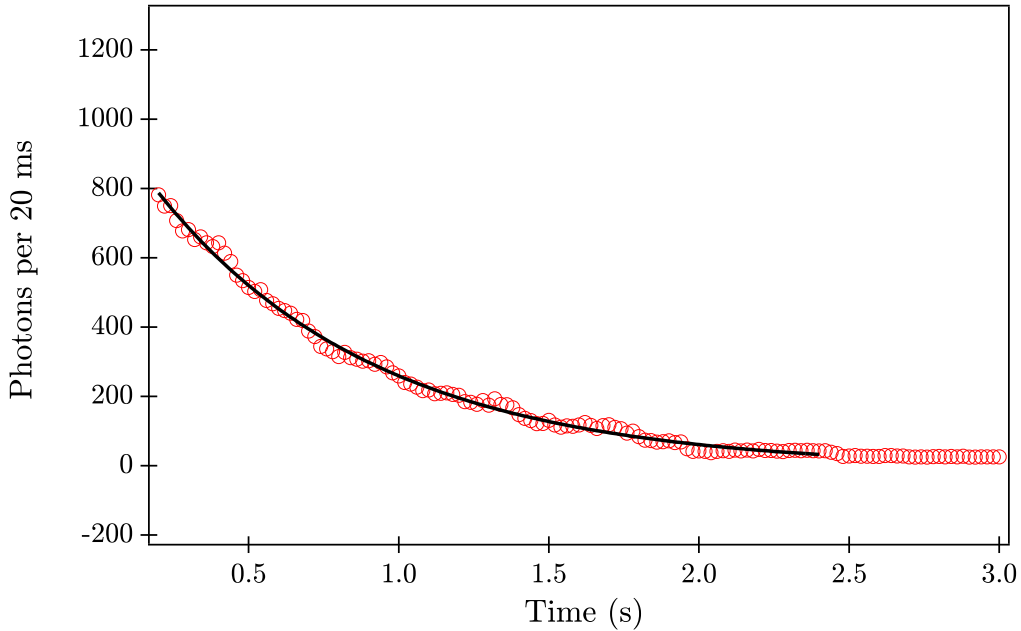


**Figure 6.13:** Lifetime measurement of atoms cooled inside the cavity. This graph is constructed from 50 runs of data with a measured lifetime of  $\tau = 0.732$  s.

For each detuning, the cavity is locked on the bare atomic resonance, and the frequency of the cooling light is changed. Figure 6.14 shows the lifetime dependence on detuning. The maximum lifetime occurs at  $\Delta_c = -8.9$  MHz, with a lifetime,  $\tau = 0.732$  s. In the theoretical section on cooling forces, Section 3.4, the maximum cooling occurs at,

$$\Delta_{c\text{Max}} = -\frac{\kappa}{\sqrt{3}}.$$

The theoretical maximum cooling occurs,  $\Delta_{c\text{Max}} = -7.88 \pm 0.83$  MHz. The maximum cooling observed in the experiment was at, -8.9 MHz which is 1.2 standard deviations from

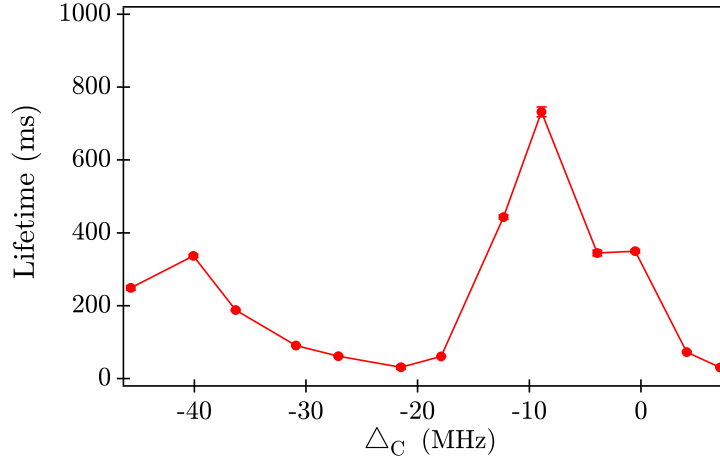


**Figure 6.14:** Results from lifetime measurement starting with 40 atoms in the MOT. The frequency of the cooling beam is varied, and lifetime is plotted versus pump-cavity detuning,  $\Delta_c$ . The frequency of the cavity is set to the bare atom resonant frequency,  $\omega_c = \omega_0$ .

the theoretical maximum value.

### 6.7 Transfer into the intra-cavity Dipole Trap

A filtering technique was developed to demonstrate the deterministic ability to move atoms in and out of the cavity mode with many atoms. In this experiment a large MOT of  $10^5$  atoms was formed and transported to the cavity. Once the atoms reach the cavity, the cooling beams are turned on and the emitted photons are detected. After 750 ms, the cooling beams are turned off along with the walking-wave optical lattice and the atoms are left in the shallow intra-cavity dipole trap. For the experiments in Figure 6.15, the trap depth of the intra-cavity trap is approximately  $50 \mu\text{K}$ , corresponding to a circulating intensity of 0.4 mW. The atoms remain in the intra-cavity dipole trap for 2 ms before the walking-wave lattice is turned on, along with the cooling beams. As seen in Figure 6.15 (a-b), some of the atoms survive the transfer. Atoms that are not exactly overlapping with the cavity mode are lost or filtered away.

In Figure 6.15 (c-d), we further explore the filtering processing. To verify that only atoms in the cavity mode remain after the filtering process, we translate the atoms in the walking-wave lattice after the filtering process. In Figure 6.15 (c), atoms are transferred and then translated 0.5 mm out of the cavity, approximately 10 cavity waists. After the atoms

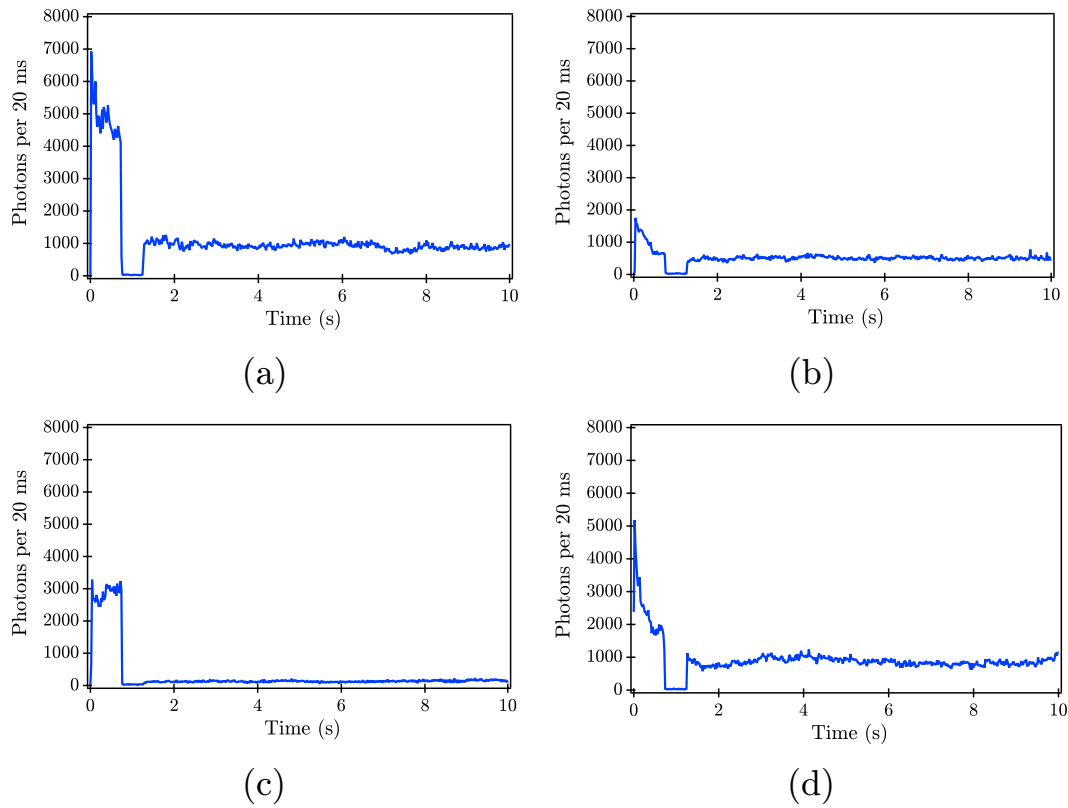


**Figure 6.15:** (a-b) Filtering atoms by the transferring them into the shallow intra-cavity dipole trap. (c) After the filtering process, atoms are transported 0.5 mm out of the cavity mode. (d) After the filtering, atoms are transported 2 mm out of the cavity mode and then 2 mm back and detected by the cavity.

have been transported, the cooling lights are turned on and the cavity does not detect any scattered photons.

In Figure 6.15 (d), we preform the same experiment as above with slight modifications. The atoms again are transfered and filtered by the intra-cavity dipole trap. After the transfer process atoms are again moved but in this experiment, the atoms are moved 2 mm away from the cavity and then back 2 mm. The atoms travel a distance of 4 mm, but returns to where they started, in the cavity mode. After the atoms have completed their movement, the cooling light is turned on. In Figure 6.15 (d), one can see that after moving 2 mm out and back into the cavity mode, the atoms remains trapped for 9.5 s.

This experiment shows the ability to deterministically put atoms in the cavity mode, observe the atoms, move them out of the mode, and finally reposition them back in the cavity and observe them again.

### ***6.8 Deterministic Delivery and Cooling of Single atoms***

Starting with a single atom in the MOT we deterministically load this atom into the cavity where it is cooled and observed. This is a different approach than other groups that rely on filtering techniques or small loading probabilities to reach the single atom regime [50, 66].

This experiment follows the general experimental protocol with a few changes. Atoms are collected and counted from the single atom MOT. After being counted in the MOT, atoms are loaded into a cross-dipole lattice trap. Since the walking-wave lattice is shallow at the MOT, this additional trap increases the efficiency of transferring atoms from the MOT to the walking-wave lattice

The cross trap is built by spatially overlapping the walking-wave lattice, with an additional lattice trap constructed from 1 W of Yb doped fiber laser power that is focused to  $w_0 = 17 \mu\text{m}$ . This additional lattice is perpendicular to the walking wave lattice, and provides a potential depth of  $U_{\text{cross}} \approx 1 \text{ mK}$ . Before the atoms are transported, the cross lattice is turned off, leaving atoms in the walking-wave lattice where the atoms are transported to the cavity.

Once inside the cavity, atoms are cooled and observed by scattering the cooling light

into the cavity. The Rabi frequency of the cooling beams is  $\Omega = 32$  MHz, the cooling beams are set to  $\omega_p = \omega_0 - 21.5$  MHz and the cavity is locked to  $\omega_c = \omega_0 - 12$  MHz. In Figure 6.16, shows individual atoms observed by the optical cavity. With a pump-cooling detuning of  $\Delta_c = -9.5$  MHz, one can see one, two, three and four atoms stored in the cavity. The one atom signal begins with one atom loaded into the MOT, the two atom signal begins with two atoms in the MOT, likewise for the three and four atom signals.

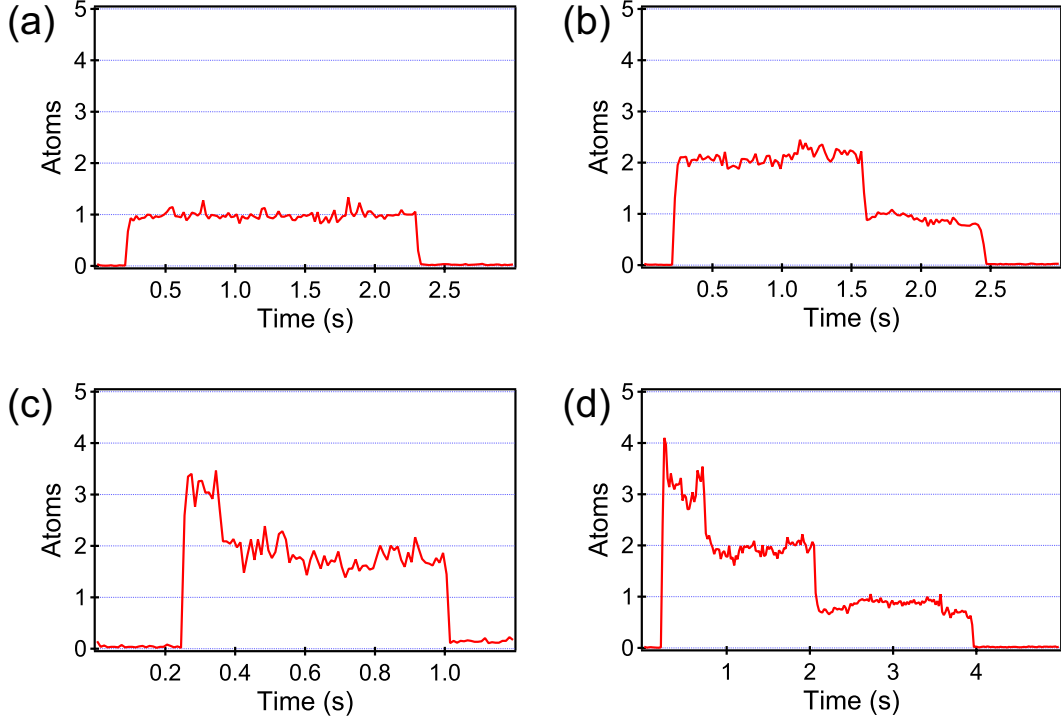


**Figure 6.16:** Individual atoms that are non-destructively observed in the cavity. (a) A MOT is formed of one atom that is then transported and detected in the cavity. In (b-d) the MOT begins with  $n = 2, 3, 4$  atoms, and then 2, 3, and 4 atoms are detected by the optical cavity. In these traces, the count rate for a single atom is 800 photons/atoms/10ms

The single atom signal in Figure 6.16 (a) is stored in the cavity for more than two seconds.

Typically, the transport efficiency of loading atoms into the cavity is 40%. In Figure 6.17, a MOT with 5 atoms is formed and in this experiment, only one atom survives the transport but once cooled inside the cavity, it is stored for 1.7 s.

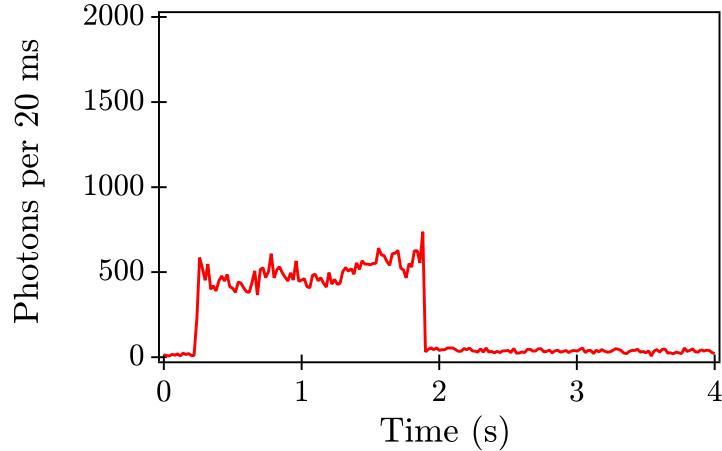


**Figure 6.17:** A MOT is loaded with 5 atoms and then transported to the cavity. Only a single atom is loaded into the cavity. In the cavity the atom is stored for 1.7 s

## 6.9 Experiments with Single Atom Scatter Rate

This section presents experiments that study the scatter rate,  $R_{\text{scat}}$  from Eq. (6.5), of a single atom with respect to the three parameters, the atom's position, the detuning of the cavity and the Rabi frequency of the cooling beams.

### 6.9.1 Scatter rate versus Atomic Position

In order to study the scattering rate versus the coupling rate  $g$ , we move the single atom across the cavity mode. The coupling rate is given by,  $g = g_0 \cos(kx) \exp(-(y^2 + z^2)/w(z)^2)$  for the  $\text{TEM}_{00}$  Gaussian mode. A single atom is transported to the high finesse cavity and then slowly moved over the mode with a velocity of  $50 \mu\text{m/s}$ . The atom travels a distance twice the cavity waist in approximately 1 s at this velocity. In Figure 6.18 (a), one can see the average of 17 single atom traces that map out the Gaussian  $\text{TEM}_{00}$  mode with a waist,  $w = 16 \mu\text{m}$ , from the Gaussian fit. From cavity theory the waist was calculated to be  $w = 20 \mu\text{m}$ , but still in good agreement with the fit.

The atom's position can be scanned in and out of the cavity mode multiple times. In Figure 6.18 (b), a single atom is moved in and out of the cavity mode 11 times with a velocity of  $440 \mu\text{m/s}$ . The signal is fit to a sum of Gaussian where the separation between each set of peaks is on average  $219 \pm 6.56 \text{ ms}$ .

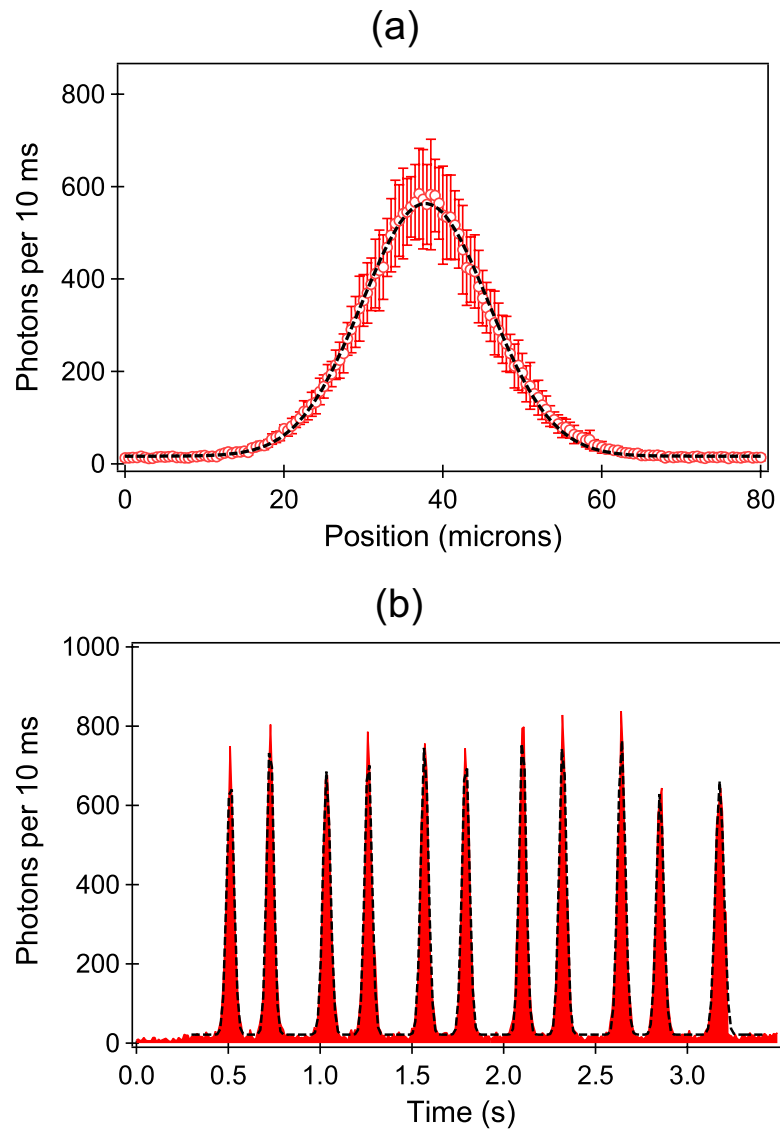


**Figure 6.18:** (a) Ramping a single atom through the cavity mode. A single atom is ramped through the cavity mode at  $50 \mu\text{m/s}$ . As the position of the atom changes, the Gaussian structure of the cavity mode is mapped. This is an average of 17 single atom runs, where error bars indicate one standard deviation, and the dashed black line is a Gaussian fit. (b) Ramping a single atom in and out of the cavity mode 11 times. The atom travels with a velocity of  $440 \mu\text{m/s}$ . The data is fit to a sum of Gaussian functions which is shown in the black dashed line.

Moving at faster velocities,  $v = 4.40$  mm/s, we have been able to record over 70 passages of the single atom through the cavity mode. Figure 6.19 shows a single atom moving over the cavity mode 79 times.

### 6.9.2 Scatter rate versus cavity-pump Detuning

To study the dependence of the scattering rate with respect to pump-cavity detuning,  $\Delta_c$ , single atoms are loaded into the optical cavity, and the detuning of the cavity is changed in real-time. This is done by changing the lock point of the cavity, which changes the resonance frequency of the cavity. The cavity detuning is ramped  $5 \kappa$  ( $\approx 70$  MHz) in one second, while the frequency of the cooling beam is held constant at  $\omega_p = \omega_0 - 21.5$  MHz. As the cavity detuning approaches zero, the atom scatters more photons into the cavity mode.

The scattering rate versus cavity detuning can be seen in Figure 6.20. The analytical scattering rate formula, Eq (6.5), is a Lorentzian function with respect to  $\Delta_c$ , for fixed  $\Omega$  and  $\Delta_a$ . The data in Figure 6.20 is fit to a Lorentzian function which is shown in black.

### 6.9.3 Scatter rate versus Rabi Frequency

To study the dependence of the scattering rate with respect to Rabi frequency, a single atom is loaded into the cavity. After a single atom enters the cavity the cooling beam power is linearly ramped from 24 nW to 24  $\mu$ W in 250 ms. The cooling beams are detuned -21.5 MHz and the cavity is detuned -12 MHz, both of these detunings are in respect to the bare atom resonance. This results in a pump-cavity detuning of,  $\Delta_c = -9.5$  MHz. The scatter rate is directly proportional to the Rabi frequency squared from Eq. (6.5). Since the optical power is proportional to the Rabi frequency squared,  $\Omega^2 \sim P$ , the scatter rate should be directly proportional to the cooling beam power. This linear dependence is shown in Figure 6.21 which is the average of 5 single atom data sets.

## 6.10 *Current Limitations of the Cavity QED System*

The preceding sections have presented a system that can study a single atom in a high finesse cavity, there are still some features that limit its performance and should be improved. The first feature to improve is the cavity's linewidth. Although the system is in the strong

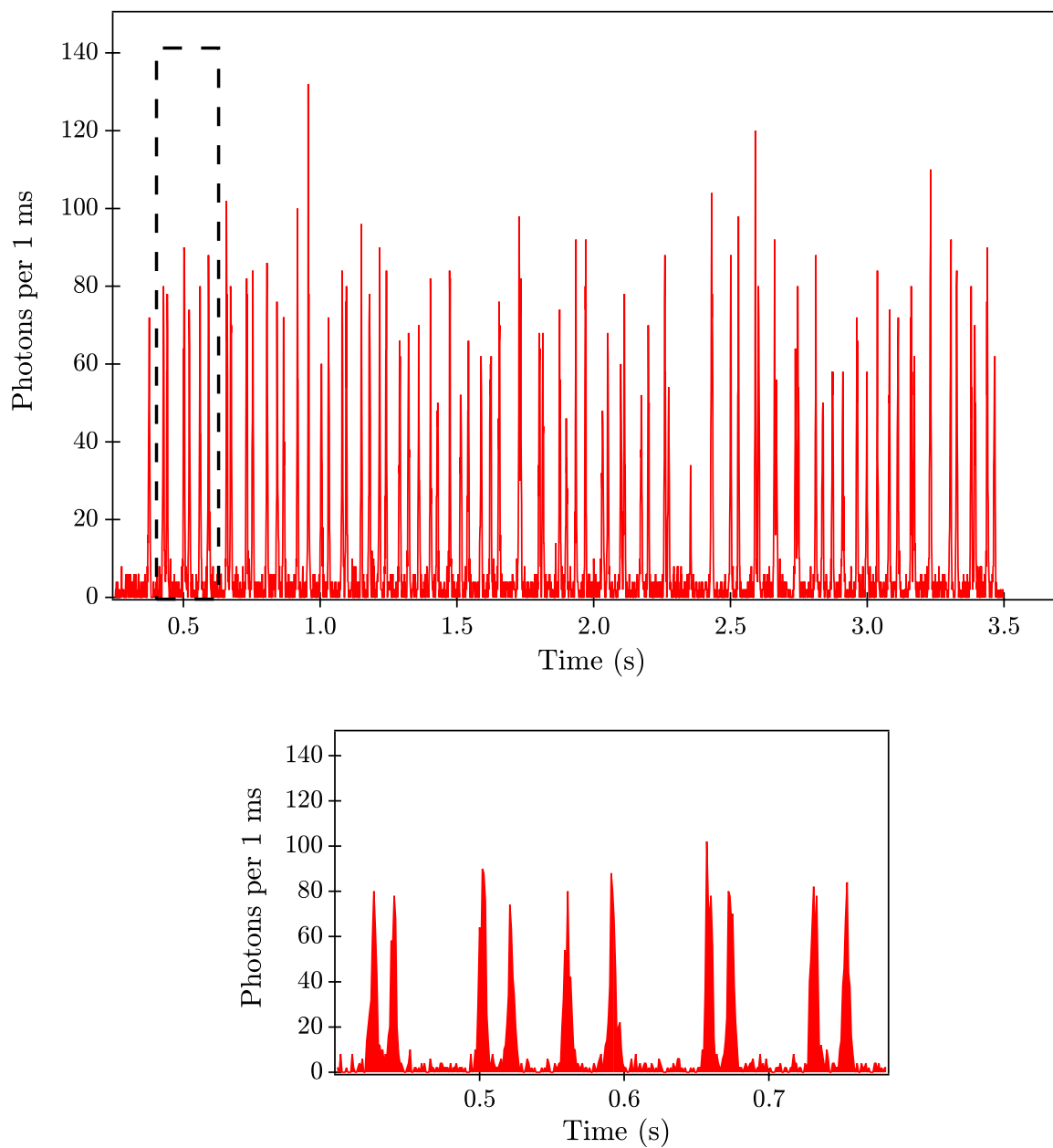


**Figure 6.19:** Moving an atom through the cavity mode 79 times at a velocity of 4.40 mm/s. The bottom graph shows a zoomed in detail of the dashed box region.

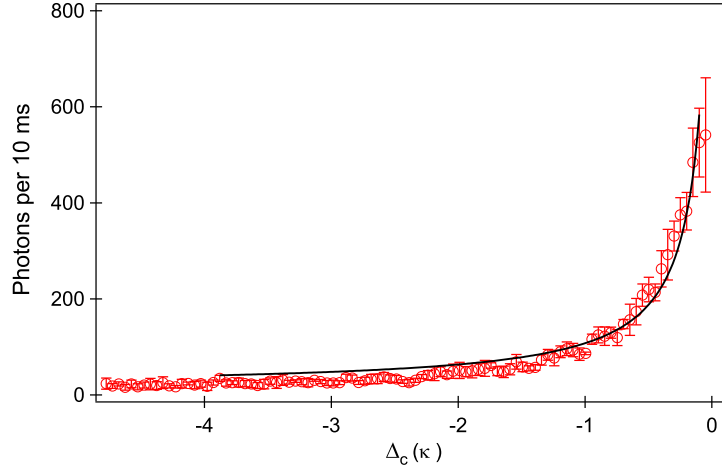


**Figure 6.20:** The scatter from a single atom as a function of the pump-cavity detuning. The cooling beams are held at a constant detuning of -21.5 MHz from the bare atom resonance. The cavity’s frequency is scanned 70 MHz in one second. The curve is an average of 4 single data sets, where the scattering rate is fit to a Lorentzian function, shown in black, with error bars indicating one standard deviation.

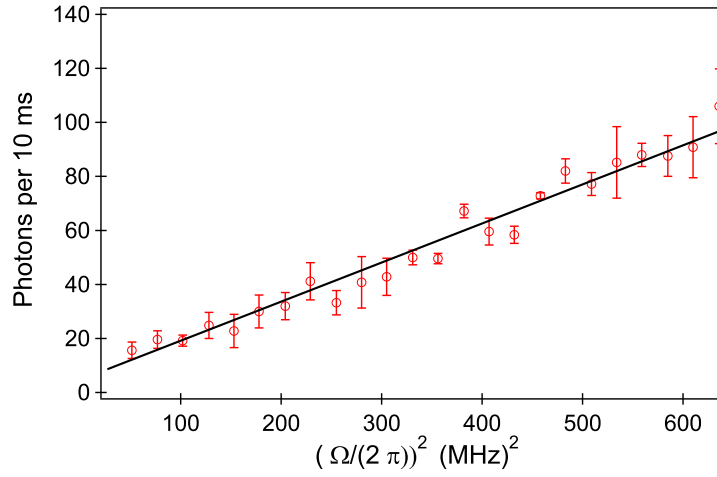


**Figure 6.21:** The single atom scatter rate as a function of cooling beam power. The optical power in the cooling beams is linearly ramped from 24 nW to 24  $\mu$ W in 250 ms with the scattering rate’s linear dependence with respect to pump power as expected from theory. The data set is acquired from 5 single atom runs that are averaged together, with the error bars indicating one standard deviation and the black curve is a linear fit.

coupling regime with  $(g, \gamma, \kappa) = (2\pi) (17.11, 6.06, 13.69)$  MHz, but the cavity linewidth is 2.5 times larger than the designed value. While cavity cooling and storage will work with this cavity, it limits the ultimate quantum information processes the cavity is designed to

perform.

Two other limitations are related to the count rate of individual atoms. First, the count rate is much smaller than the value predicted by theory. This small count rate hurts the signal to noise ratio, and increases the time required to detect an atom above the noise floor. Possible explanations of this small count rate are presented in the next section, 6.10.1. Secondly, we observe strange continuous decay of count rate, which is inconsistent with the discrete nature of atoms which is addressed in section 6.10.2.

### 6.10.1 Count Rate

When the theoretical count rate differs so much from the experimental value, the natural question to ask is where are the missing photons. The typical count rate for a single atom in this system ranged from 15-20 photons/atom/ms depending on the detuning. For a small number of data sets, the count rate of atoms was about three-four times larger than normal. These data sets were presented in Figures 6.18 and 6.16 where the count rate was 50-80 photons/atoms/ms, roughly a factor of four larger. It should be noted that these datasets of higher count rate started with a single atom MOT.

For the higher count rate values, as in Figure 6.18, the single atom count rate was 55 photons/atom/ms, for a pump-cavity detuning of  $\Delta_c = -9.5$  MHz and  $\Omega = 32$  MHz and a calculated Stark shift detuning of  $\Delta_s = 75$  MHz. Using Eq. (6.5), the theoretically predicted count rate is 8970 photons/atom/ms, which is approximately 163 times larger than the measured value.

The first source to explain this error is the polarization sensitive optics that are used to separate the science light from the locking light. The atoms will emit a randomly polarized photon, and the detection scheme will only collect half of these photons. This brings the discrepancy down to a factor of 81.5.

The second source is inefficient re-pumping of the atoms. The atoms experience a large Stark shift due to the optical trap, approximately  $\Delta_s = 75$  MHz. Since the repump is set to the bare atom transition  $F = 1 \rightarrow F' = 2$ , the repump is detuned by more than 12 linewidths from the Stark shifted atom. This detuning makes the repump process inefficient

and the atom emit less photons in the cavity because it spends more time in the  $F = 1$  dark state. In the work by Nußman *et al.* [66], the single atom count rate was a factor of 5 smaller than the theoretical value. To explain this discrepancy, they introduced a “blinking” factor of  $1/5$  due to poor re-pumping efficiency. For the repump in the cooling beams, the probability of exciting a Stark detuned atom is  $p_{ee} \approx 0.1$ , compared to  $p_{ee} \approx 0.5$ , for the bare atom. Adopting a blinking factor of  $1/5$  which brings the discrepancy in count rate to a factor of 16.30. The dependence of the scattering rate with respect to repump detuning should be measured explicitly.

The typical experimental count rate, as in Figure 6.10, the count rate was 15 photons/ms. The theoretical count rate is 12300 photons/s and making the same arguments as above the detected count rate is 84 times smaller than the theoretical value.

This discrepancy can be attributed to the calculation of atom-cavity coupling,  $g_0$ , where the value of the electric dipole moment,  $\mu$ , was average over all Zeeman states. In actuality there are many Zeeman states and some with smaller atom-cavity coupling.

### 6.10.2 Drifting count rates

One problem observed in some datasets is a linear drifts of the count rates for a single atom. Figure 6.22 shows an example of these linear drifts. In Figure 6.22 (a), one can see discrete steps of atoms cooled in the cavity and Figure 6.22 (b), shows data for the same setting where there are discrete atom steps, and then drifts continuously from 1 atom to zero atoms.

This drift could be due to physics. As the atom is cooled to the bottom of the optical trap potential, it will experience a larger Stark shift. So as the atom cools it will emit less photons. However, it is difficult to imagine this process taking so long.

The most likely culprit is a technical problem with the quality of the RF sources that generate the walking wave-lattice. The location of the atom in the cavity mode is crucial and the position dependence was presented in Figure 6.18. If the atom starts at the center of the cavity mode and is slowly dragged to the right or left of the mode, the count rate will decrease. This agrees with the experimental results where the drift is observed to only

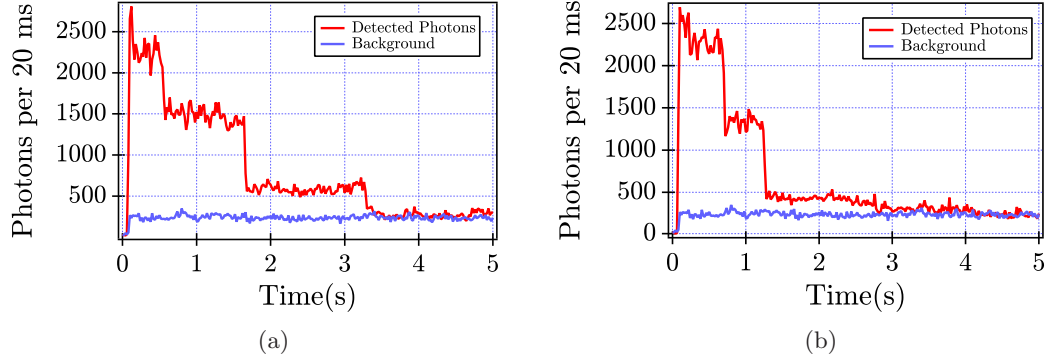


**Figure 6.22:** (a) Discrete atomic steps observed from cooling many atoms inside the cavity. The data is binned in 20 ms time bins. (b) Discrete atomic steps, but the last atom continuously decays to the background level.

decrease the count rate.

The quality of the RF sources was measured by setting each source to 40 MHz and mixing the signals to measure the beat frequency. The output from the mixer was low pass filtered and a 1.5 Hz oscillation was observed. This frequency difference corresponds to velocity of the walking wave of  $v = 0.8 \mu\text{m/s}$ . An atom beginning at the center of the cavity mode moving will exit the cavity mode in 20 seconds at this velocity. As the atom moves out of the mode, the count rate will decrease. While we observe faster drifts, improvements of the RF sources needs to be investigated.

### 6.11 Summary of Atom-Cavity System Results

This chapter presents a full realization of a working cavity QED system with the implementation of a stable long-lifetime Yb doped fiber based optical trap, an active locking scheme of the science cavity. This flexible system allows the study of individual atoms interacting with individual photons to study cavity QED. This system employs a completely deterministic technique to load individual atoms into the cavity.

This chapter demonstrates the ability to deterministically load and probe atoms using the intra-cavity probe. In addition, this chapter develops the ability to cool atoms in the optical cavity with the addition of cooling beams. With these cooling beams a single atom can be stored in the optical cavity for many seconds. The maximum observed lifetime of a

single atom was 10 seconds in the cavity. This is roughly a factor 10,000 fold improvement if the atoms are just probed with the cavity field.

This chapter presents experiments on the dependence of the scattering rate of a single atom with respect to the atom's position, the detuning of the cavity and the cooling beam's Rabi rate. Additionally, we have demonstrated the ability to move an atom in out of the cavity mode over 70 times. One can imagine performing an operation on a qubit (atom) inside the cavity and then pulling out the atom, in order to perform a operation on a different atom. These techniques provide framework to implement this protocol.

## CHAPTER VII

### CONCLUSION AND OUTLOOK

In this thesis, a complete rebuild of the cavity QED experiment has been presented. This flexible new system allows for the study of trapped individual atoms. This new system allows the next generation of experiments to continue to advance the state of the art in cavity QED.

This work has developed techniques to detect single atoms by construction of a single atom MOT and a large numerical aperture imaging system. These individual atoms were loaded into an optical trap and were continuously cooled and observed in free space. This non-destructive technique increased the lifetimes in the optical trap to greater than two minutes. This longer lifetime is 1000 times larger than the original titanium sapphire laser traps used to deterministically load atoms in a high finesse cavity.

This thesis developed techniques to non-destructively observe atoms in a high finesse cavity. This technique increased the storage times of a single atom to greater than 10 seconds. Comparing to individual atoms probed using the cavity field, this cavity assisted cooling increases the storage time by a factor of 10,000! This long storage time, and cooling was made possible by implementing a flexible active locking system.

#### ***7.1 Future Directions***

##### **7.1.1 Qubit in a cavity**

With the long storage time of individual atoms, this system is poised to prepare the first neutral atom qubit in a high finesse cavity. To prepare the qubit the atom is prepared initially in the  $|F, m_F\rangle = |1, 0\rangle = |0\rangle$  state. The required rotations can be performed using microwaves, on the clock-transition which is the magnetic field insensitive transition between the  $|1, 0\rangle$  and  $|1\rangle = |2, 0\rangle$  hyperfine states.

The ability to drive microwave transitions has already been developed in this system. In Figure 7.1, microwaves on the clock-transition were used to drive Rabi transitions from

the  $F = 1$  ground state to the  $F = 2$  ground state in  $^{87}\text{Rb}$  for atoms trapped in an optical lattice. After a microwave pulse, atoms are imaged with  $F = 2 \rightarrow F' = 3$  light. As the pulse width of the microwave is varied the Rabi flopping spectrum is observed. This measurement was performed on 10,000  $^{87}\text{Rb}$  atoms trapped in an optical lattice

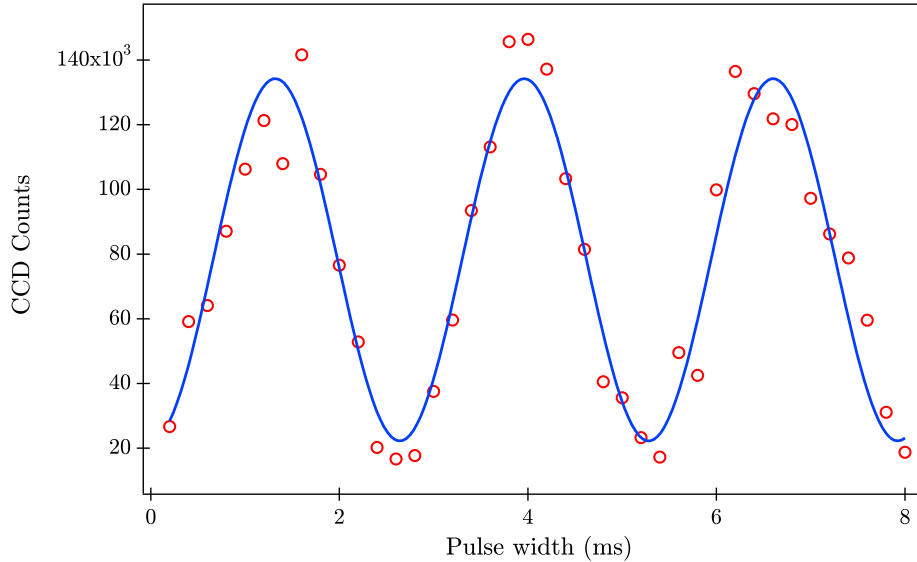


**Figure 7.1:** Rabi flopping in an optical lattice with a static DC bias field of 300 mG. Atoms are driven from the  $F = 1$  hyperfine line to  $F = 2$  with the use of microwaves tuned on the clock transition. After the microwave pulse atoms are imaged on the  $F = 2 \rightarrow F' = 3$  cycling transition. From the graph three complete Rabi flops are evident.

The protocol to prepare the qubit would be as follows: optically pump the atom into the  $|1,0\rangle$  state and then with a microwave pulse to prepare the atom in an arbitrary superposition state. Using the cavity, the state of the atom is measured. The experiment sequence would be done quickly, less than 10 ms for a complete cycle, allowing for many measurements to be performed on one single atom.

To perform many measurements on a single atom, it will be necessary to develop a more sophisticated experimental control that would include feedback. An example of this feedback would be if two atoms are loaded in the cavity, the software would dump the trap and try again until a single atom is loaded. Additionally, it will be necessary to use a pulsed cooling scheme where the atom is cooled for a short period of time (10 ms), followed by a time when the cooling light is turned off. While the cooling light is turned off, the atom

is optical pumped, exposed to microwave pulse and state is read by the cavity. When the experiment sequence is completed, the atom is cooled again. This pulsed cooling technique should be straight forward to implement as it has already been implemented in the free space cooling experiments.

### **7.1.2 Two Lattices in the Cavity**

With a longer cavity one can construct two optical lattices to transport atom into the cavity as depicted in Figure 3.6. The qubits (atoms) are stored in two independent lattices each of which can be translated. With two trapped atoms in the cavity it will be possible to perform a two-qubit gate and this implementation provides a mechanism for entangling qubits in a controlled fashion. This new cavity system will build upon the technological advances presented in thesis to advance experimental cavity QED research.

## REFERENCES

- [1] L. Allen and J. H. Eberly, *Optical Resonance and Two-Level Atoms* (Dover Publications, Inc., New York, 1975).
- [2] D. J. Wineland and H. G. Dehmelt, “Proposed  $10^{14}\delta\nu < \nu$  laser fluorescence spectroscopy on  $\text{TI}^+$  mono-ion oscillator III,” *Bull. Am. Phys. Soc* **20**, 637 (1975).
- [3] T. W. Hänsch and A. L. Schawlow, “Cooling of gases by laser radiation,” *Opt. Commun.* **13**, 68 (1975).
- [4] M. H. Anderson, J. R. Ensher, M. R. Matthews, C. E. Wieman, and E. A. Cornell, “Observation of Bose-Einstein Condensation in a Dilute Atomic Vapor,” *Science* **269**, 198 (1995).
- [5] S. Chu, “The manipulation of neutral particles,” *Rev. Mod. Phys.* **70**, 685 (1998).
- [6] C. N. Cohen-Tannoudji, “Manipulating atoms with photons,” *Rev. Mod. Phys.* **70**, 707 (1998).
- [7] W. D. Phillips, “Laser cooling and trapping of neutral atoms,” *Rev. Mod. Phys.* **70**, 721 (1998).
- [8] E. A. Cornell and C. E. Wieman, “Nobel Lecture: Bose-Einstein condensation in a dilute gas, the first 70 years and some recent experiments,” *Rev. Mod. Phys.* **74**, 875 (2002).
- [9] W. Ketterle, “Nobel lecture: When atoms behave as waves: Bose-Einstein condensation and the atom laser,” *Rev. Mod. Phys.* **74**, 1131 (2002).
- [10] R. P. Feynman, “Simulating physics with computers,” *Int. J. Theor. Phys.* **21**, 467 (1982).
- [11] D. Deutsch, “Quantum theory, the Church-Turing principle and the universal quantum computer,” *Proc. R. Soc. Lond. A* **400**, 97 (1985).
- [12] P. Shor, “Algorithms for quantum computation: Discrete logarithms and factoring,” in *Proceedings of the 35th Annual Symposium on Foundations of Computer Science* pp. 124–134 Los Alamitos, CA 1994 IEEE Computer.
- [13] R. L. Rivest, A. Shamir, and L. Adleman, “A method of obtaining digital signatures and public-key cryptosystems,” *Comm. Assoc. Comput. Mach.* **21**, 120 (1978).
- [14] L. Grover, “Quantum mechanics helps in searching for a needle in a haystack,” *Phys. Rev. Lett.* **79**, 325 (1997).
- [15] J. I. Cirac and P. Zoller, “Quantum Computations with Cold Trapped Ions,” *Physical Review Letters* **74**, 4091 (1995).

- [16] C. Monroe, D. M. Meekhof, B. E. King, W. M. Itano, and D. J. Wineland, “Demonstration of a Fundamental Quantum Logic Gate,” *Phys. Rev. Lett.* **75**, 4714 (1995).
- [17] Q. A. Turchette, C. S. Wood, B. E. King, C. J. Myatt, D. Leibfried, W. M. Itano, C. Monroe, and D. J. Wineland, “Deterministic Entanglement of Two Trapped Ions,” *Phys. Rev. Lett.* **81**, 3631 (1998).
- [18] M. D. Barrett, J. Chiaverini, T. Schaetz, J. Britton, W. M. Itano, J. D. Jost, E. Knill, C. Langer, D. Leibfried, R. Ozeri, and D. J. Wineland, “Deterministic quantum teleportation of atomic qubits,” *Nature (London)* **429**, 737 (2004).
- [19] H. Häffner, W. Hänsel, C. F. Roos, J. Benhelm, D. C. al kar, M. Chwalla, T. Köber, U. D. Rapol, M. Riebe, P. O. Schmidt, C. Becher, O. Gühne, W. Dür, and R. Blatt, “Scalable multiparticle entanglement of trapped ions,” *Nature (London)* **438**, 643 (2005).
- [20] M. Riebe, H. Häffner, C. F. Roos, W. Hänsel, J. Benhelm, G. P. T. Lancaster, T. W. Körber, C. Becher, F. Schmidt-Kaler, D. F. V. James, and R. Blatt, “Deterministic quantum teleportation with atoms,” *Nature (London)* **429**, 734 (2004).
- [21] K. A. Brickman, P. C. Haljan, P. J. Lee, M. Acton, L. Deslauriers, and C. Monroe, “Implementation of Grover’s quantum search algorithm in a scalable system,” *Phys. Rev. A* **72**, 050306(R) (2005).
- [22] B. B. Blinov, D. L. Moehring, L.-M. Duan, and C. Monroe, “Observation of entanglement between a single trapped atom and a single photon,” *Nature (London)* **428**, 153 (2004).
- [23] D. Kielpinski, C. Monroe, and D. J. Wineland, “Architecture for a large-scale ion-trap quantum computer,” *Nature (London)* **417**, 709 (2002).
- [24] R. Hughes, “A Quantum Information Science and Technology Roadmap,” 2004.
- [25] D. P. DiVincenzo, “The Physical Implementation of Quantum Computation,” *Fortschr. Phys.* **48**, 771 (2000).
- [26] T. Sleator and H. Weinfurter, “Realizable Universal Quantum Logic Gates,” *Phys. Rev. Lett.* **74**, 4087 (1995).
- [27] J. A. Sauer, K. M. Fortier, M. S. Chang, C. D. Hamley, and M. S. Chapman, “Cavity QED with optically transported atoms,” *Phys. Rev. A* **69**, 051804(R) (2004).
- [28] E. L. Raab, M. Prentiss, A. Cable, S. Chu, and D. E. Pritchard, “Trapping of Neutral Sodium Atoms with Radiation Pressure,” *Phys. Rev. Lett.* **59**, 2631 (1987).
- [29] S. Chu, L. Hollberg, J. E. Bjorkholm, A. Cable, and A. Ashikin, “Three-Dimensional Viscous Confinement and Cooling of Atoms by Resonance Radiation Pressure,” *Phys. Rev. Lett.* **55**, 48 (1985).
- [30] H. J. Metcalf and P. van der Straten, *Laser Cooling and Trapping* (Springer, New York, 1999).
- [31] C. J. Foot, *Atomic Physics* (Oxford University Press, Oxford, 2005).

- [32] P. D. Lett, R. N. Watts, C. I. Westbrook, W. D. Phillips, P. L. Gould, and H. J. Metcalf, "Observation of Atoms Laser Cooled below the Doppler Limit," *Phys. Rev. Lett.* **61**, 169 (1988).
- [33] P. J. Ungar, D. S. Weiss, E. Riis, and S. Chu, "Optical molasses and multilevel atoms: theory," *J. Opt. Soc. Am. B* **6**, 2058 (1989).
- [34] J. Dalibard and C. Cohen-Tannoudji, "Laser cooling below the Doppler limit by polarization gradients: simple theoretical models," *J. Opt. Soc. Am. B* **6**, 2023 (1989).
- [35] M. D. Barrett, J. A. Sauer, and M. S. Chapman, "All-Optical Formation of an Atomic Bose-Einstein Condensate," *Phys. Rev. Lett.* **87**, 10404 (2001).
- [36] M. Takamoto, F.-L. Hong, R. Higashi, and H. Katori, "An optical lattice clock," *Nature (London)* **435**, 321 (2005).
- [37] A. Corney, *Atomic and Laser Spectroscopy* (Oxford University Press, Oxford, 1977).
- [38] A. Ashkin, "Acceleration and Trapping of Particles by Radiation Pressure," *Phys. Rev. Lett.* **24**, 156 (1970).
- [39] A. Ashkin, "Trapping of Atoms by Resonance Radiation Pressure," *Phys. Rev. Lett.* **40**, 729 (1978).
- [40] S. Chu, J. E. Bjorkholm, A. Ashkin, and A. Cable, "Experimental Observation of Optically Trapped Atoms," *Phys. Rev. Lett.* **57**, 314 (1986).
- [41] J. D. Miller, R. A. Cline, and D. J. Heinzen, "Far-off-resonance optical trapping of atoms," *Phys. Rev. A* **47**, R4567 (1993).
- [42] R. Grimm, M. Weidemüller, and Y. Ovchinnikov, "Optical dipole traps for neutral atoms," *Adv. At. Mol. Opt. Phys.* **42**, 95 (2000).
- [43] E. Hecht, *Optics*, Fourth ed. (Pearson Addison Wesley, San Francisco, CA, 2002).
- [44] B. E. A. Saleh and M. C. Teich, *Fundamentals of Photonics* (Wiley-Interscience, New York, 1991).
- [45] A. E. Siegman, *Lasers* (University Science Books, Sausalito, CA, 1986).
- [46] Y.-N. Zeng, X.-J. Zhou, J.-B. Chen, and X.-Z. Chen, "Magic Wavelength for Caesium Transition Line  $6S_{1/2} - 6P_{3/2}$ ," *Chin. Phys. Lett.* **23**, 1687 (2006).
- [47] R. L. Kurucz and B. Bell, "1995 Atomic Line Data," Kurucz CD-ROM No. 23.
- [48] A. B. R. L. Targat, X. Baillard, M. Fouché, and P. Lemonde, "Hyperpolarizability Effects in a Sr Optical Lattice Clock," *Phys. Rev. Lett.* **96**, 103003 (2006).
- [49] S. G. Porsev, A. Derevianko, and E. N. Fortson, "Possibility of an optical clock using the  $6^1S_0 \rightarrow 6^3P_0^0$  transition in  $^{171,173}\text{Yb}$  atoms in an optical lattice," *Phys. Rev. A* **69**, 021403(R) (2004).
- [50] J. McKeever, J. R. Buck, A. D. Boozer, A. Kuzmich, H. C. Nagerl, D. M. Stamper-Kurn, and H. J. Kimble, "State-insensitive cooling and trapping of single atoms in an optical cavity," *Phys. Rev. Lett.* **90**, 133602 (2003).

- [51] D. Meschede, *Optics, Light and Lasers: The Practical Approach to Modern Aspects of Photonics and Laser Physics* (Wiley-VCH, Verlag GmbH, 2004).
- [52] E. T. Jaynes and F. W. Cummings, “Comparison of Quantum and Semiclassical Radiation Theories with Application to the Beam Maser,” *Proc. IEEE* **51**, 89 (1963).
- [53] J. M. Raimond, M. Brune, and S. Haroche, “Colloquium: Manipulating quantum entanglement with atoms and photons in a cavity,” *Rev. Mod. Phys.* **73**, 565 (2001).
- [54] H. Mabuchi, Q. A. Turchette, M. S. Chapman, and H. J. Kimble, “Real-time detection of individual atoms falling through a high-finesse optical cavity,” *Opt. Lett.* **21**, 1393 (1996).
- [55] P. Meystre and M. Sargent III, *Elements of Quantum Optics*, Second ed. (Springer-Verlag, Berlin, 1990).
- [56] P. R. Berman, editor, *Cavity Quantum Electrodynamics* (Academic Press, Inc., San Diego, 1994).
- [57] J. A. Sauer, *Cold Atom Manipulation for Quantum Computing and Control*, PhD thesis Georgia Institute of Technology 2004.
- [58] K. Murr, S. Nußman, T. Puppe, M. Hijlkema, B. Weber, S. C. Webstera, A. Kuhn, and G. Rempe, “Three-dimensional cavity cooling and trapping in an optical lattice,” *Phys. Rev. A* **73**, 063415 (2006).
- [59] P. Horak, G. Hechenblaikner, K. M. Gheri, H. Stecher, and H. Ritsch, “Cavity-Induced Atom Cooling in the Strong Coupling Regime,” *Phys. Rev. Lett.* **79**, 4974 (1997).
- [60] G. Hechenblaikner, M. Gangl, P. Horak, and H. Ritsch, “Cooling an atom in a weakly driven high-Q cavity,” *Phys. Rev. A* **58**, 3030 (1998).
- [61] V. Vuletić and S. Chu, “Laser Cooling of Atoms, Ions, or Molecules by Coherent Scattering,” *Phys. Rev. Lett.* **84**, 3787 (2000).
- [62] T. Fischer, P. Maunz, T. Puppe, P. W. H. Pinkse, and G. Rempe, “Collective light forces on atoms in a high-finesse cavity,” *New. J. Phys.* **3**, 11 (2001).
- [63] H. W. Chan, A. T. Black, and V. Vuletić, “Observation of Collective-Emission-Induced Cooling of Atoms in an Optical Cavity,” *Phys. Rev. Lett.* **90**, 063003 (2003).
- [64] P. Maunz, T. Puppe, I. Schuster, N. Syassen, P. W. H. Pinkse, and G. Rempe, “Cavity cooling of a single atom,” *Nature (London)* **428**, 50 (2004).
- [65] A. D. Boozer, A. Boca, R. Miller, T. E. Northup, and H. J. Kimble, “Cooling to the ground state of axial motion for one atom strongly coupled to an optical cavity,” *Phys. Rev. Lett.* **97**, 83602 (2006).
- [66] S. Nußmann, K. Murr, M. Hijlkema, B. Weber, A. Kuhn, and G. Rempe, “Vacuum-stimulated cooling of single atoms in three dimensions,” *Nature Phys.* **1**, 122 (2005).
- [67] T. Pellizzari, S. A. Gardiner, J. I. Cirac, and P. Zoller, “Decoherence, Continuous Observation, and Quantum Computing: A Cavity QED Model,” *Phys. Rev. Lett.* **75**, 3788 (1995).

- [68] J. Pachos and H. Walther, “Quantum Computing with Trapped Ions in an Optical Cavity,” *Phys. Rev. Lett.* **89**, 187903 (2002).
- [69] X. X. Yi, X. H. Su, and L. You, “Conditional Quantum Phase Gate between Two 3-State Atoms,” *Phys. Rev. Lett.* **90**, 097902 (2003).
- [70] C. Klempt, T. van Zoest, T. Henninger, O. Topic, E. Rasel, W. Ertmer, and J. Arlt, “Ultraviolet light-induced atom desorption for large rubidium and potassium magneto-optical traps,” *Phys. Rev. A* **73**, 13410 (2006).
- [71] C. C. Bradley, J. Chen, and R. G. Hulet, “Instrumentation for the stable operation of laser diodes,” *Rev. Sci. Instrum.* **61**, 2097 (1990).
- [72] K. G. Libbrecht and J. L. Hall, “A low-noise high speed diode laser current controller,” *Rev. Sci. Instrum.* **64**, 2133 (1993).
- [73] W. Demtröder, *Laser Spectroscopy*, Second ed. (Springer, Berlin, 1996).
- [74] W. Z. Zhao, J. E. Simsarian, L. A. Orozco, and G. D. Sprouse, “A computer-based digital feedback control of frequency drift of multiple lasers,” *Rev. Sci. Instrum.* **69**, 3737 (1998).
- [75] S. M. Jaffe, M. Rochon, and W. M. Yen, “Increasing the frequency stability of single-frequency lasers,” *Rev. Sci. Instrum.* **64**, 2475 (1993).
- [76] B. G. Lindsay, K. A. Smith, and F. B. Dunning, “Control of long-term output frequency drift in commercial dye lasers,” *Rev. Sci. Instrum.* **62**, 1656 (1991).
- [77] C. J. Hood, *Real-time Measurements and Trapping of Single Atoms by Single Photons*, PhD thesis California Institute of Technology 2000.
- [78] D. W. Vernooy, *Cold Atoms in Cavity QED for Quantum Information Processings*, PhD thesis California Institute of Technology 2000.
- [79] Q. A. Turchette, *Quantum optics with single atoms and single photons*, PhD thesis California Institute of Technology 1997.
- [80] J. H. Moore, C. C. Davis, and M. A. Coplan, *Building Scientific Apparatus* (Addison Wesley Publishing Company, 1989).
- [81] E. D. Black, “An introduction to Pound-Drever-Hall laser frequency stabilization,” *American Journal of Physics* **69**, 79 (2000).
- [82] R. W. P. Drever, J. L. Hall, F. V. Kowalski, J. Hough, G. M. Ford, A. J. Munley, and H. Ward, “Laser phase and frequency stabilization using an optical resonator,” *Appl. Phys. B* **31**, 97 (1983).
- [83] T. A. Savard, K. M. O’Hara, and J. E. Thomas, “Laser-noise-induced heating in far-off resonance optical traps,” *Phys. Rev. A* **56**, R1095 (1997).
- [84] C. S. Adams, J. J. Lee, N. Davidson, M. Kasevich, and S. Chu, “Evaporative Cooling in a Crossed Dipole Trap,” *Phys. Rev. Lett.* **74**, 3577 (1995).

- [85] D. Haubrich, H. Schadwinkel, F. Strauch, B. Ueberholz, R. Wynands, and D. Meschede, “Observation of individual neutral atoms in magnetic and magneto-optical traps,” *Europhys. Lett.* **34**, 663 (1996).
- [86] Y. Miroshnychenko, D. Schrader, S. Kuhr, W. Alt, I. Dotsenko, M. Khudaverdyan, A. Rauschenbeutel, and D. Meschede, “Continued imaging of the transport of a single neutral atom,” *Opt. Express* **11**, 3498 (2003).
- [87] D. Schrader, I. Dotsenko, M. Khudaverdyan, Y. Miroshnychenko, A. Rauschenbeutel, and D. Meschede, “Neutral atom quantum register,” *Phys. Rev. Lett.* **93**, 150501 (2004).
- [88] D. A. Steck, “Rubidium 87 D Line Data,” <http://steck.us/alkalidata/>; accessed July 2006 2003.
- [89] C. J. Hood, H. J. Kimble, and J. Ye, “Characterization of high-finesse mirrors: Loss, phase shifts, and mode structure in an optical cavity,” *Phys. Rev. A* **64**, 33804 (2001).
- [90] S. Nußmann, M. Hijlkema, B. Weber, F. Rohde, G. Rempe, and A. Kuhn, “Submicron positioning of single atoms in a microcavity,” *Phys. Rev. Lett.* **95**, 173602 (2005).
- [91] J. T. Verdeyen, *Laser Electronics*, Third ed. (Prentice Hall, Upper Saddle River, NJ, 1995).
- [92] S. M. Tan, “A computational toolbox for quantum and atomic optics,” *Journal of Optics B: Quantum and Semiclassical Optics* **1**, 424 (1999).
- [93] R. J. Thompson, G. Rempe, and H. J. Kimble, “Observation of Normal-Mode Splitting for an Atom in an Optical Cavity,” *Phys. Rev. Lett.* **68**, 1132 (1992).
- [94] C. J. Hood, M. S. Chapman, T. W. Lynn, and H. J. Kimble, “Real-time cavity QED with single atoms,” *Phys. Rev. Lett.* **80**, 4157 (1998).
- [95] J. Ye, D. W. Vernooy, and H. J. Kimble, “Trapping of single atoms in cavity QED,” *Phys. Rev. Lett.* **83**, 4987 (1999).
- [96] P. W. H. Pinkse, T. Fischer, P. Maunz, and G. Rempe, “Trapping an atom with single photons,” *Nature (London)* **404**, 365 (2000).